The Thesis Committee for Madalyn Marie Liebum
Certifies that this is the approved version of the following thesis:

Characterization of an Alkyl Diamine Surfactant for Gas Mobility Control in Gas Enhanced Oil Recovery and Conformance Control

APPROVED BY
SUPERVISING COMMITTEE:

Quoc P. Nguyen, Supervisor

David DiCarlo

Characterization of an Alkyl Diamine Surfactant for Gas Mobility Control in Gas Enhanced Oil Recovery and Conformance Control

by

Madalyn Marie Liebum, B.S.E.E.

Thesis

Presented to the Faculty of the Graduate School of

The University of Texas at Austin

in Partial Fulfillment

of the Requirements

for the Degree of

Master of Science in Engineering

The University of Texas at Austin

May 2016

Dedication

To my family.

Acknowledgements

I would like to acknowledge Dr. Quoc P. Nguyen for his guidance and support throughout the entire process. I also would like to thank Dr. David DiCarlo for being my second reader and teaching me the realm of thermodynamics.

Thank you Dr. Ian Riddington and team for your guidance and patience. Additionally, I would like to thank the past and current member of the Gas EOR team for all their hard work: Christian, Galang, Heather, Nilanka, and Tyler.

Abstract

Characterization of an Alkyl Diamine Surfactant for Gas Mobility Control in Gas Enhanced Oil Recovery and Conformance Control

Madalyn Marie Liebum, M.S.E

The University of Texas at Austin, 2016

Supervisor: Quoc P. Nguyen

The objective of this research is to characterize the properties and performance of an amine-based "switchable" surfactant, Duomeen TTM, at various environmental conditions. In particular, bulk characterization measurements namely, aqueous stability, solubility, partition, and rheological behavior were tested and applied in core flooding experiments using carbonate rock saturated in very saline brine.

Aqueous stability provides insight about how Duomeen TTM solutions tolerate with changes in salt concentration, pH, and temperature. This surfactant becomes more hydrophilic as pH decreases and transforms into a viscoelastic solution at moderate to high salt concentrations. This viscoelasticity is intensified by changes in pH, temperature, and surfactant concentration of the solution, where surfactant concentration limits the aggregation density of the solution, pH influences the protonation process in the head group, and temperature controls the minimization of free energy by breaking, reformation, and branching of micellar networks.

Furthermore, solubility measurements were conducted for a series of pressures and temperatures in pure CO_2 as well as in gas mixtures composed of CO_2 and CH_4. It is shown that Duomeen TTM is very soluble in CO_2, but becomes less soluble when methane is present in the system. Partition experiments amongst brine and CO_2 reveal Duomeen TTM is very water soluble at low pH, in agreement with the aqueous stability results.

Finally, these bulk characterization results were applied in core flooding experiments where in-situ viscoelasticity or gel development capabilities were tested with surfactant dissolved in solution at different salinities. In-situ viscosification is mainly dependent on the salinity contrast between the injective solution and resident brine as well as the rheological behavior of the surfactant solution at different salinities. This in-situ gel development provides mobility control by blocking thief zones and high permeable regions in porous media. In all, this ability to viscosify in-situ makes Duomeen TTM applicable for near-wellbore conformance control and CO_2 mobility control in CO_2 enhanced oil recovery.

Table of Contents

List of Tables xii

List of Figures xiii

Chapter 1: Introduction 1

1.1 Use of Surfactants in Subsurface Applications 1

1.2 Research Objectives 2

1.3 Description of Chapters 3

Chapter 2: Literature Review 6

2.1 Fundamental Concepts of Surfactants 6

2.1.1 Fundamentals 6

2.1.2 Thermodynamic Relationship for CMC and Hydrophobic Effect 7

2.1.3 Classes of Surfactants 8

2.1.4 HLB Concept 9

2.2 Amine-Based "Switchable" Surfactants 12

2.2.1 Definition 12

2.2.2 Water Solubility of Amine-Based Surfactants 13

2.2.3 Aqueous Stability and Phase Behavior 13

2.2.4 Degree of Protonation 16

2.3 Solubility in Supercritical and Gaseous Phase 17

2.4 Viscoelastic Surfactants 22

2.5 Rheology 28

2.5.1 Surfactant Morphology Models 28

2.6 Foam in Porous Media 31

2.6.1 Foam Properties 31

2.6.2 Mobility Control 33

2.7 Surfactant Use in Petroleum Applications 34

2.7.1 Conformance Control 35

2.7.2 Enhanced Oil Recovery 36

2.7.3 Matrix Stimulation 37

Chapter 3: Aqueous Stability of Duomeen TTM....39
3.1 Introduction....39
3.2 Materials and Procedure....39
3.2.1 Materials....39
3.2.2 Procedure....40
3.3 Results and Discussion....41
3.3.1 Phase Behavior: 0.2 wt.% Duomeen TTM Solution....41
3.3.2 Critical pH: 0.2 wt.% Duomeen TTM Solution....43
3.3.3 Critical pH: 1 wt.% Duomeen TTM Solution....45
3.4 Conclusion....48
Chapter 4: Surfactant Solubility in Mixed Gas and CO_2/Brine Phase Partition of Alkyl Amines....49
4.1 Introduction....49
4.2 Materials and Procedure....50
4.2.1 Materials....50
4.2.2 Procedure....51
4.3 Results and Discussion....57
4.3.1 Pure CO_2 Results....58
4.3.2 Surfactant Solubility in the Mixture of CO_2 and CH_4....65
4.3.3 Partition Results....70
4.4 Conclusion....71
Chapter 5: Rheological Characterization of Alkyl Amine Surfactants....73
5.1 Introduction....73
5.2 Materials and Procedure....74
5.3 Results and Discussion....75
5.3.1 Effects of Salinity for Duomeen TTM....75
5.3.2 Effects of pH for Duomeen TTM....82
5.3.3 Effects of Temperature for Duomeen TTM....84
5.3.4 Effects of Chemical Structure....88
5.4 Conclusion....92

Chapter 6: Bulk Rheology vs. Rheology in Porous Media 94
6.1 Introduction 94
6.2 Materials and Procedure 95
6.2.1 Materials 95
6.2.2 Preparation 96
6.2.3 Pore Volume Calculations 96
6.2.4 Permeability Measurement 97
6.2.5 Glass Beads Setup 98
6.2.6 Core Setup 100
6.3 Results and Discussion 102
6.3.1 Bulk Rheology Results 102
6.3.2 Glass Beads Results 103
6.3.3 Limestone Core Results 105
6.2.4 Discussion 105
6.4 Conclusion 107

Chapter 7: Surfactant In-Situ Viscosification during Single -Phase Flow in Limestone Cores 108
7.1 Materials and Procedure 108
7.1.1 Materials 108
7.1.2 Preparation and Procedure 109
7.2 Results 112
7.2.1 Salinity Gradient Experimental Series 112
7.3 Conclusion and Discussion 119

Chapter 8: Conclusion and Recommendations 120
8.1 Conclusion 120
8.1.1 Aqueous Stability and Critical pH 120
8.1.2 Solubility and Partition 121
8.1.3 Bulk Rheology 121
8.1.4 Core Flooding 122
8.2 Recommendations 122

8.2.1 Bulk Characterization 122
8.2.2 Foam Flooding 122
Appendices 124
Appendix A: Additional Information for Chapter 4 124
Appendix B: Relaxation Times for Duomeen TTM Viscoelastic Solutions 126
B.1 Dynamic Rheological Response 126
Appendix C: Diagram of In-Situ Viscosification 130
References 131
Vita 143

List of Tables

Table 2.1: Ranges of HLB and Application Use/ Properties 9

Table 2.2: Chemical Structures Analyzed: Properties and HLB Values 11

Table 2.3: Factors that Enhanced Surfactant Solubility in Water 13

Table 2.4: List of Surfactants that Contain Viscoelastic Properties.....24

Table 2.5: Morphology of Micellar Aggregation Based on Packing Parameter.....30

Table 2.6: Geometrical Relations for Different Aggregate Shape.....30

Table 6.1: Intrinsic Properties for Glass Bead Setup. 99

Table 6.2: Intrinsic Properties for Core Flood Setup. 101

Table 7.1: Run 1: 0.5 wt.% Duomeen TTM with 5 wt.% NaCl 113

Table 7.2: Run 2: 0.5 wt.% Duomeen TTM with 10 wt.% NaCl.....115

Table 7.3: Run 3: 0.5 wt.% Duomeen TTM with 15 wt.% NaCl.....117

Table B.1: List of Relaxation Times for Each Solution 129

List of Figures

Figure 2.1: Surfactant Structural Composition....8
Figure 2.2: Ethomeen C12: Hydroxyethyl cocoalkylamine....14
Figure 2.3: Critical pH of Ethomeen C12. 15
Figure 2.4: Ethomeen C12 in 22 wt.% synthetic formation brine (Left) and Ethoduomeen T13 in 22 wt.% synthetic formation brine (Right) 15
Figure 2.5: Degree of protonation for Ethoduomeen T13 in DI water and 22 wt.% TDS Brine 16
Figure 2.6: Span-Wagner CO_2 Diagram at 40 and 60°C.....18
Figure 2.7: CO_2 PVT EOS comparison at 40°C.....18
Figure 2.8: CO_2 PVT EOS comparison at 60°C.....19
Figure 2.9: Comparative viscosity profiles for Ethomeen C12 at different foam qualities from 30 to 90% in 22 wt.% TDS brine and DI water.....33
Figure 2.10: Comparative viscosity profiles for Ethomeen C12 at different foam qualities from 30 to 90% in 22 wt.% TDS brine, one at room temperature and the other at 120°C. 33
Figure 2.11: Visualization of Improved Mobility Control 34
Figure 2.12: Gel Conformance Control Diagram....36
Figure 3.1: Unaltered “natural” pH at 60℃.....42
Figure 3.2: 0.2 wt.% Duomeen TTM with NaCl salinities ranging from 0 to 10 wt.% and pH adjusted to 3 43
Figure 3.3: Critical pH of Duomeen TTM at 0.2 wt.% in a range of salinities from 2 to 10 wt.% NaCl. Three temperatures were analyzed to decouple changes in critical pH.....44

Figure 3.4: Phase behavior of 1 wt.% Duomeen TTM solution in 20 wt.% NaCl brine at high temperatures to test stability from 25 to 120°C. 46
Figure 3.5: Viscoelastic surfactant solutions composed of 1 wt.% Duomeen TTM and 20 wt.% NaCl with changes in pH. 47
Figure 3.6: Steady shear rate of 1 s^{-1} for pH solutions imaged above. 47
Figure 4.1: Pictures of High-Pressure Cell. 51
Figure 4.2: Solubility Experiment Layout. 52
Figure 4.3: Density of mixed gas with different fractions of methane. 54
Figure 4.4: Partition Experiment Layout 55
Figure 4.5: CO_2 PVT Chart to show all experiments were conducted in the supercritical CO_2 region 58
Figure 4.6: Duomeen TTM solubility in CO_2 at 40°C 60
Figure 4.7: Duomeen TTM carbon number tail distribution in CO_2 at a given pressure (40ºC) 60
Figure 4.8: Duomeen TTM solubility in CO_2 at 60°C. 61
Figure 4.9: Duomeen TTM carbon number tail distribution in CO_2 at a given pressure (60ºC) 61
Figure 4.10: Armeen DMCD, Duomeen TTM and Ethoduomeen T13 solubility in CO_2 at 40°C. 63
Figure 4.11: Armeen DMCD carbon number tail distribution in CO_2 at a given pressure (40ºC) 64
Figure 4.12: Ethoduomeen T13 carbon number tail distribution in CO_2 at a given pressure (40ºC) 64
Figure 4.13: Duomeen TTM solubility in different CO_2/CH_4 ratios at 40 and 60°C. .66

Figure 4.14: Duomeen TTM carbon number tail distribution at different mixed gas fractions at 2650 psig and 40ºC. 66
Figure 4.15: Duomeen TTM carbon number tail distribution at different mixed gas fractions at 2650 psig and 60ºC. 67
Figure 4.16: Armeen DMCD, Duomeen TTM and Ethoduomeen T13 solubility in different CO_2/CH_4 ratios at 40°C. 68
Figure 4.17: Armeen DMCD carbon number tail distribution at different mixed gas fractions at 2650 psig and 40ºC. 69
Figure 4.18: Ethoduomeen T13 carbon number tail distribution at different mixed gas fractions at 2650 psig and 40ºC. 69
Figure 4.19: Partition coefficient for Duomeen TTM at different pressures and temperatures. 70
Figure 5.1: Changes in Duomeen TTM concentration (wt.%) at a fixed shear rate (10 s^{-1}) conducted at 40°C. 77
Figure 5.2: Steady-state shear rate at 40^{o}C and pH around 5 to 7. Each plot has a different salinity value ranging from 10 wt.% to 25 wt.% NaCl, the solid lines represent the viscosity profile and dotted lines signify shear stress at various surfactant concentrations from 0.2 wt.% to 2 wt.% Duomeen TTM. 82
Figure 5.3: Steady shear rheology with various amounts of HCl added for pH adjustment conducted at 1 wt.% Duomeen TTM solution, 20 wt.% NaCl, and 40°C. 84
Figure 5.4: Steady-State shear rheology at 1 wt.% Duomeen TTM, 20 wt.% NaCl solution at temperatures ranging from 25°C to 80°C with pH around 5 to 7.....86

Figure 5.5: Fixed shear rate of 1 s^{-1} and 10 s^{-1} for 1 wt.% and 0.5 wt.% Duomeen TTM at 20 wt.% NaCl Solution with pH around 5 to 7.....87
Figure 5.6: Chemical Structures analyzed for viscoelasticity 88
Figure 5.7: Viscoelastic comparison amongst chemical structures: 25 and 20 wt.% NaCl with 1 wt.% surfactant concentration at 40°C.. 89
Figure 6.1: Glass Beads Setup.....99
Figure 6.2: Limestone Core Flood Setup 101
Figure 6.3: Bulk rheology results for 0.5 wt.% Duomeen TTM and 20 wt.% NaCl. Displays pseudo-plasticity and shear thinning trend. 102
Figure 6.4: Glass Beads Setup results 104
Figure 6.5: Rheology comparison for glass beads setup.. 104
Figure 6.6: Limestone Core flood results.....105
Figure 6.7: Relaxation time at 0.5 wt.% Duomeen TTM and 20 wt.% NaCl. 106
Figure 7.1: Schematic of the core flood. 111
Figure 7.2: Viscosity profile of 0.5 wt. % Duomeen TTM solution at different salinities. 112
Figure 7.3: Core flood results for 0.5 wt.% Duomeen TTM and 5 wt.% NaCl brine solution.....114
Figure 7.4: Core flood results for 0.5 wt.% Duomeen TTM and 10 wt.% NaCl brine solution.....116
Figure 7.5: Core flood results for 0.5 wt.% Duomeen TTM and 15 wt.% NaCl brine solution.....118
Figure A.1: Duomeen TTM calibration carbon tail distribution.. 124
Figure A.2: Armeen DMCD calibration carbon tail distribution. 125
Figure A.3: Ethoduomeen T13 calibration carbon tail distribution. 125

Figure B.1: Left: 2 wt.% Duomeen TTM in 20 wt.% NaCl Brine at 20°C. Right: 2 wt.% Duomeen TTM in 15 wt.% NaCl Brine at 20°C.....127
Figure B.2: Left: 1 wt.% Duomeen TTM in 20 wt.% NaCl Brine at 20°C. Right: 1 wt.% Duomeen TTM in 15 wt.% NaCl Brine at 20°C.....127
Figure B.3: Left: 0.5 wt.% Duomeen TTM in 20 wt.% NaCl Brine at 20°C. Right: 0.5 wt.% Duomeen TTM in 15 wt.% NaCl Brine at 20°C.....128
Figure B.4: 0.2 wt.% Duomeen TTM in 20 wt.% NaCl Brine at 20°C.....128
Figure C.1: Diagram of in-situ viscosification for Chapter 7. The phases illustrate the successive steps of gel development.....130

Chapter 1: Introduction

The chapter provides background information about surfactant use in foam assisted gas flooding and about the challenges of gas enhanced oil recovery in reservoirs with harsh saline conditions. Next, research objectives are mentioned followed by a brief description of the remaining chapters in this thesis.

1.1 Use of Surfactants in Subsurface Applications

More than 60% of the world's oil is held in carbonate reservoirs (Schlumberger, 2007). Primary and secondary recovery factors in carbonate reservoirs are lower than 35% due to its complex pore networks and structures, heterogeneities and oil-wet/mixed-wet conditions (Sheng, 2013). Therefore, to recover additional OOIP, tertiary recovery is employed using surfactants, polymers, or a combination of both (SP). These chemicals, injected either in the gas phase or more commonly the liquid phase, improves the sweep efficiency, stability, and mobility of the flood leading to "enhanced" recovery. However, the recovery from polymer flooding specifically in carbonate reservoir is relatively low on average 5% due to poor injectivity, compatibility issues between hard brine and polymer, as well as the size of the chemical (Lake, 1989). Thus, surfactant-foam flooding is a sought out as a favorable alternative to polymer flooding.

The concept of foam as a mobility control agent has been used for several decades to improve gas flooding by alleviating poor macroscopic sweep efficiency, and gravity override. Foaming surfactant and foam process designs have improved significantly over the past decade with progress in developing reservoir-specific surfactants and defining the interrelation between surfactant and rock properties. However, limestone and carbonate

reservoirs pose a problem for most conventional anionic and nonionic surfactants especially at harsh saline and temperature conditions.

Therefore, amine-based surfactants can improve the recovery in carbonate reservoirs, since this type of surfactant has "switchable" capabilities of converting from a nonionic to a cationic surfactant by the adjustment of pH. Some types of amine-based surfactants can stabilize foam, sustain harsh conditions (high salinity and high temperature), and are reasonably CO_2 and water soluble depending on the protonation and terminal structure of the head group.

CO_2 is one common solvent used for gas and foam flooding due to its supercritical properties. Understanding how surfactant solubility changes with alterations in gas composition is important for designing of foam floods to attain optimal efficiency. In addition, some surfactant's viscosity can be enhanced by "triggers", therefore transforming the surfactant solution from a Newtonian to polymer-like material. This viscoelastic fluid can be used as foam enhancer, gas-blocking, diverting or gel treatment agents thereby improving the sweep efficiency of the flood.

1.2 RESEARCH OBJECTIVES

The goal of this research is to contribute findings for a "switchable" amine-based surfactant with high degree of methylation. This thesis comprises a piece of an extensive project to design and optimize the use of amine-based surfactants in carbonate reservoirs. In all, the following is the scope and research objectives for this thesis.

- Determine if an alkyl diamine surfactant is water-soluble at a range of salinities, temperatures, and pH values for use in carbonate reservoirs.

- Analyze how surfactant solubility or uptake in CO_2 changes with the presence of methane in the system. Result will be compared with two other amine surfactants to observe how changing chemical structure impacts solubility in CO_2 or gas mixture.
- Decouple the environmental factors for initiating and intensifying the viscoelasticity of an alkyl diamine surfactant in the aqueous phase.
- Understand if bulk rheology results for viscoelastic surfactant solutions translates to the viscosity observed in porous media.
- Conduct a series of core floods to study in-situ viscosification of the surfactant solution at different injective salinities. A salinity gradient is formed between the injective and resident brines, thus these experiments identify the lowest injective salinity required to form gel in the porous media. The in-situ generation of gel can be used to block high permeable regions or thief zones for conformance control and recovery purposes.

1.3 DESCRIPTION OF CHAPTERS

Chapter 2: Literature review of topics related to surfactant chemistry, characterization, and flow through porous media.

Chapter 3: Aqueous stability will be studied to determine if Duomeen TTM is applicable at viable reservoir and injective conditions. Temperature variations at a fixed surfactant concentration at 0.2 wt.% Duomeen TTM, with a range of salinities up to 10 wt.% NaCl was conducted. High temperature aqueous stability will also be conducted to for a fixed surfactant concentration and salinity of 1 wt.% Duomeen TTM and 20 wt.% NaCl, respectively.

Chapter 4: This study analyzes the changes in solubility of Duomeen TTM in pure carbon dioxide and in carbon dioxide-methane mixtures at different molar fractions. In addition, partition of 0.2 wt.% Duomeen TTM in 1 wt.% NaCl brine and CO_2 was investigated at two temperatures to identify the chemical's affinity with changes in pressure.

Chapter 5: The basis of this study is to identify the versatility of N, N, N' trimethyl-N'-tallow-1,3- diaminopropane, Duomeen TTM, for oil/gas applications, namely conformance control, enhanced oil recovery, and matrix acidizing in high-salinity carbonate reservoirs. Duomeen TTM, a viscoelastic fatty-alkyl diamine surfactant, is examined with the presence of NaCl and no co-solvents to understand how triggers such as salt, pH, temperature, surfactant concentration, and steady state shear rate influences the viscoelastic response and micellar morphology of the surfactant solution. These parameters were decoupled to conduct sensitivity analysis for this surfactant. As with most viscoelastic surfactants (VES), viscosity is highly dependent on the addition and type of salt ultimately reducing electrostatic repulsion amongst molecules and leading to self-assembled rod-like or elongated worm-like micellar structures. Other parameters mentioned fine-tune and optimize the strength of the induced viscoelastic response. Using steady-state rheometry data, it was found that this chemical has the capability of transitioning from a foam-bearing to viscoelastic state at surfactant concentrations above 0.2 wt.% Observations also include compelling temperature and pH-induced viscoelasticity as well as the presence of a stress plateau at high salt and surfactant concentrations perhaps signifying the presence of worm-like micelles for this surfactant.

Chapter 6: Core flood and glass bead experiments were carried out to characterize the rheology of a viscoelastic surfactant solution in porous media with respect to the shear rate. To associate the apparent viscosity with the measured bulk viscosity, a relationship between apparent shear rate inside the core and fluid injection rate was used. Compared to bulk viscosity, resembling shear thinning behavior, the apparent viscosity in porous media displays a shear thickening response and deviates significantly from the bulk viscosity at higher shear rates. Experiments consist of solutions comprised of 0.5 wt.% Duomeen TTM and 20 wt.% NaCl. At this state, the surfactant's viscoelastic properties resemble that of flexible polymer. Discussion will generalize the potential reasons for this rheological shift in viscoelastic surfactant solutions.

Chapter 7: Core flood experiments were performed to test the viscoelastic response of Duomeen TTM when exposed to high saline resident brine (25 wt.% NaCl). Injective conditions consist of 0.5 wt.% Duomeen TTM in either 5, 10 or 15 wt.% NaCl brine at low viscosities. When the injected solution interacts with the resident brine, it is hypothesized that the solution will thicken in-situ predicted by the rise in pressure drop.

Chapter 8: Conclusions and recommendations for future experimental work.

Chapter 2: Literature Review[1]

This chapter embodies the literature and background review of the thesis. Topics will span from the fundamental concepts of surfactants, specifically amine-based and viscoelastic-based surfactants, rheology, solubility, flow in porous media and petroleum applications.

2.1 FUNDAMENTAL CONCEPTS OF SURFACTANTS

This section provides a brief summary about surfactants. It will go over fundamental aspects, thermodynamic relationships, classes of surfactants, and HLB concept.

2.1.1 Fundamentals

Surfactants, also known as surface-active agents, are amphiphilic chemicals composed of a hydrophobic tail and a hydrophilic head group that alter surface and interfacial properties amongst immiscible mediums (Schramm, 2010). These molecules reside at the interface and orient based on its affinity to the respective mediums. At dilute surfactant concentrations, the molecules form a monolayer at the interface portraying a solution with normal electrolytes, but at higher concentrations, the solution behaves differently due to the formation of organized, self-assembled molecular structures called micelles. Normally, micelles are arranged where the hydrophobic/lipophilic group cluster in the interior of the micelles, while the hydrophilic parts contact and interact with the aqueous medium through dipole-dipole or ion-dipole interactions (Schramm and Wassmuth, 1994). The onset of micellar formation is referred to as critical micelle

[1] Parts of Section 2.4 and Section 2.5.1 are adopted from the March 2016 SPE manuscript "Salt-Induced Viscoelastic Response of Alkyl Amine Surfactant", Manuscript ID: SJ-0316-0062, Status: Pending. Journal article written by Madalyn M. Liebum and co-authored by Dr. Quoc P. Nguyen. Dr. Nguyen's contribution included peer reviewing article before submission and providing resources to conduct this research.

concentration (CMC). This property is dependent on factors namely temperature, thermal forces, electrostatic forces, electrolytes in solution, and molecular mass of the tail (Schramm and Wassmuth, 1994).

2.1.2 Thermodynamic Relationship for CMC and Hydrophobic Effect

The equation below expresses the thermodynamic association of the onset of CMC given the chemical potential of the system.

$$\Delta G^{\circ}_{micelle} = \mu^{\circ}_{micelle} - \mu^{\circ}_{solvent} = RTln(CMC) \quad (2.1)$$

The behavior of the lipophilic tail in water is dominated by enthalpy and entropy of the reaction rather than intermolecular forces, such as Van der Waals (Than, 2016). This is due to the breaking of hydrogen bonds to make room for the hydrophobic tails in the system (Than, 2016). Entropy, the largest contributor, of the system decreases as the hydrogen bonds restructure around the hydrophobic region consequently making the hydrophobic section more structured (Than, 2016). Furthermore, enthalpy is based on the new hydrogen bonding structure to its original structure (Than, 2016). The interactions amongst hydrophobes, i.e. surfactant tails, is based on Gibbs Energy, where a positive value promotes hydrophobic interaction in the system (Than, 2016).

The strength of the hydrophobic interaction is based on temperature, carbons atoms and shape of the hydrophobic parts of the surfactant molecule (Than, 2016). A branched tail group can result in lower hydrophobic interaction due to the production of steric hindrance, and the increase in carbon atoms or temperature boost hydrophobic interaction in the system (Than, 2016). More information can be found in Chapter 1 of "Surfactants: Fundamentals and Applications in the Petroleum Industry" (Schramm, 2010).

2.1.3 Classes of Surfactants

There are four classes of surfactants based on their hydrophilic moiety of the head group (Schramm, 2010; AkzoNobel, 2010):

- *Nonionic:* Head group has no net charge. Molecules are insensitive to changes in salinity. Surfactant Class Examples: alcohols, hydroxyethyl acids, alkanolamides, hydroxyethyl amines, and amine oxides.
- *Cationic:* Head group has a positive charge when surfactant molecule dissociates. Molecules are sensitive to salinity and zeta potential of the reservoir matrix (negative-charged: sandstone and clay). Surfactant Class Examples: quaternary ammonium salts
- *Anionic*: Head group is negative when the molecule dissociates. Molecules are sensitive to salinity and zeta potential of the reservoir matrix (positive-charged: limestone). Surfactant Class Examples: alkyl sulfates or sulfonates, lignin sulfonates, phosphate esters, sulfosuccinate esters, and carboxylates
- *Amphoteric/Zwitterionic:* Head group contains both negative and positive charge. The ionic character depends on pH of the solution. Molecules are sensitive to salinity and zeta potential of the reservoir matrix. Surfactant Class Examples: carboxylbetaines and sulfobetaines

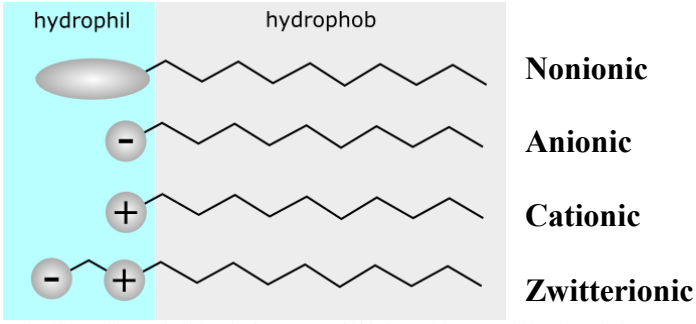

https://upload.wikimedia.org/wikipedia/commons/d/d1/TensideHyrophilHydrophob.png

Figure 2.1: Surfactant Structural Composition

2.1.4 HLB Concept

HLB, meaning hydrophilic-lipophilic balance, represents the surfactant's solubilization and emulsion behavior based on the interactions amongst the head and tail groups as well as the media of interest. The Davies' equation, which is used for ionic surfactants, takes in account the effect of stronger and weaker head groups by using the equation below, where hydrophilic numbers are positive and lipophilic or hydrophobic numbers are negative in value (Davies 1957). Table 2.1 predicts the surfactant properties of a molecule based on the HLB value. High HLB values signify polarity and water solubility, while low HLB values have good nonpolar solubility (AkzoNobel, 2010).

$$\text{HLB} = 7 + \sum(\text{hydrophilic group numbers}) + \sum(\text{lipophilic group numbers}) \qquad (2.2)$$

Table 2.1: Ranges of HLB and Application Use/ Properties (Davies, 1957)

Range of HLB Values	Application and Properties
0 to 6	Hydrophobic (Oil Soluble)
1.5 to 3	Anti-Foaming Agent
3.5 to 6	W/O Emulsifier
6 to 10	Water Dispersible
7 to 9	Wetting and Spreading Agent
8 to 18	O/W Emulsifier
10 to above	Hydrophilic (Water Soluble)
13 to 15	Detergent
15 to 18	Solubilization or Hydrotrope

https://en.wikipedia.org/wiki/Hydrophilic-lipophilic_balance

The inverse of the HLB provides information about how micelles aggregate with respect to the hydrophobic and hydrophilic state of the system. If 1/HCB < 1, it insinuates the head groups will be submerged in the water phase and the tails orient inwards and entangle with other tail groups forming C/W emulsions. If 1/HCB>1, then the molecules will aggregate as reverse micelles and partition more toward the CO_2 phase (Adkins et al., 2010).

$$\frac{1}{\mathrm{HCB}} = \frac{A_{TC} - A_{TT} - A_{CC}}{A_{HW} - A_{HH} - A_{WW}} \tag{2.3}$$

where, the interaction A_{ij} between surfactant tail (T), CO_2 (C), surfactant head group (H) and water (W). This equation will be useful for assessing and analyzing reactive flow mechanisms, e.g. solubility and partition, of the system.

Table 2.2 provides the HLB value for the chemicals analyzed in this thesis. Duomeen TTM will be the primary chemical investigated, while the remaining three are used for comparative analysis of how chemical structures influence the results. Refer to AkzoNobel for more information about each chemical.

Table 2.2: Chemical Structures Analyzed: Properties and HLB Values (AkzoNobel, 2010)

Chemical	Chemical Structure	Amine Derivative	Fatty Chain	HLB
Duomeen TTM	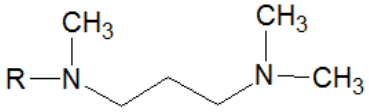	N, N, N'-trimethyl-N'-tallow-1,3-diaminopropane	Tallow	**14.2**
Ethoduomeen T/13	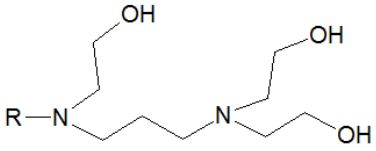	Ethoxylated (3) N-tallow-1,3-diaminopropane	Tallow	**19**
Armeen DMCD	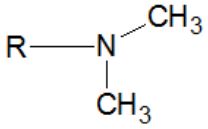	Cocoalkyl-dimethylamines	Coco	**9.4**
Ethomeen C12	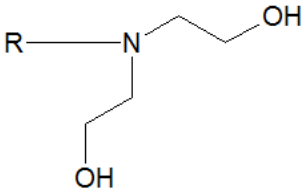	Ethoxylated cocoalkylamines	Coco	**12.2**

The use of fatty acids, such as tallow and coco causes significant variations in tail length and composition of the alkyl chain (Mohamed et al., 2011). This variation alters the surfactant's surface-active properties leading to uncertainty and errors in the interpretation of the results and in performance (Mohamed et al., 2011).

2.2 AMINE-BASED "SWITCHABLE" SURFACTANTS

This section discusses the aspects and capabilities of amine surfactants, namely general information, water solubility, aqueous stability, and degree of protonation. The "switchable" factor transforming the compound from a nonionic to ionic state makes this type of surfactant attractive in subsurface applications.

2.2.1 Definition

Amine surfactants exhibit nonionic and cationic properties depending on pH of the solution. These surfactants are water insoluble at neutral to high pH, and can be protonated in the presence of hydrogen ions, H^+, resulting in the formation of amine salts and a positively charged hydrophilic head (cationic). Ionic surfactants have great solubility at high temperature, pressures, and salinity as well as withstand low adsorption in carbonate reservoirs. The following are examples of general protonation reactions for mono- and diamines analyzed in this thesis. Typically, one protonated amine group is sufficiently hydrophilic to solubilize tail groups containing up to 12 carbons, however for the larger alkyl chain lengths, two protonated amino groups are required at low pH (AkzoNobel, 2010).

Duomeen TTM

$$\mathrm{RN(CH_3)(CH_2CH_2CH_2)N(CH_3CH_3)} + 2\mathrm{H^+} \rightarrow \mathrm{RN^+(CH_3)(CH_2CH_2CH_2)N^+(CH_3CH_3)} \quad (2.4)$$

Ethoduomeen T13

$$\mathrm{R(N(CH_2CH_2OH)(CH_2CH_2CH_2)(N(CH_2CH_2OH)_2)} + 2\mathrm{H^+} \rightarrow \mathrm{R(N^+(CH_2CH_2OH)(CH_2CH_2CH_2)(N^+(CH_2CH_2OH)_2)} \quad (2.5)$$

Armeen DMCD

$$\mathrm{RN(CH_3CH_3)} + \mathrm{H^+} \rightarrow \mathrm{RN^+(CH_3CH_3)} \quad (2.6)$$

Ethomeen C12

$$\mathrm{RN(CH_2CH_2OH)_2} + \mathrm{H^+} \rightarrow \mathrm{RN^+(CH_2CH_2OH)_2} \quad (2.7)$$

2.2.2 Water Solubility of Amine-Based Surfactants

Improving water solubility of amine surfactants are governed by the following factors listed in Table 2.3:

Table 2.3: Factors that Enhanced Surfactant Solubility in Water (AkzoNobel, 2010)

Factors	Reasons
Influence of Alkyl Chain	• Decreases in chain length or molecular mass • Increase in unsaturation or branching
Influence of Nitrogen Moiety	• Increase in number of functional groups • Increase in degree of ethoxylation • Formation of salts • Quaterernization
Influence of Medium	• Decreasing pH

The hydrophilic character of the amine surfactant is determined by the polarity of the head group as well as pH, temperature or the degree of ethoxylation (AkzoNobel, 2010). An increase in ethoxylation makes the surfactant more water soluble, while an increase in tail length will make it more lipophilic (AkzoNobel, 2010).

2.2.3 Aqueous Stability and Phase Behavior

Aqueous stability tests identify limitations and screen chemicals for a particular application. If the solution appears cloudy, precipitated, or separated under a set of defined conditions, surfactant consumption and retention in the porous media will prevail leading to poor sweep efficiency, recovery, and formation damage due to permeability reduction.

Typical experiments consist of a salinity, surfactant concentration, pH and temperature scan to define the tolerance and setbacks for the surfactant.

For the temperature scan, as temperature increases, the solubility of many salts also increase, however surfactants characteristically degrade at elevated temperatures. Therefore, surfactant solutions should be tested at a variety of temperatures to understand its thermal-based solubility, which is important when applying this solution at different reservoir conditions.

Cui (2014) and Elhag et al. (2014) studied a similar chemical to Duomeen TTM called Ethomeen C12 comprising of single nitrogen and hydroxyethylated head branches, illustrated in Figure 2.2.

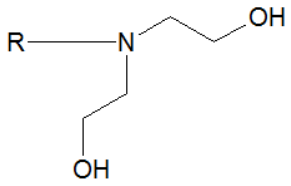

Figure 2.2: Ethomeen C12: Hydroxyethyl cocoalkylamine

From Cui's research, phase behavior of this chemical was conducted at 1 wt.% surfactant solution with temperatures spanning from 20°C to 130°C. Phase behavior was analyzed with the surfactant immersed in DI water as well as synthetic formation brine (22 wt.% TDS), shown in Figure 2.3. In particular, Ethomeen C12 can tolerate high temperatures and low pH due to its short terminal EO groups by reducing the electrolyte effect and promoting steric blocking.

In addition, Elhag et al. (2014) and Chen et al. (2015) performed aqueous stability tests for Ethomeen C12 in 22 wt.% TDS brine with temperatures spanning up to 90°C. Along with Ethomeen C12, Elhag et al. (2014) investigated the phase behavior of

Ethoduomeen T13, a diamine surfactant with hydroxyethyl groups, at 1 wt.% surfactant and 22 wt.% TDS brine. The results are shown in Figure 2.4.

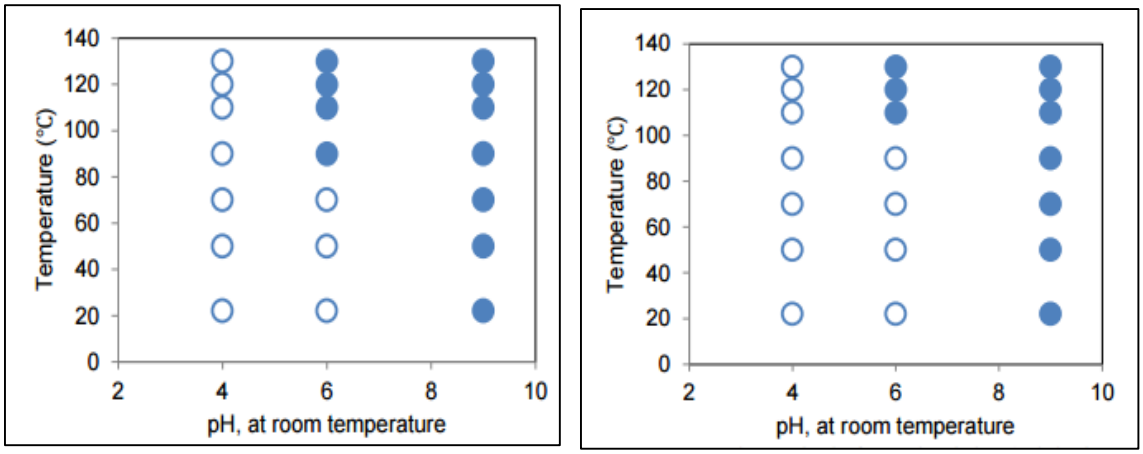

Figure 2.3: Critical pH of Ethomeen C12 at 1 wt.% concentration in (Left) DI or (Right) 22 wt.% synthetic brine (Cui, 2014).

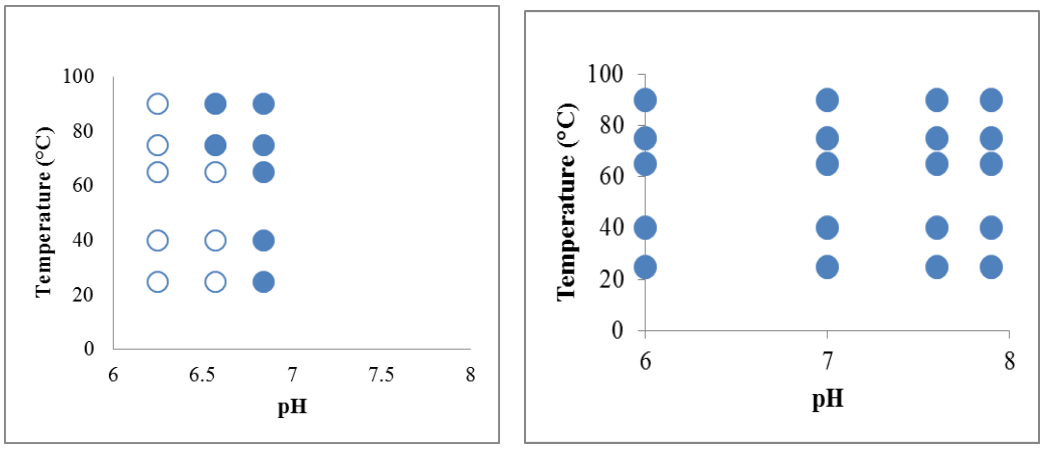

Figure 2.4: 1 wt.% Ethomeen C12 in 22 wt.% synthetic formation brine (Left) and 1 wt.% Ethoduomeen T13 in 22 wt.% synthetic formation brine (Right) (Chen et al., 2015; Elhag et al., 2014)

2.2.4 Degree of Protonation

This term defines the ratio of protonated to unprotonated molecules present in the solution. Degree of protonation, α, ranges from 0 (unprotonated) to 1 (protonated). The protonation process is dependent on factors, namely the nitrogen moiety, salinity, functional groups and temperature of the solution.

Full protonation occurs faster for chemicals containing a single nitrogen ion in the head group than a diamine, this is due to the simple requirement that monoamines necessitate 1 H^+ ion to protonate and 2 H^+ ions for a diamine surfactant. So, adding HCl to the solution dissociates and provides the H^+ ions required for protonation.

The addition of salt increases the protonation rate. Elhag et al. (2014) reported this observation with Ethoduomeen T13 using DI and 22 wt.% brine, in Figure 2.5, which contain hydroxyethyl groups. DI water exponentially increases compared to the saline solution that sharply rises then stabilizes when approaching full protonation. This can be due to the critical pH rising from the addition of salt.

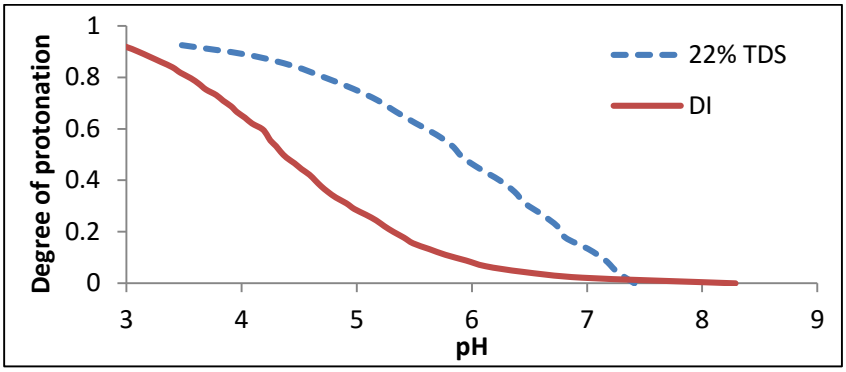

Figure 2.5: Degree of protonation for Ethoduomeen T13 in DI water and 22 wt.% TDS Brine. The addition of salt increases the rate of protonation. (Elhag, 2014)

Additionally, functional groups consisting of methyl groups readily protonate and enhances surfactants' water solubility because methyl groups have better electron donating properties, smaller group size, and larger steric hindrance than hydroxyethyl groups.

2.3 SOLUBILITY IN SUPERCRITICAL AND GASEOUS PHASE

This section will discuss CO_2 properties, EOS, CO_2-philic surfactant properties, methane effects on solubility, and attributes for enhanced oil recovery application.

Carbon Dioxide Properties

Carbon dioxide is a low cost, recyclable, chemically inert, non-toxic, readily-accessible weak solvent (Tc= 31.1°C, Pc= 1070.4 psi) (Eckert et al., 1996; Adkins et al. 2010b). Due to its low viscosity, density and surface tension, CO_2 is able to wet structured materials, heat and mass transfer more effectively than most liquids (Girard et al., 2016). Even though CO_2 is considered a weak solvent due to its low cohesive density, this chemical is classified as a weak Lewis acid and reacts with strong Lewis bases, such as amines (Hoefling et al., 1993; Girard et al., 2016). This property is advantageous for CO_2 dissolving amine-based surfactants in applications related to carbon capture, enhanced oil recovery and other subsurface application (Girard et al., 2016).

Altering the pressure and temperature of the system fine-tunes the CO_2 density, which influences the surfactant tail solvation in CO_2 (Eastoe et al., 2003). For the most part, due to weak intermolecular forces and poor solubilizing power, supercritical CO_2 remains an unsuitable solvent for polar and high molecular weight solutes (Consani and Smith, 1990).

CO_2 Equation of State

Different equation of states (EOS) characterize the pressure and temperature dependence of the CO_2 density. The most common EOS is Span and Wagner, Figure 2.6, that specifically describes CO_2 thermodynamics. Moreover, Figure 2.7 and 2.8 compare various EOS including Span and Wagner, Peng Robinson and SRK methods at different temperatures. Span and Wagner EOS will be used in Chapter 4.

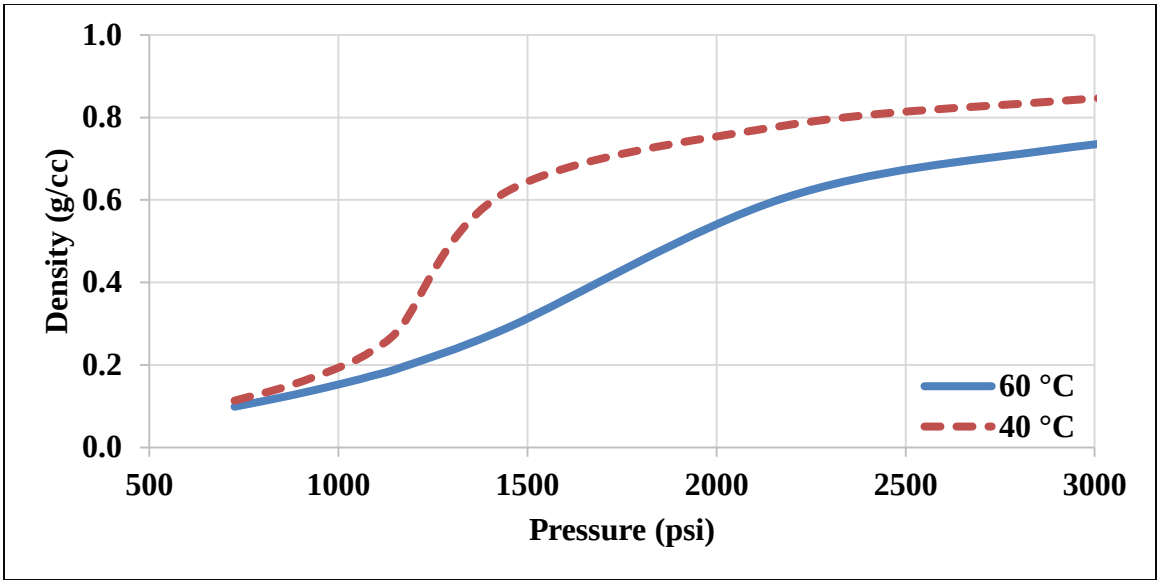

Figure 2.6: Span-Wagner CO_2 Diagram at 40 and 60°C. At lower temperatures the density gradient is steeper and more gradual at higher temperatures.

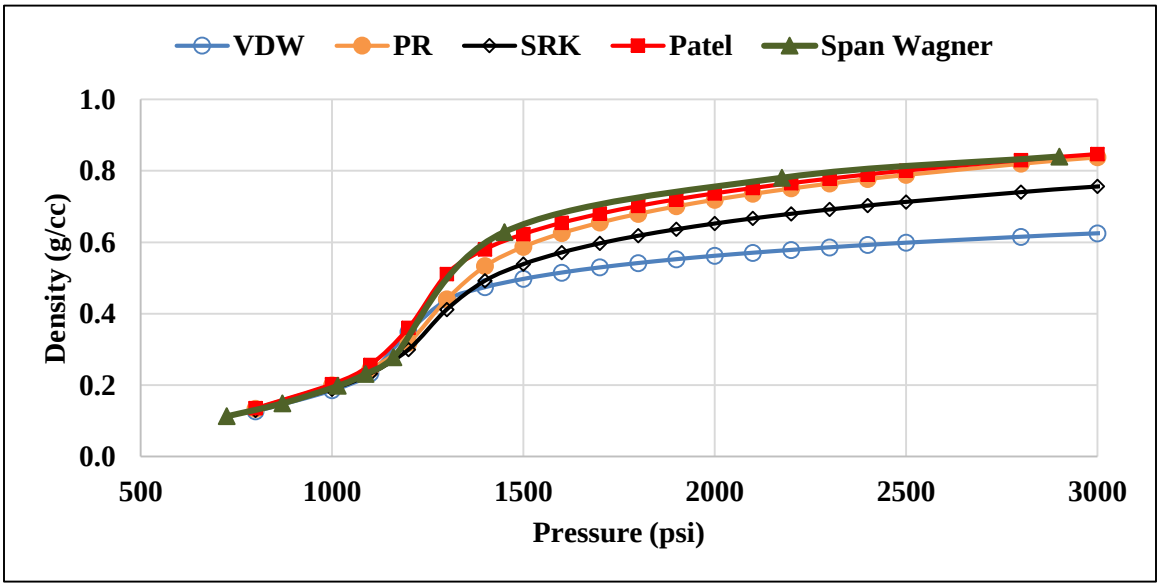

Figure 2.7: CO_2 PVT EOS comparison at 40°C.

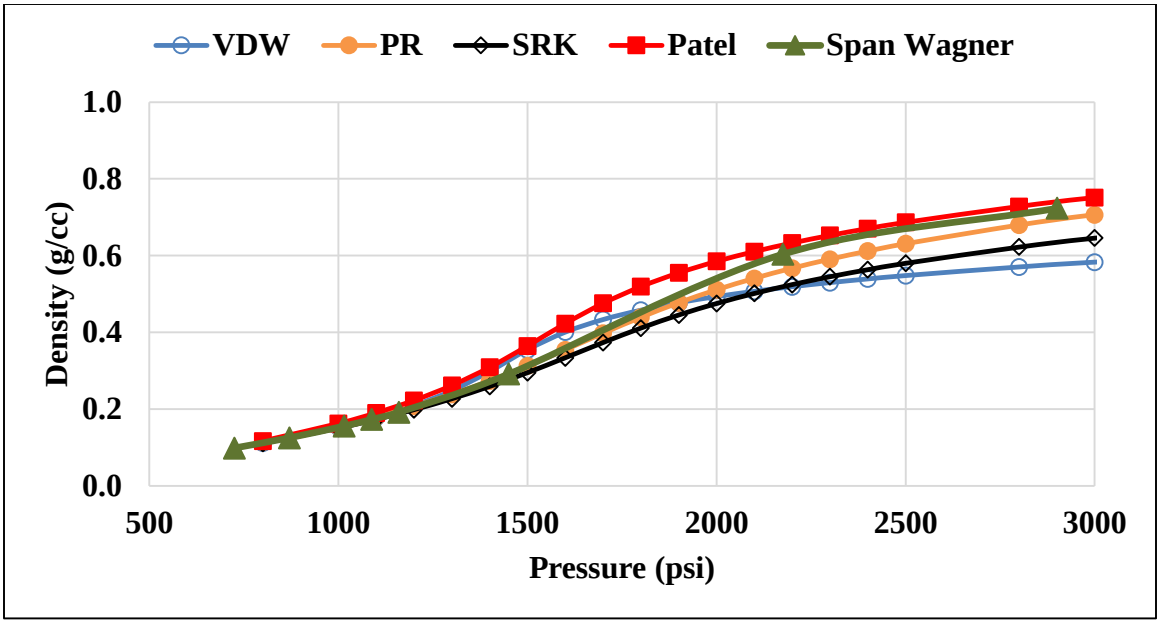

Figure 2.8: CO_2 PVT EOS comparison at 60°C.

Surfactant Solubility in CO_2

The pioneer classes of surfactants that exhibit reasonable solubility in CO_2 comprise of fluorocarbons, phosphates, sulfonates and silicones due to its low cohesive density and polarizability (Eastoe et al., 2003). These types of surfactants, in particular fluorinated and silicone-based hydrophobes, can lower intermolecular interactions of the surfactants thereby increasing the surfactant solubility in CO_2 (Ren et al., 2014). However, these types of compounds are expensive, require special synthesis and non-environmentally friendly (Eastoe et al., 2003). To mitigate these issues, recent advances in developing non-fluorinated and hydrocarbon-based surfactants provide a low-cost and effective option for solubilizing surfactant in CO_2 (Eastoe et al., 2003). The goal of designing non-fluorinated CO_2-philic surfactants is to lessen the intermolecular interactions amongst molecules and maximize the interaction with CO_2 (Sanders et al.,

2010; Adkins et al., 2010; Wang et al., 2009). Some CO_2-philic features include: low molecular weight hydrophobes, tail branching, methylation of chain tips, oxygenation of the tail with C=O groups, Lewis basic side chains, and non-ionic (Eastoe et al., 2001; Fan et al., 2005; Sanders et al., 2010; Adkins et al., 2010, 2010b).

Tail Structure:

Much research has been conducted to make hydrocarbon-based tails very CO_2-philic in order to replace non-environmental and expensive compounds containing fluorides and phosphates. According to Eastoe et al. (2001) and other researchers, specially tailored CO_2-philic hydrocarbon tails can exhibit high levels of CO_2 solubility compared to fluorinated surfactants. This includes tails consisting of oligo lactic acid, sugar acetates, oligo butylene glycol, oligo vinyl acetate, PPO, and highly methylated alkyl groups (Xing et al., 2010, Fan et al., 2005). It is also reported that branched tails are more soluble than its linear counterparts (Ryoo et al., 2003). Branching and methylation reduces the tail-tail interaction of molecules therefore promoting a rise in CO_2 solubility and improving aqueous stability (Ghaicha et al., 1992; Adkins et al., 2010). In addition, Stone et al. (2003) and Adkins et al. (2010b) stated that stubby and/or branched hydrocarbon surfactants are promising, since molecules are able to cover more surface area per unit surfactant and block the interfacial contact between CO_2 and water more effectively.

Head Group Structure:

In regards to changes in head group composition, Sagisaka et al. (2003), reported that subtle alterations of terminal functional groups dramatically alters the surfactant behavior due to changes in intermolecular interaction and packing efficiency of the molecules. Oxygenated functional groups, such as ethoxylated, propylene oxide (PO), ethylene oxide (EO) and carbonyl, are CO_2-philic due to Lewis acid-base interactions between CO_2 and oxygen (Kilic et al., 2009). Surfactants with shorter EO or PO chain

lengths increase the solubility in CO_2 due to the reduction of intermolecular interactions amongst surfactant molecules (Ren et al., 2014) In addition, Eastoe et al. (2003) reports that highly methylated chains lower surface energy and interact with CO_2 by electron donation therefore promoting solubilization.

Nonionic vs. Ionic Surfactants

In literature, it has been stated that nonionic surfactants, such as 2-ethyl-1-heaxanol-(propylene oxide)$_n$ -(ethylene oxide)$_m$, exhibit higher solubility in supercritical CO_2 than ionic surfactants (Ren et al., 2014). Solubilizing ionic surfactants in CO_2 require pressures higher than the MMP and are practically insoluble due to its CO_2-phobic head group and high molecular weight (Consani and Smith, 1990; Le et al., 2008; Xing et al., 2010).

Amine-Based Surfactants

Particularly, "switchable" amine-based surfactants can achieve high solubility in CO_2 in its nonionic or unprotonated state but digress with the addition of water and acid. This behavior is notable for mass transfer of surfactant from the CO_2 to aqueous phase in the reservoir, due to the protonation aspect of the amine-based surfactant. According to Lapaumier et al. (2009), diamines, such as Duomeen TTM, are CO_2-philic due to its second amine function having close properties to alcohols (soluble in both CO_2 and water), therefore increasing the CO_2 adsorption capacity (Eastoe et al., 2003). In addition, unlike single nitrogen moieties, diamines can tolerate degradation from thermal, CO_2 and oxidative factors leading to an increase in chemical stability when exposed to high pressures and temperatures (Lapaumier et al., 2010).

CO_2 Solubility Alterations with Methane Dilution

The presence of methane in the system will deter the solvation of the surfactant tails in the CO_2 phase (Zheng et al., 2015). This will make the surfactant less CO_2-philic because methane has a lower solvent strength than CO_2 (Zheng et al., 2015). In comparison, CO_2 has charge separations amongst the oxygen terminals and central carbon inducing dipole-quadrupole interactions, also considered a "non-dipolar solvent" (McHugh et al., 1998; Girard et al., 2016). This allows CO_2 to solvate polar substances, which methane or other hydrocarbons are not capable of (Girard et al., 2016). In comparison, methane has no polar moment, low dispersive forces, no Lewis acid properties and does not carry any lone pair of electrons. In all, the solubility in hydrocarbons is dependent of the alkyl chain length, degree of unsaturation and on the cationic character of the head group's nitrogen moiety (AkzoNobel. 2010).

2.4 VISCOELASTIC SURFACTANTS

Surface-active agents, more widely known as surfactants, are amphiphilic compounds composed of a hydrophobic tail and hydrophilic head group that reside at the interface between the polar and nonpolar media (Schramm, 2010). Surfactant molecules at the interface begin to self-assemble into organized micelles above a certain concentration called the critical micelle concentration (CMC). Held by physical attraction, the interior of the micelle typically embodies the hydrophobic components of the surfactant while the head group is exposed to the aqueous medium (Schramm, 2010; Gaudino et al., 2015; van Zanten, 2011).

Microstructural aggregation and morphology of the micelles impart changes in macroscopic behavior and flow properties of the surfactant solution under certain conditions (Trickett and Eastoe, 2008). In general, the packing parameter classifies the

structure of the micelles under four divisions; spherical, cylindrical/worm-like, vesicles, or lamellar micelles (Lequeux, 1995). Solutions with spherical or short-rod micelles tend to have Newtonian behavior at low viscosities. Depending on internal and external parameters, the morphology can transition from one state to another. When the micelles organize into cylindrical aggregates or entangled worm-like structures, the solution transforms into a viscoelastic state described by its a gel-like consistency and suspended, trapped air bubbles when shaken (Hull et al., 2015; Koehler, 2000).

Viscoelastic surfactants (VES) are characterized as having viscous and elastic properties that deform under applied shear, stress and/or strain. However unlike polymer, the removal of force allows VES solutions to quickly recover and reform back to its natural state at a specified relaxation time giving it the name “living polymer” (Cates and Candau, 1990). In addition, depending on the type of surfactant, adjustments in salinity, temperature, surfactant concentration, and pH can fine-tune the viscoelastic response and macroscopic fluid behavior of the solution (Nasr-El-Din, 2009). These reasons considerably make viscoelastic surfactants attractive and practical for petroleum application in the realm of conformance control (gel and foam treatment), matrix acidizing (acid delivery) and chemical enhanced oil recovery (diverting fluid and gas-flood mobility control). In literature, many types of surfactants, especially ionic-type, exhibit a viscoelastic response. Notable ones are listed below in Table 2.4.

Table 2.4: List of Surfactants that Contain Viscoelastic Properties

Surfactant	References
cetylpyridinium bromide (CPyBr)	Kuperkar et al., 2011
cetylpyridinium chloride (CPyCl)	Tung et al., 2007
cetyltrimethylammonium bromide (CTAB)	Barentin, 2001 Kuperkar et al., 2011 Rehage and Hoffmann, 1991
cetyltrimethylammonium chloride (CTAC)	Kuperkar et al., 2011
cetyltrimethylammonium p-toluenesulfonate (CTAT)	Rojas et al., 2008 Truong, 2002
erucyl bis(hydroxyethyl) methylammonium bromide (EHAB)	Raghavan and Kaler, 2001
erucyl bis(hydroxyethyl) methylammonium chloride (EHAC)	Kalur et al., 2005
erucyl trimethylammonium chloride (ETAC)	Raghavan and Kaler, 2001
p-dodecyloxy benzyl dimethyl amine oxide	Brinchi et al., 2010
trimethylammonium bromide	Brinchi et al., 2010
amine and dimethylamine-oxide based	Aryanpanah and Nasr-El-Din, 2014 Brinchi et al., 2010 Li et al., 2010 Maeda et al., 2001

Theory

A viscoelastic surfactant exhibits viscous and elastic properties under deformation from shearing forces. According to Hooke's Law, when elastic materials are deformed, the material tends to return to its original configuration (Sheng, 2011).

$$\tau = G'\gamma \tag{2.8}$$

where, G' is defined as the elastic modulus, τ is stress and γ is the strain or displacement of the object from its original state. Correspondingly, a purely viscous fluid abides by the following Newton's equation, in which $\dot{\gamma}$ is shear rate and μ is viscosity of the fluid (Sheng, 2011):

$$\tau = \mu\dot{\gamma} \tag{2.9}$$

For viscoelastic solutions, both laws are incorporated leading to the Maxwell constitutive model that relates stress and strain of the fluid (Sheng, 2011). The fluid behaves Newtonian as the derivative, $\left(\frac{\delta\tau}{\delta t}\right)$ approaches 0 insinuating stress does not change with time.

$$\frac{\tau}{\mu} + \frac{1}{G'}\left(\frac{\delta\tau}{\delta t}\right) = \dot{\gamma} \tag{2.10}$$

Two stress responses are produced for viscoelastic solutions, G' the elastic or storage modulus and G" the loss or viscous modulus. Typically, G" is the governing response at low shear rates or frequencies (ω), then crossovers where the elastic modulus becomes prominent at high shear environments (Sheng, 2011). This crossover marks a shift in fluid behavior and provides an estimated relaxation time (λ) of the solution. The relaxation time is the inverse frequency at which G' and G" crossover and defines the time it takes for the solution to adjust to changes in flow conditions (Sheng, 2011).

$$\text{Elastic Modulus: } G'(\omega) = \sum_k G_k \left(\frac{\omega^2\lambda_k^2}{1+\omega^2\lambda_k^2}\right) \tag{2.11}$$

$$\text{Viscous Modulus: } G''(\omega) = \sum_k G_k \left(\frac{\omega\lambda_k}{1+\omega^2\lambda_k^2}\right) \tag{2.12}$$

Theoretically, when the capillary tubes are at a constant diameter, the solution behaves as a viscous fluid, but when the diameters of these tubes change erratically, then the viscoelastic micellar chains are pulled, snapped and contracted representing elastic fluid behavior (Sheng, 2011). The latter behavior resembles flow through porous media.

For the most part, viscoelastic materials undergo shear thinning in a rheometer, but some may experience a shear thickening response in porous media due to the elongation of the micellar chains when being stretched at the pore level. Elastic instabilities occur at low to medium flow rates due to large normal stresses and tension along streamlines (Miller, 2007).

In addition, from the equations below, when viscosity in porous media departs from bulk viscosity, the difference between the apparent and bulk viscosities is considered the elongation-induced viscosity term. This also applies for pressure gradient, where an increase in pressure gradient indicating flow thickening and coincides with the onset of elastic instabilities in porous media (Howe et al., 2015). For more information on expanding these expressions, refer to Hirasaki and Pope (1974), Delshad et al. (2008), and Sheng (2011).

$$\mu_{app} = \mu_{shear} + \mu_{elongation} \tag{2.13}$$

$$\Delta P_{apparent} = \Delta P_{shear} + \Delta P_{elongation} \tag{2.14}$$

Flow Instability Parameters for Non-Newtonian, Viscoelastic Flow

Reynolds Number

This dimensionless number represents the degree of flow turbulence in the system. Low Reynolds numbers below critical flow is considered laminar and friction factors are

predetermined. The incorporation of porosity and intrinsic velocity of fluids in the pores leads to the Reynolds number stated below (Ergun, 1952; Zeng and Grigg, 2005). From literature, the critical value for non-Darcy flow is between 3-10 depending on application (Zeng and Grigg, 2005). In the equation below, D_p represents particle diameter, u is intrinsic velocity, μ is the viscosity of the fluid, ρ is the density of the fluid and ϕ is porosity.

$$\mathrm{Re} = \frac{\rho D_p u}{\mu}\left(\frac{1}{1-\phi}\right) \tag{2.15}$$

Deborah Number

This dimensionless value differentiates the flow of solids and liquids by comparing the relaxation time to the observation time of the surfactant solution. At high Deborah numbers (De), the material behaves solid-like and more elastic, and at low numbers the material has more fluidity (Miller, 2007). Deborah number can be expressed below where it states the ratio of elastic and viscous forces in viscoelastic flows (Miller, 2007). In this equation, λ is the relaxation time of the material and shear rate, $\dot{\gamma}$.

$$\mathrm{De} = \lambda\dot{\gamma} \tag{2.16}$$

Weissenberg Number

This term is similar to Deborah number since it also relates time of observation of the surfactant solution. Weissenberg number (Wi) defines the elastic forces dominating flow behavior for viscoelastic solutions (Miller, 2007). The equation below incorporates relaxation time, average velocity, U, and characteristic length, L.

$$\mathrm{Wi} = \lambda\left(\frac{\mathrm{U}}{\mathrm{L}}\right) \tag{2.17}$$

To predict the onset of elastic flow instabilities, McKinley et al. (1996) defined a dimensionless number, M, where a value greater than $\sqrt{21.17}$ resembles an unstable viscoelastic surfactant solution (Howe et al., 2015).

$$\mathrm{M} = \sqrt{\mathrm{Wi} * \mathrm{De}} \tag{2.18}$$

2.5 RHEOLOGY

Strengthening the surfactant's liquid viscosity can add resistance to the thinning of thick films and rupturing of foam (Schramm and Wassmuth, 1994). Increasing the viscosity can also impede the draining rate and promote foam stability in the system (Schramm and Wassmuth, 1994). Therefore, rheology plays a significant role in the stability and flow of the solution through porous media.

2.5.1 Surfactant Morphology Models

Rheological behavior links both the microstructure and morphology elements of a solution (Rounds, 1994). In this study, a classical qualitative model called Israelachvili's packing parameter, "P", was used to characterizes the micellar morphology (size and shape) of the solution. This model was derived from the Tanford's Model where changes in thermodynamics and free energy conditions of the system evoke micellar transformations (Raghavan, 2009; Hull et al., 2015; Collura et al., 2001). As the chemical potential of the state becomes negative, the micelles will self-assemble into micelles. Three main chemical potential mechanisms describe the basic features of 'micellization' exist in the Tanford's model, eqn. 2.19-20 (Hull et al., 2015; Nagarajan, 2014):

- *Transfer* signifies the repulsive behavior of the hydrophobic tail and water as the tails transfer from the aqueous to the lipophilic environment, this is responsible for the aggregation of micellization,
- *Interface* is the residual contact between the tail and water thus promoting the growth of aggregates,
- *Head* is the repulsion between surfactant head groups hence limiting the aggregation size of the micelles, and
- *Packing* was a later edition to the model. It is a shape dependent factor based on the influence of the hydrocarbon tail length to the head group area (Nagarajan, 2014).

$$\left(\frac{\Delta\mu^{\circ}_{g}}{kT}\right) = \left(\frac{\Delta\mu^{\circ}_{g}}{kT}\right)_{\text{Transfer}} + \left(\frac{\Delta\mu^{\circ}_{g}}{kT}\right)_{\text{Interface}} + \left(\frac{\Delta\mu^{\circ}_{g}}{kT}\right)_{\text{Head}} + \left(\frac{\Delta\mu^{\circ}_{g}}{kT}\right)_{\text{Packing}} \tag{2.19}$$

$$\ln(CMC) = \left(\frac{\Delta\mu^{\circ}_{g}}{kT}\right)_{\text{Tran.}} + \left[\left(\frac{\sigma}{kT}\right)a\right]_{Inter.} + \left[\left(\frac{\alpha}{kT}\right)\left(\frac{1}{a}\right)\right]_{Head} + \left[\left(\frac{\alpha+\frac{2QkT}{a}}{\sigma}\right)^{\frac{1}{2}}\right]_{Packing} \tag{2.20}$$

where, α is repulsion, σ is interfacial tension, "a" is equilibrium head group area, "k" is the Boltzmann constant, T is temperature in Kelvin and Q is the coefficient for $1/a^2$ depending on aggregate size and L is the characteristic length (typically 4.6Å).

Moreover, shown in eqn. 2.21, Israelachvili's packing parameter value, "P", relates the volume (v) and maximum length (l) of the tail as well as the effective head group area (a) of the surfactant molecules to various micellar structures categorized as either spherical, cylindrical, vesicle or lamellar shown in Table 2.5 (Hull et al., 2015). Moreover, Table 2.6 provides geometrical equations for specific variables used in this model and mentioned in eqn. 2.19-21.

$$\text{Packing Parameter: } P = \frac{v}{al} \tag{2.21}$$

Table 2.5: Morphology of Micellar Aggregation Based on Packing Parameter (Adopted from Chemistry and Technology of Surfactants by Richard Farn)

Spherical	**Cylindrical /Wormlike**	**Vesicles /Ring**	**Lamellar /Bilayer**
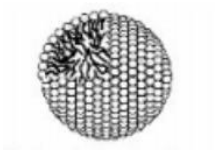			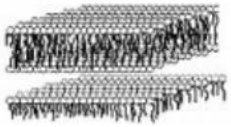
P< 1/3	1/3 < P < 1/2	1/2 < P < 1	P = 1

Table 2.6: Geometrical Relations for Different Aggregate Shapes (Nagarajan, 2014)

Geometrical Variables		**Sphere**	**Cylinder**	**Bilayer**
Volume of Core	V=gv	$4\pi R^3/3$	πR^2	2R
Surface Area of Core	A=ga	$4\pi R^2$	$2\pi R$	2
Area per Molecule	a	3v/R	2v/R	v/R
Packing Parameter	v/al	$v/al \leq 1/3$	$v/al \leq 1/2$	$v/al \leq 1$
Largest Aggregation Number	g_{max}	$4\pi l^3/3v$	$\pi l^2/v$	2l/v
Aggregation Number	g	$g_{max}(3v/al)^3$	$g_{max}(2v/al)^2$	$g_{max}(v/al)$
Coefficient for $1/a^2$	Q	(27/8)vL	(20/8)vL	(10/8)vL

External factors such as salt type, concentration, pH, and temperature can influence the micellar structure and alter the packing parameter. For instance, upon the addition of salt, the head size “a” shrinks from the reduction of electrostatic repulsion amongst other head groups therefore increasing “P” and transforming the micellar morphology of the solution (Gaudino et al., 2015; Hull et al., 2015; van Zanten, 2011).

2.6 FOAM IN POROUS MEDIA

Foam is a dispersion of a gas in a liquid. The foam system has regions called lamella that consist of thin liquid film, the interface between the gas and liquid, and the junction amongst other lamella (Schramm and Wassmuth, 1994). The behavior of foam is dependent on the connectivity, geometry, and body to pore throat distribution in porous media (Kovscek and Radke, 1994)

The addition of surfactant in the solution promotes thin-film stability and persistence to the foam structure by reducing the interfacial tension amongst phases (Schramm and Wassmuth, 1994). Lowering interfacial tension lessens the amount of mechanical energy required to form foam in the system (Schramm and Wassmuth, 1994). The initiation of foam is sensitive to the following parameters: oil/water saturation, surfactant concentration and formulation, gas flow rate, water flow rate, resident brine salinity, heterogeneity, capillary pressure, temperature and pressure of the system (Talebian et al., 2014). In addition, the stability of foam is constituted by these solution and interfacial properties: viscosity, gravity drainage, capillary suction, surface elasticity, electric double-layer repulsion, dispersion force attraction, and steric repulsion (Schramm and Wassmuth, 1994). Therefore, it is important to understand the physical and environmental aspects involved in foam flow through porous media when screening surfactants and other foaming agents.

2.6.1 Foam Properties

Mechanisms of Foam Formation and Coalescence.

According to Kovscek and Radke (1994), four mechanisms, namely snap-off, lamella division, leave-behind, and gas evolution, generate foam lamella in porous media, while foam coalescence is based on the limiting capillary and disjoining pressures. As

temperature increases, foam coalescence and thermal degradation prevail leading to challenges of foam propagation in the far-field reservoir.

Foam Quality

There are two meanings for foam quality. First, foam quality is defined as the gas fraction in foam, eqn. 2.22. Second, in eqn. 2.23, foam quality represents the ratio amongst the gas and aqueous injection rate. Altering the quality, changes the dryness and wetness as well as the strength, generation, and development of foam (Heller, 1994).

$$\text{Foam Quality} = \frac{V_{gas}}{V_{gas}+V_{aqueous}} \tag{2.22}$$

$$\text{Foam Quality} = \frac{Q_{gas}}{Q_{gas}+Q_{aqueous}} \tag{2.23}$$

Cui (2014) tested how foam quality impacts the strength of foam for Ethomeen C12. These experiments include results for WAG and co-injection schemes with surfactant in either DI or 22 wt.% TDS brine and pure CO_2 at the following conditions: at 20°C and 3400 psi using Silurian dolomite at flow rate of 4 ft/day. Shown in Figure 2.9, salinity promotes stabilization of foam by decreasing the electrostatic repulsion between molecules leading to an increase in packing density at the interface (Cui, 2014). It is also noted that disjoining pressure increases initially with salinity concentration followed by a downturn (Cui, 2014). As disjoining pressure decreases, the foam stability weakens and becomes unstable (Cui, 2014). Furthermore, in Figure 2.10, the influence of temperature plays a role in the strength of the foam, as temperature increases the strength of foam decreases due to thermal motion and coalescence of foam (Cui, 2014).

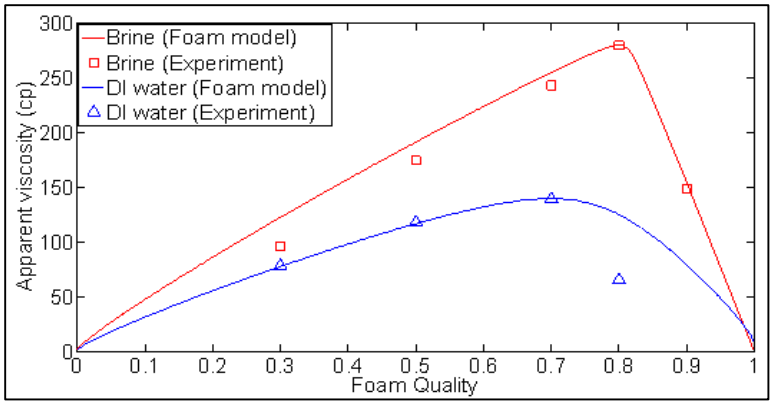

Figure 2.9: Comparative viscosity profiles for Ethomeen C12 at different foam qualities from 30 to 90% in 22 wt.% TDS brine and DI water (Cui, 2014).

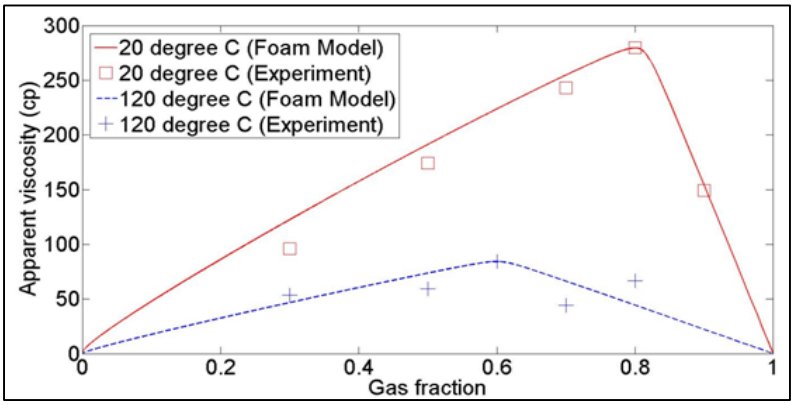

Figure 2.10: Comparative viscosity profiles for Ethomeen C12 at different foam qualities from 30 to 90% in 22 wt.% TDS brine, one at room temperature and the other at 120°C (Cui, 2014).

2.6.2 Mobility Control

Mobility ratio compares the mobility of the displacing phase (D) to the mobility of the displaced phase (d). As the mobility ratio decreases below 1, typically by increasing the viscosity or decreasing relative permeability of the displacing fluid, this signifies an improved sweep efficiency. From the equation below the mobility of the phase, λ relates the permeability, "k", to the viscosity, μ, of the phase.

$$M = \frac{\lambda_D}{\lambda_d} = \frac{k_D \mu_d}{k_d \mu_D} \tag{2.24}$$

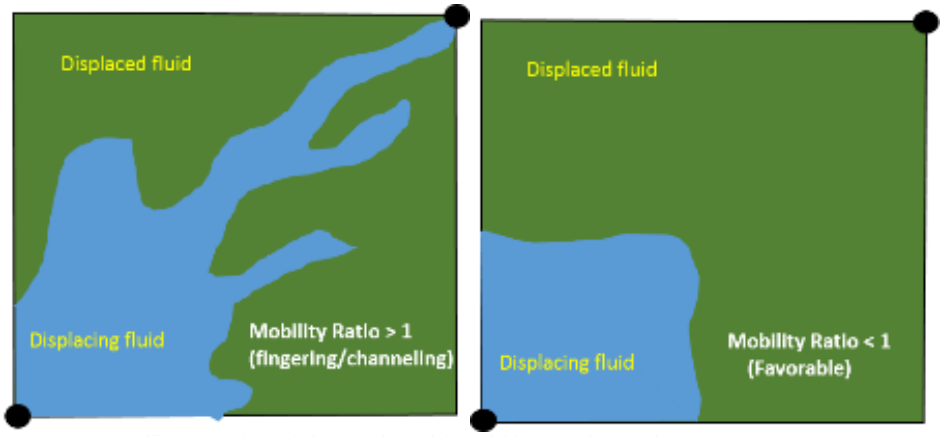

http://large.stanford.edu/courses/2015/ph240/aldousary1/images/f2big.png

Figure 2.11: Visualization of Improved Mobility Control

CO_2 Mobility Control

Due to its low viscosity at 0.1 cp, the mobility of CO_2 is higher than that of the displaced fluid resulting in instability, poor sweep efficiency, fingering and channeling, especially in heterogeneous reservoirs, followed by premature breakthrough at the production well (Heller, 1994; Lee et al., 1991). The lower density has a tendency to migrate upwards, known as gravity override, causing additional reduction in sweep efficiency (Talebian et al., 2014).

When surfactant is incorporated into the system, foam increases the viscosity of the gas phase thereby decreasing the mobility ratio and promoting an improved sweep efficiency and recovery. The use of foam can be used for diverting the displacing fluid into low permeable or unswept regions by blocking pores in the high permeable region.

2.7 SURFACTANT USE IN PETROLEUM APPLICATIONS

This section comprises of three applications suited for surfactant use: conformance control, enhanced oil recovery and matrix stimulation. In all, choosing an appropriate

surfactant for oil and gas applications can be challenging since the surfactant should include the following aspects (Yang, 2002; Anderson, 2006; Enick, 2012; Lee et al., 1991):

- Not chemically or thermally degrade at injected or reservoir temperatures and pressures
- Stable in the presence of salts (low and high concentrations)
- Stable at low pH conditions either from exposure to CO_2 or acid treatment
- Not adsorb excessively to the media, so has to be rock-compatible
- For viscoelastic surfactants:
    - Remain viscoelastic at reservoir temperature and pressures, fast relaxation time under applied shear, and sustain gel or viscoelasticity for long periods of time and not become unstable

These conditions are major indicators of the value of a surfactant for the following petroleum applications (Lee et al., 1991).

2.7.1 Conformance Control

Conformance control consist of strategies to enhance sweep efficiency, relieve coning problems, reduce permeability, hinder gravity override, and improve near well-bore regions, illustrated in Figure 2.12. Two conformance control technologies namely gel and foam treatments pertain to the alteration of micellar structures to treat and enhance the fluid system. Gel treatments generally function as a plugging agent by blocking high permeable stratums, anomalies, and thief zones. This allows the injected fluids to divert into low permeable as well as unswept regions containing trapped oil for an improved sweep efficiency and oil recovery. Some measures are required for gel treatments, this includes that the surfactant has to be insensitive to gas contact, stable at reservoir conditions and be applicable over a wide range of pH and temperature values. Moreover, foams can be applied as mobility control agents for enhanced oil recovery initiatives or function as

blockers near the well-bore to reduce gas coning depending on the strength and stability of the foam (Enick, 2012; Sydansk and Southwell, 2000; Heller, 1994).

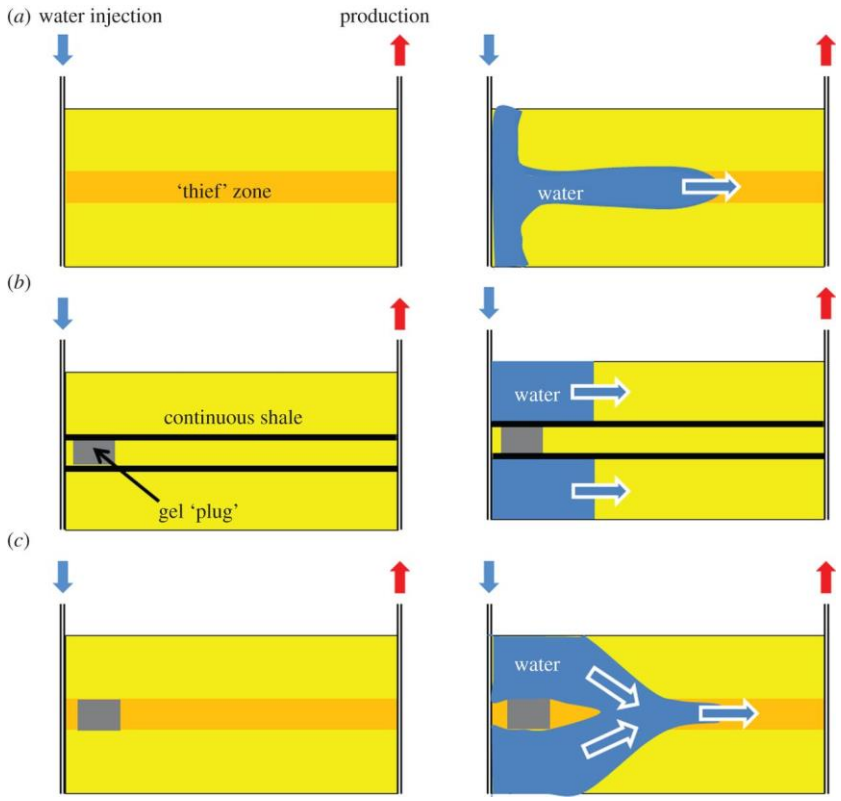

http://d29qn7q9z0j1p6.cloudfront.net/content/roypta/372/2006/20120320/F7.large.jpg

Figure 2.12: Gel Conformance Control Diagram

2.7.2 Enhanced Oil Recovery

Surfactant use in enhanced oil recovery (EOR), particularly during CO_2 floods, can increase the viscosity of the injected fluid by forming foam or an emulsion amongst the vapor and aqueous phase therefore improving the sweep efficiency and providing mobility control for far-field applications. When surfactant is dissolved in CO_2, it ensures that surfactant is available for foam generation with respect to where CO_2 is flowing at the subsurface (Le et al., 2008). Foam generation for EOR poses weak viscoelasticity and

resides under a set of conditions beyond which gel-like consistency arises and becomes more pertinent to gel conformance control. Thus, it is important to understand the impacts and sensitivity of temperature, salinity, pH, and surfactant concentration on the macroscopic behavior of the surfactant solution. In all, the span of this transition from foam to gel can provide other great strategic features, hence providing gel-treatment far-field by triggering a modifiable parameter, such as salinity (Enick, 2012).

2.7.3 Matrix Stimulation

Besides conformance control and enhanced oil recovery, viscoelastic surfactants can be used for matrix stimulation in carbonate formations if the surfactant solution's viscosity changes with pH and can withstand high concentrations of HCl or other compatible acids (Hull et al., 2015; Nasr-El-Din et al., 2009). For matrix stimulation, a highly acidic surfactant solution is transferred into the reservoir, then as HCl in the solution depletes from matrix dissolution, the pH as well as the viscosity rises, which stem the creation of viscoelastic gel (Hull et al., 2015). The gel obstructs high permeable channels (similar to conformance control) therefore diverting fresh acid into low permeable and un-contacted zones by the propagation of wormholes. These wormholes provide a highly conductive flow channel to transport trapped hydrocarbons to production (Hull et al., 2015).

Note, this pH-dependency is prone to amine-based surfactants because as pH decreases, the degree of amine protonation increases (α =1) leading to more ionized surfactant molecules and vice versa. When more molecules have alike charges, this leads to smaller micellar structures due to the intensification of electrostatic repulsion amongst molecules. In other cases, with little to no protonation above the surfactant's critical pH (α =0), molecules have no charge (non-ionic) and become unaffected by the presence of salt

compared to ionized surfactant molecules, thus the micellar structures remain small and non-viscoelastic (Wang et al., 2008). Consequently, for matrix acidizing, understanding the protonation characteristics for the particular surfactant is vital to attain optimal viscoelasticity in the subsurface.

Chapter 3: Aqueous Stability of Duomeen TTM

3.1 INTRODUCTION

It is imperative to select a surfactant that has reasonable water solubility for subsurface applications. If water-soluble, the surfactant solution will be able to propagate through the porous media leading to an improved sweep efficiency. If the solution appears cloudy, phase separated, or precipitated at given conditions, this can lead to excessive retention and chemical consumption of the surfactant.

Temperature and salinity scans were conducted for Duomeen TTM at typical reservoir and injective conditions. These experiments had a fixed surfactant concentration of 0.2 wt.% with salinities ranging up to 10 wt.% NaCl and temperature from 40 to 80°C. High temperature and viscoelastic aqueous stability tests were also conducted at a fixed surfactant concentration and salinity of 1 wt.% Duomeen TTM and 20 wt.% NaCl, respectively.

3.2 MATERIALS AND PROCEDURE

3.2.1 Materials

95% active Duomeen TTM from AkzoNobel was used as received. To prepare solutions, mixtures of surfactant, deionized water, lab-grade NaCl, and 2N hydrochloric acid were used. A Hanna Instruments™ 2020 edge multiparameter pH meter with Hanna Instruments™ Electrode 11310, three controlled temperature ovens, BUCHI 461 Water Bath, Sartorius Scale™, and Eppendorf Repeater™ plus were used to measure pH, heat, weigh and measure samples for this series of experiments.

3.2.2 Procedure

Phase Behavior: 0.2 wt.% Duomeen TTM Solutions

Sixty solutions were prepared comprising of 0.2 wt.% Duomeen TTM and salinities ranging from 0 to 10 wt.% NaCl. Mixtures of bulk solutions consisting of 0.8 wt.% Duomeen TTM, 20 wt.% NaCl and DI water produced the sample variety. For 30 samples, the pH was adjusted to 3 by the addition of 2N HCl in the Duomeen TTM bulk solution. The other 30 samples had no pH adjustment; the unaltered pH of Duomeen TTM is around 9. Furthermore, 5 mL of each solution was injected into a flame-sealed glass pipette and placed in three ovens designated at 40, 60, and 80°C for two weeks. Observations were recorded every other day.

Critical pH: 0.2 wt.% Duomeen TTM Solutions

Three bulk solutions consisting of 0.8 wt.% Duomeen TTM, DI water and 2N HCl were prepared. The pH of each mixture was adjusted using hydrochloric acid. The 0.2 wt.% Duomeen TTM samples consisted of three bulk solutions: deionized water, 20 wt.% sodium chloride with no pH adjustment, and 0.8 wt.% Duomeen TTM bulk solutions with altered pH. Three sets of nine samples were produced, nine for each of the three ovens set to temperatures of 40°C, 60°C, and 80°C. Each set has 0.2 wt.% Duomeen TTM, but with varied pH and salinities: 2.0, 5.0, and 10.0 wt.%. The samples were allowed 12 hours to protonate before being placed in their respective ovens and remained there for one week. Then, solutions were then taken out of the ovens for immediate observation and pH recording. The samples rested in a thermobath at either 40,60 or 80°C when pH readings were taken. The recordings noted the solution's appearance as to whether it appeared clear, translucent, opaque when gently stirred.

Critical pH: 1 wt.% Duomeen TTM Solutions

This series examined solutions consisting of 1 wt.% Duomeen TTM and 20 wt.% NaCl to observe if samples are stable at high temperatures up to 120°C. All solutions had variable pH adjustments using HCl. Depending on pH, some solutions encompass viscoelastic/polymer-like properties at higher HCl dosages. The HCl dosages administered were 150, 200, 250, 300, 350, 400, 450, and 500 μL HCl for a 19-gram solution. Furthermore, the solutions were filled in flame-sealed glass pipettes and placed in an oven. The temperature ranged from 25 to 120°C and remained at that temperature for one week in order to age. Periodic observations were recorded.

3.3 RESULTS AND DISCUSSION

3.3.1 Phase Behavior: 0.2 wt.% Duomeen TTM Solution

These experiments depict that pH adjustment is crucial for making amine-based "switchable" surfactants water-soluble. It can be seen in Figure 3.1 that not adjusting the pH leads to Duomeen TTM phase-separating and residing as a white/yellow film at the interface. At all temperatures and salinities observed, when gently shaken, the solution turns opaque and separates after time.

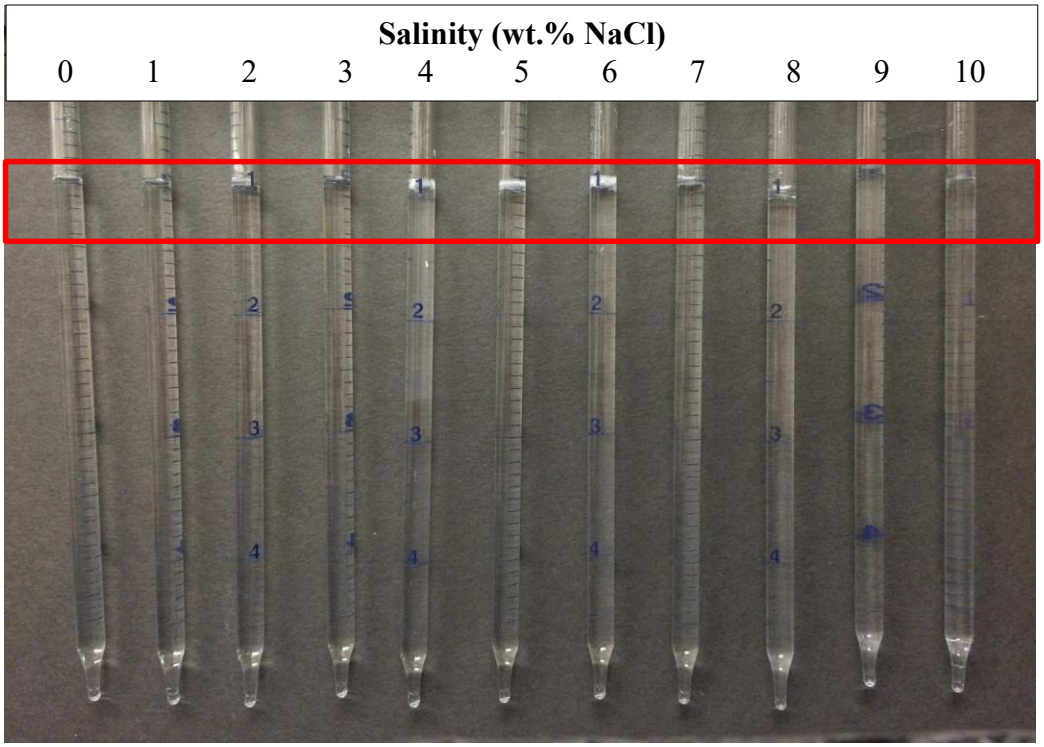

Figure 3.1: Unaltered "natural" pH at 60°C - notice the thin film of surfactant at the interface. Also there is cloudiness present on the 4% NaCl pipette. For this case, surfactant concentrations are at 0.2 wt.% Duomeen TTM with NaCl salinities ranging from 0 to 10 wt.%.

On the other hand, illustrated in Figure 3.2, the solutions with pH adjusted to 3 remained clear at all temperatures and salinities observed. These samples remained stable and no apparent film was present throughout the time of observation. Protonation of the amine head group allows Duomeen TTM to solubilize in the aqueous medium. As seen in Figure 3.1, when the amine group is unprotonated (little to no pH adjustment), the surfactant acts as a fatty acid leading to phase separation and insolubility, similar behavior as an immiscible oil/water mixture. In conclusion, Duomeen TTM solutions requires a pH adjustment to become stable in the aqueous medium. The next sought out question is at what critical pH does the solution become unstable/opaque at different salinities, temperatures and surfactant concentrations.

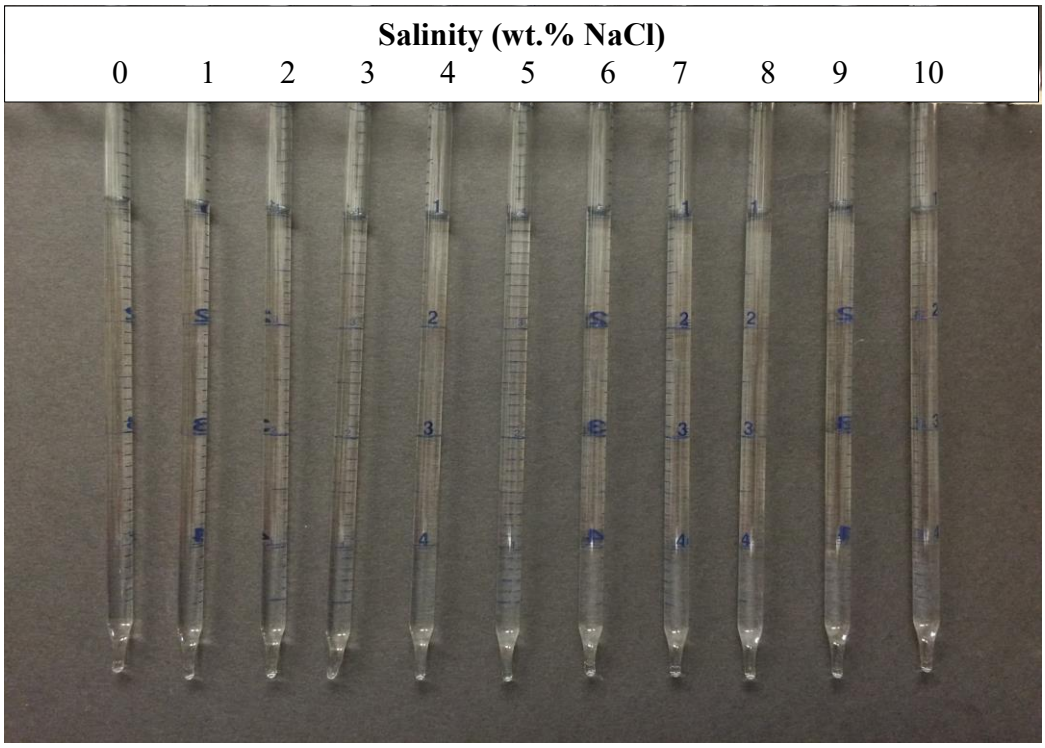

Figure 3.2: 0.2 wt.% Duomeen TTM with NaCl salinities ranging from 0 to 10 wt.% and pH adjusted to 3 at 60°C. Solutions remained stable under acidic conditions.

3.3.2 Critical pH: 0.2 wt.% Duomeen TTM Solution

Results are presented in Figure 3.3; each chart characterizes the critical pH of 0.2 wt.% Duomeen TTM at a specified temperature. Three salinities were analyzed: 2, 5, and 10 wt.% NaCl. In addition, it can be seen from the figure below, as temperature increases then critical pH decreases, and as salinity increases at a fixed temperature, then critical pH increases. Salinity promotes hydration for ionic surfactants thereby increasing the water-solubility of Duomeen TTM in solution and decreases electrostatic repulsion between surfactant molecules. Temperature elevation drives the surfactant to become less hydrophilic eventually becoming unstable.

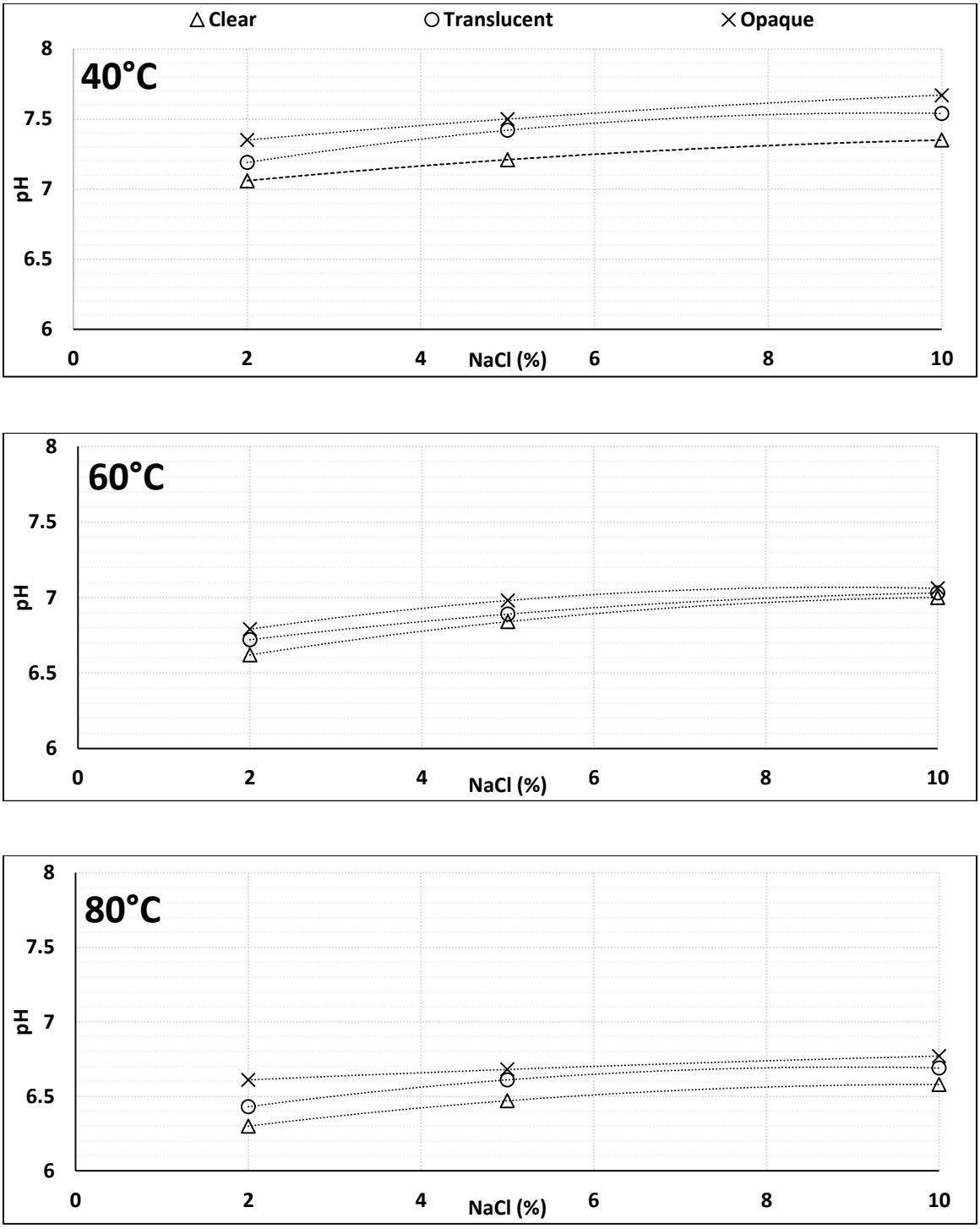

Figure 3.3: Critical pH of Duomeen TTM at 0.2 wt.% in a range of salinities from 2 to 10 wt.% NaCl. Three temperatures were analyzed to decouple changes in critical pH.

3.3.3 Critical pH: 1 wt.% Duomeen TTM Solution

At conditions of 1 wt.% Duomeen TTM and 20 wt.% NaCl, viscoelasticity can be visually observed for solutions below a certain pH. This type of viscous fluid resembles polymer-like consistency, but does not pose the same environmental behavior that polymer entails. As salinity increases above the CMC, the aggregation of micelles form long micellar networks that elongate and entangle forming the viscous counterpart. Salt is known to decrease the electrostatic repulsion between surfactant molecules thus "triggering" this viscoelastic occurrence.

Figure 3.4 and 3.5 illustrates and displays the solutions analyzed for this experiment. The first figure defines the critical pH of the 1 wt.% Duomeen TTM and 20 wt.% NaCl solution at temperatures spanning up to 120°C. Filled circles represent opaque solutions, hatch circles are solutions having a faint translucent appearance, circles with a green fill are phase separated solutions and circles with no fill are clear solutions. Phase separation at 120°C did not occur instantly. The solutions initially appeared faintly translucent, but by the end of the week, a yellow-white film was apparent at the interface. When re-mixed into the solution, it went back to a translucent appearance. At low pH levels below 1, the color of the solution turns to a yellow tint after a week of exposure to high temperatures. The solutions with a pH in between these extremities seem to remain clear with no apparent film at the interface.

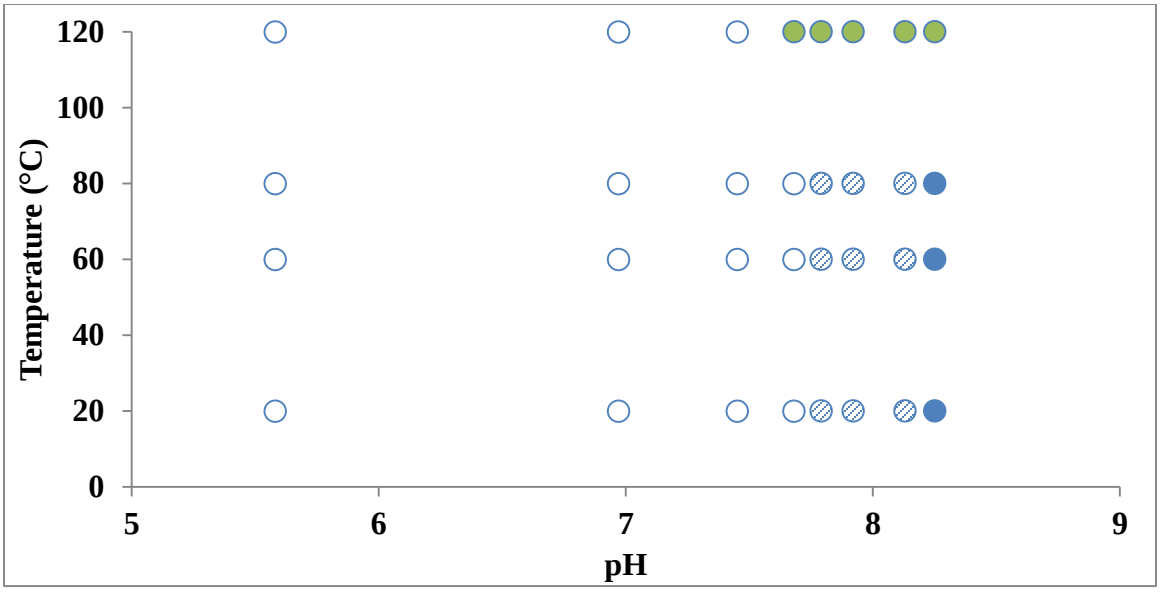

Figure 3.4: Phase behavior of 1 wt.% Duomeen TTM solution in 20 wt.% NaCl brine at high temperatures to test stability from 25 to 120°C. Some solutions resemble viscoelastic surfactant solutions.

The images shown in Figure 3.5 visualize the onset of viscoelasticity at room temperature. Viscoelasticity in this nature is termed for air bubbles trapped and suspended in solution. Figure 3.6 displays the viscosity profile at 1 s^{-1} of the exact solutions imaged in Figure 3.5. Viscoelasticity commences around the same pH as critical pH and weakens as temperature increases and strengthens as pH decreases. It can be seen that viscosity escalates in the neutral region between a pH of 7 and 8 and then stabilizes around 2000 cp at the lower pH spectrum. As it will be mentioned in Chapter 5, the strongest viscoelasticity occurs at the half protonation state of the solution, where 1 is fully ionized (lower pH) and 0 is non-ionized (higher pH).

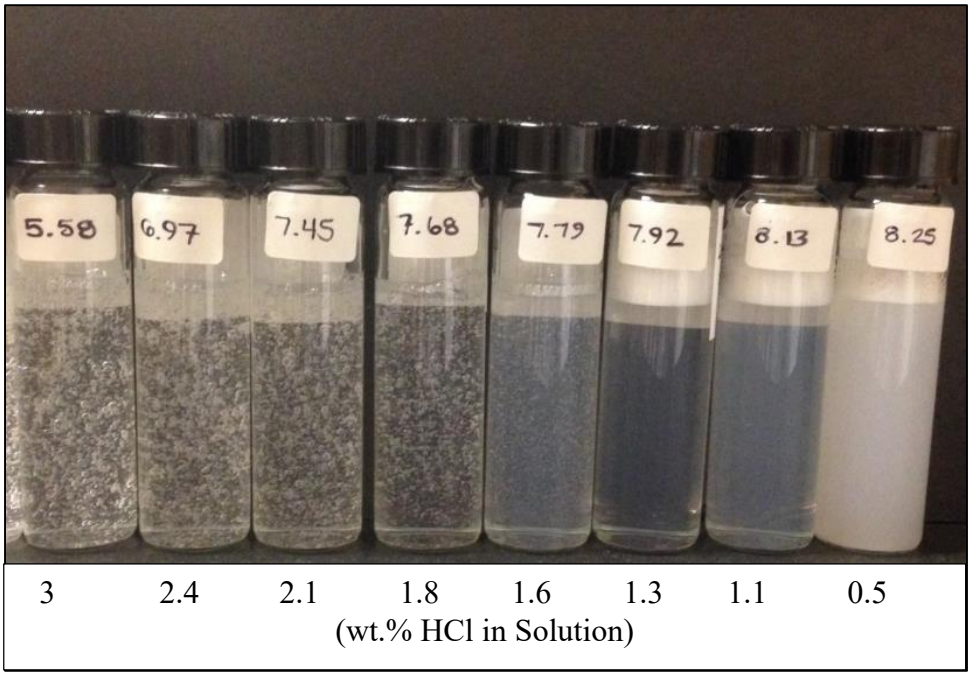

Figure 3.5: Viscoelastic surfactant solutions composed of 1 wt.% Duomeen TTM and 20 wt.% NaCl with changes in pH. The pH value for each solution is written on the designated glass jar.

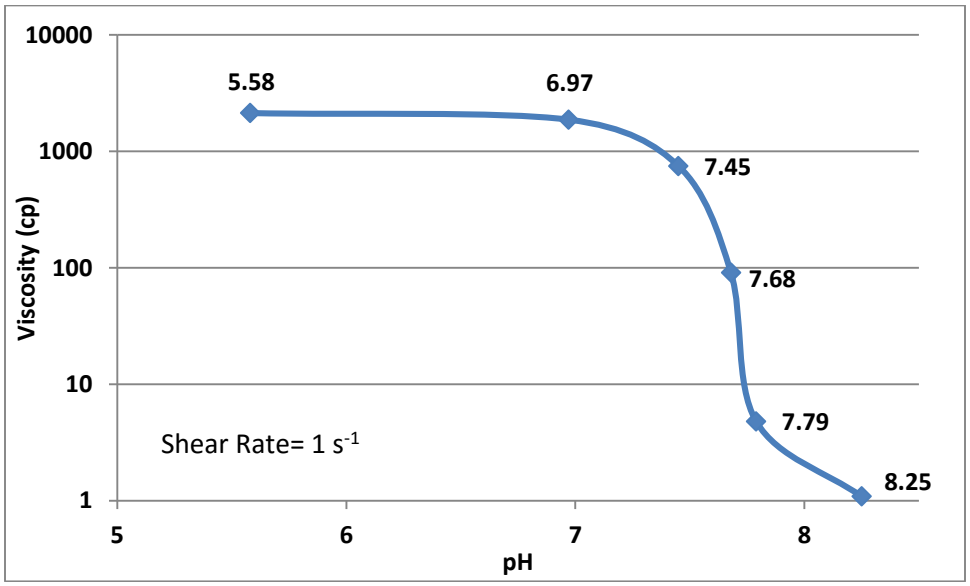

Figure 3.6: Steady shear rate of 1 s^{-1} for pH solutions imaged above. Viscosity dramatically increases after surpassing the critical pH (7.79).

3.4 CONCLUSION

The following remarks summarize the results from this chapter:

- Duomeen TTM is water soluble when pH is adjusted accordingly. As HCl is added to the solution, more H^+ ions are available to bind to the two nitrogen ions in the head group creating ammonium salt counterparts. This process makes the surfactant molecules significantly more water-soluble.
- At low surfactant concentrations, the critical pH of the solution increases with increasing salt concentration. Salinity promotes aggregation of micelles above the CMC due to reducing the electrostatic repulsion amongst molecules. In addition, adding salt decreases the CMC of the solution for ionic surfactants.
- As temperature increases, it negatively impacts surfactant's solubility in water and can cause instability and phase separation depending on salt concentration and pH of the solution.
- Viscoelastic surfactants can still exhibit phase separation at high temperatures. The stability of the solution is time-dependent and may not appear until the solution has been aged at that specific temperature. The onset of viscoelasticity occurred close to where the critical pH of the solution lies.
- Once surpassing the critical pH, it seems that the viscosity rises due to the formation of entangled and elongated micelles that resemble polymer. Theoretically, maximum viscosity occurs at the halfway degree of protonation point, even though it is not shown in these results.

The following chapters took consideration of these aqueous stability results. All surfactant solutions have a pH less than 6.5 to ensure it does not surpass the critical pH boundary.

Chapter 4: Surfactant Solubility in Mixed Gas and CO_2/Brine Phase Partition of Alkyl Amines

4.1 INTRODUCTION

Surfactant transport in multi-phase flow is strongly influenced by surfactant solubility and partition in each phase.

Solubility

The concentration of surfactant in the gas phase can be predicted using either the cloud point or HPLC coil method. Both provide estimated surfactant solubilities in the vapor phase, but the HPLC coil method also characterizes the mass and carbon-tail distribution of the dissolved solute at a given temperature and pressure. This reason led us to analyze Duomeen TTM's solubility by using the HPLC coil method. The goal of this study is to provide trends and estimated solubility values of Duomeen TTM in CO_2 and impure CO_2 with methane dilution at different temperature and pressure values.

The presence of methane or other impurities is common amongst petroleum applications. In practice, the CO_2 is recaptured and reused for ongoing enhanced oil recovery purposes, therefore the purity of CO_2 degrades overtime and additional gas components, such as lighter hydrocarbons, are incorporated into the reuse mixture. Aspects of CO_2 contaminated mixtures will be discussed in this chapter. Solubility was analyzed for five types of gas mixtures based on partial pressure: pure CO_2 or 0% CH_4, 100% CH_4, 75% CH_4, 50% CH_4, and 25% CH_4.

Partition

Along with solubility, the partition coefficient identifies if Duomeen TTM prefers the aqueous or vapor phase at different environmental conditions. This ratio near 0 means the surfactant tends to reside in the aqueous or above 1 favoring the vapor phase. Based on

the results from Chapter 3, it is predicted that Duomeen TTM will have a low partition coefficient under acidic conditions.

4.2 MATERIALS AND PROCEDURE

This section discusses the materials and methodology for the solubility and partition experiments.

4.2.1 Materials

Duomeen TTM, Ethoduomeen T13 and Armeen DMCD were obtained from AkzoNobel and used as received. CO_2 and CH_4 from Matheson Tri-Gas was used as received. Custom fabricated 67 cm^3 stainless steel pressure cells (maximum pressure: 5000 psi, Figure 4.1) with Aflas chemical resistant O-rings, magnetic stir bars, and either a spigot or 2.5 cm^3 coil tubing were used for the study as well as a convection oven, quizix pump, Omegadyne pressure transducers, and two custom fabricated accumulators equipped with a floating piston. The internal volumes of the accumulators are 2000 cm^3 and 450 cm^3, used for pressurizing incoming gas and storing acidic water for rinsing, respectively. The acidic water to rinse the surfactant out of the coil was adjusted to a pH of 2 by adding 20 mL of 2N HCl into 4000 g of Millipore DI water.

For solubility experiments, pure surfactant was used without additives, while for partition experiments, the surfactant solution consisted of 0.2 wt.% Duomeen TTM and 1 wt.% NaCl adjusted to a pH of 3 with the intention of reducing the significance of CO_2 dissolution in water.

Finally, the mass spectrometer and liquid chromatography (LCMS) was used to analyze concentration of the rinsed coil solution or spigot solution. The LCMS is similar to the HPLC, but provides the mass distribution of the chemical at a certain dropout time.

Figure 4.1: Pictures of High-Pressure Cell. At Left, Solubility Setup with Coil. At Right, Partition Setup with Spigot at Bottom.

4.2.2 Procedure

Calibration

Prepare surfactant concentrations that range from 0.01% to 0.00005 wt.% using pure surfactant and acidic water. Acquire a 2 mL sample of each concentration and run it through the LCMS or HPLC along with experimental samples. The results from the LCMS will provide each sample with a distinct area and height value for all peaks indicative of the surfactant. To simplify analysis, overlap base peak option was selected. Finally, plot total area vs. surfactant concentration and use this data to convert experimental LCMS data to concentration. In all, LCMS data is based on analyst interpretation of the data, results may vary based on technique used. It is advisable to run all samples at once to eliminate reading errors associated with cross contamination from other samples tested.

Solubility Method

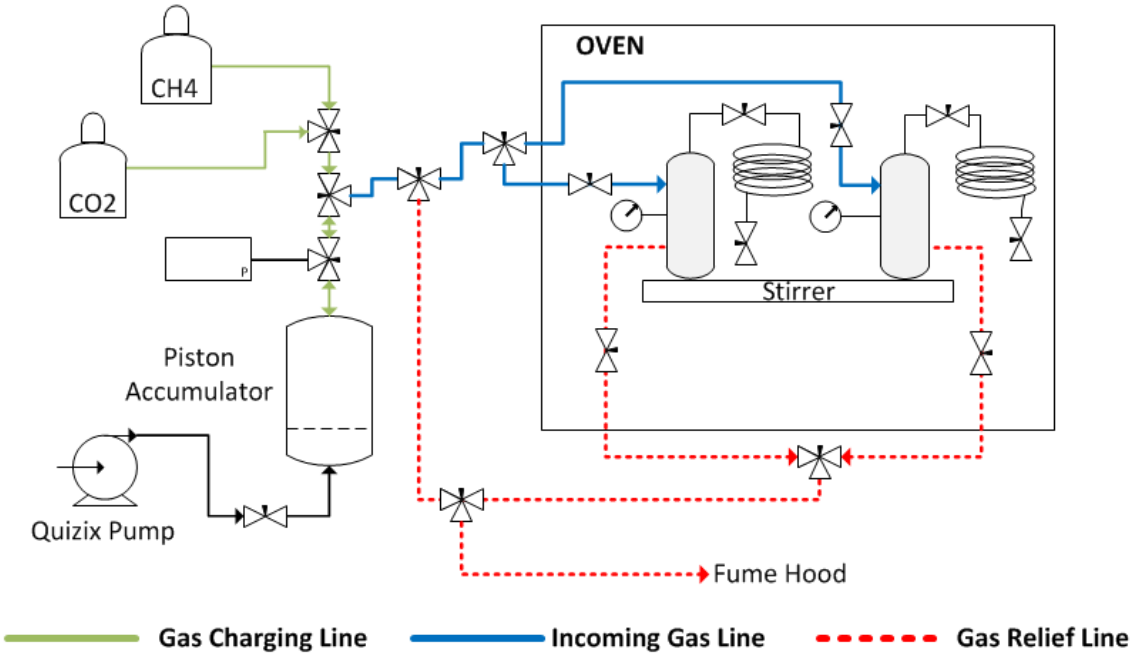

Figure 4.2: Solubility Experiment Layout.

Using the repeater, dispense 1 mL of pure surfactant into the pressure cell before placing in the oven. Connect incoming gas line, gas relief line, pressure line, and solubility coil to the pressure cell, as shown in Figure 4.2.

Next the cells were preflushed with nitrogen to detect any leaks in the system, then liberated through the gas relief line into the fume hood and vacuumed for 2 to 5 seconds. Vacuuming for a short period ensures the liquid contents remain in the cell while removing nitrogen from the system. All valves connected from the accumulator to the pressure cells are then closed. The oven was heated to the target temperature of either 40 or 60°C. While the oven is heating, charge the 2000 mL piston accumulator with 350 psi of pure CO_2 or gas mixture using partial pressure and pressurize the accumulator using a Quizix pump. Open valves from the piston accumulator to the cells and allow the pressures to equilibrate.

The slower flow rate allows the CO_2/mixture to adjust to the oven's temperature resulting in a lower pressure drop inside the cell. Close valves and turn on mixing for 2.5 hours until pressures are near or at equilibrium. Turn off mixing and allow another 4 hours for pressure to stabilize again near or at equilibrium and allow the surfactant to settle in the CO_2. Note, near equilibrium would be considered less than a 2 psig drop per hour.

In a timely manner, open the entrance valve to the solubility coil until equilibrium is achieved (typically 2 minutes). Then turn off oven and gas relief the cell. Remove coil from the cell and invert it where the exit valve is above the entrance valve. Attach and submerse a 2-inch tubing line, which is connected to the entrance valve, into 2.5 mL of pH 2 DI water and open the entrance valve slowly until all the gas bubbles are liberated from the coil, typically 5 minutes. Connect the pH 2 water line to the exit valve and place the 2-inch tubing line into a jar larger than 250 mL. Rinse coil with pH 2 water at a flow rate of 2 mL/min to a volume of 200 mL. This rinse will solubilize and protonate residual surfactant that was not collected from the first extraction. Note, the H^+ ions in the acidic water will protonate the surfactant making it more water-soluble and flow, if no acid was added to the water, then most surfactant will remain in the coil during the rinsing process resulting in low removal efficiency. The last step, place the 2.5 mL from the first extraction into the 200 mL rinse, and record mass of sample.

Acquire 2 mL from the sample and place into the LCMS to determine concentration of surfactant in the aqueous phase through calibration data. Use the following equation to convert surfactant concentration in the aqueous phase to surfactant concentration in the vapor phase (i.e. CO_2 or mixed gas).

$$C_{s_{gas}(\%)} = \frac{\frac{C_{sw(\%)}}{100} * W_{aqueous(g)}}{V_{coil(cc)} * \rho_{gas}\left(\frac{g}{cc}\right) + \frac{C_{sw(\%)}}{100} * W_{aqueous(g)}} * 100 \quad (4.1)$$

Where Cs_{gas} is the concentration of surfactant (wt.%) in the CO_2 or mixed gas phase, C_{SW} is the surfactant concentration in the aqueous phase (wt.%), $W_{aqueous}$ is the weight of the total aqueous solution from rinsing process (g), V_{coil} is the total coil volume (2.5 cc), and ρ_{gas} is the density of CO_2 or mixed gas with changes in temperature and pressure (g/cc). Figure 4.3 expresses the applied ρ_{gas} equation under conditions in this scope of work.

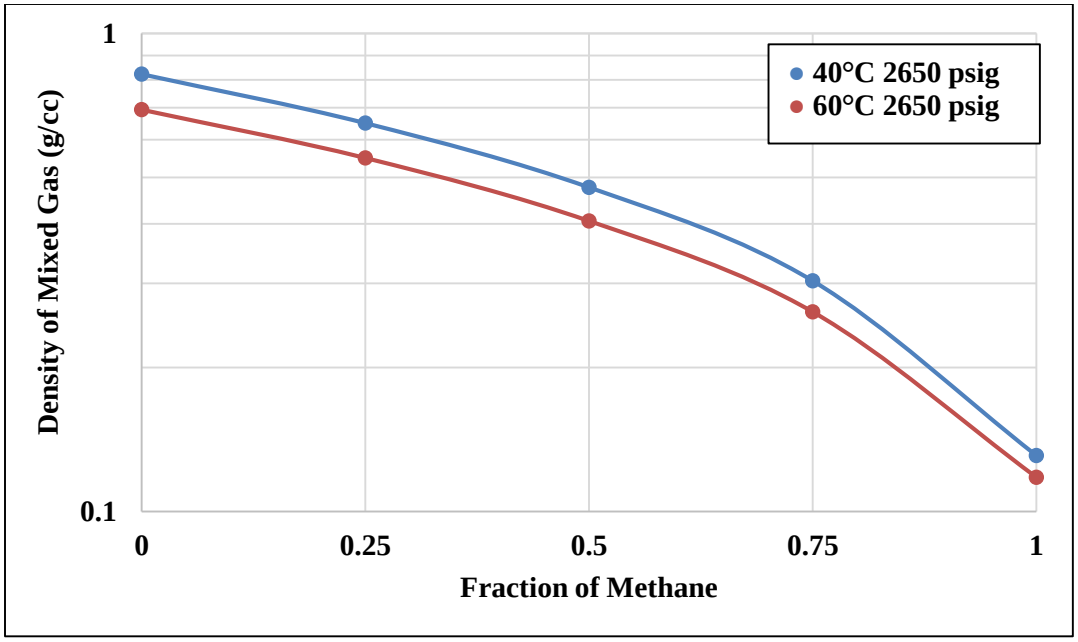

Figure 4.3: Density of mixed gas with different fractions of methane. Source: peace software: http://www.peacesoftware.de/einigewerte/

Partition Method

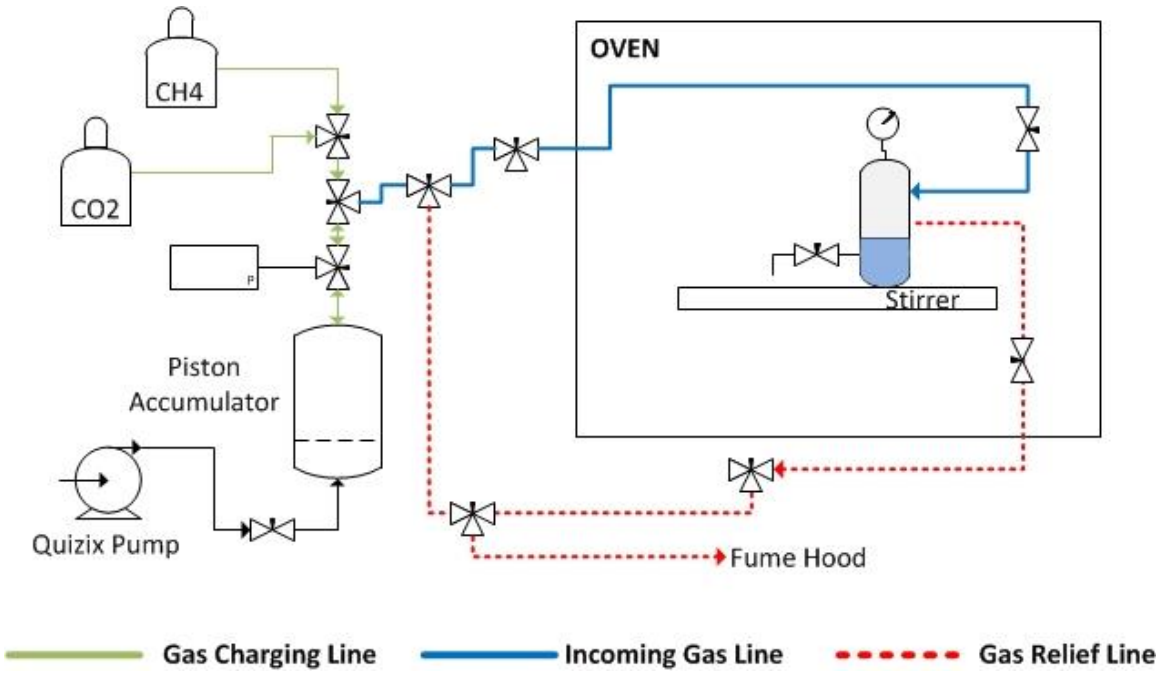

Figure 4.4: Partition Experiment Layout

Using the repeater, dispense 15 mL of 0.2 wt.% surfactant solution with 1 wt.% NaCl into the pressure cell before placing in the oven. Connect incoming gas line, gas relief line, and pressure line to the pressure cell, as shown in Figure 4.4.

Next the cells were pre-flushed with nitrogen to detect any leaks in the system, then liberated through the gas relief line into the fume hood and vacuumed for 2 to 5 seconds. Vacuuming for a short period of time ensures the liquid contents remain in the cell while removing most of the nitrogen from the system. All valves are then closed except for the incoming gas line valve inside. The oven was heated to the target temperature of either 60 or 80°C. While the oven is heating, charge the piston accumulator with pure CO_2 and pressurize using the Quizix pump. Open valves from the piston accumulator to the cell and allow the pressures to equilibrate. The slower flow rate allows the CO_2 to adjust to the

oven's temperature resulting in a lower pressure drop inside the cell. Close valves and turn mixing on for 2.5 hours until pressures are near or at equilibrium. Turn off mixing and allow another 15 hours for pressure to stabilize near or at equilibrium. Near equilibrium would be considered less than a 2 psig drop per hour.

In a timely manner, place a tube under spigot, then open the partition spigot until a 40 psig pressure drop is achieved, this is to avoid extracting the interface and free gas. The extraction contents should only be originating from the aqueous phase. Then turn off oven and gas relief the cell. Remove spigot from the cell and rinse with water.

Dilute the first extracted sample by 20x in order to analyze using the LCMS. Acquire 2 mL from the diluted initial and final sample and place into the LCMS to determine concentration of surfactant in the aqueous phase through calibration data. Use the following equation to convert surfactant concentration in the aqueous phase to surfactant partition coefficient between the vapor phase and aqueous phase.

$$k = \frac{\frac{m_{sCO_2}}{m_{sCO_2}+m_{gas}}}{\frac{m_{sw}}{m_{sw}+m_w}} \tag{4.2}$$

$$m_w = \rho_{solution\left(\frac{g}{cc}\right)} * V_{solution(cc)} \tag{4.3}$$

$$RF = 1 - \left(\frac{LCMS_{final}}{LCMS_{intial}}\right) \tag{4.4}$$

$$m_{sw} = (1 - RF) * \frac{C_{initial}}{100} * m_{w(g)} \tag{4.5}$$

$$m_{sCO_2} = \frac{C_{initial}}{100} * m_{w(g)} - m_{sw(g)} \tag{4.6}$$

$$m_{gas} = \rho_{gas\,(\frac{g}{cc})} * (V_{cell_{total}(cc)} - V_{solution(cc)}) \quad (4.7)$$

where, k is the partition coefficient, m_{sCO2} is mass of surfactant in the vapor phase (g), m_w is the mass of initial solution with density depending on salinity (g), m_{gas} is the mass of vapor occupied in the cell with density depending on temperature and pressure (g), m_{SW} is the residual mass of surfactant in the aqueous phase after extraction (g), $C_{initial}$ is the initial surfactant concentration in solution (wt.%), ρ_{gas} and $\rho_{solution}$ is the density of CO_2 and surfactant solution, respectively (g/cc), and V_{cell} and $V_{solution}$ is the volume of the cell (67 cc) and the volume of surfactant solution occupied in cell (15 cc). RF is the reduction factor that uses LCMS data to compare the surfactant loss in the final versus the initial sample.

4.3 RESULTS AND DISCUSSION

This section embodies primarily the solubility results of Duomeen TTM at different pressures, temperatures, and methane fraction. For comparative analysis, two other amine surfactants, Ethoduomeen T13 and Armeen DMCD, were tested at different pressures and fractions of methane dilution at a fixed temperature of 40°C. Surfactant solubilities were analyzed in the supercritical region, as shown in Figure 4.5, at pressures ranging from 1450 to 2650 psig at chosen temperatures of 40 and 60°C, while partition experiments were conducted at 60 and 80°C.

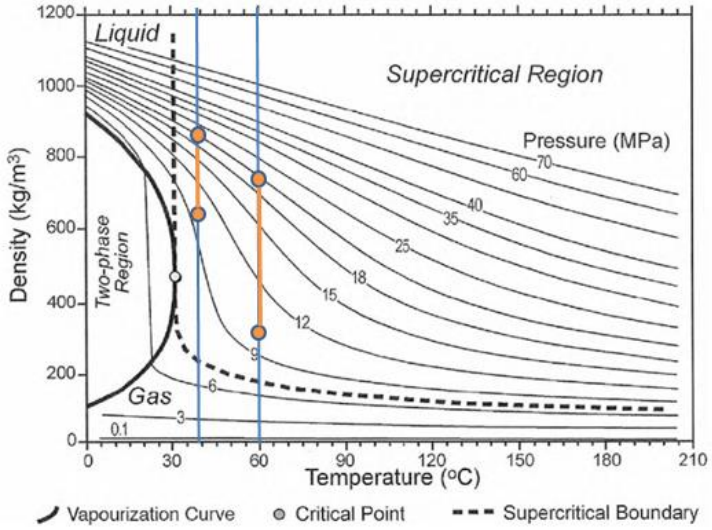

https://hub.globalccsinstitute.com/sites/default/files/publications/94506/advanced/fig-008.jpg

Figure 4.5: CO_2 PVT Chart to show all experiments were conducted in the supercritical CO_2 region

4.3.1 Pure CO_2 Results

Effect of Temperature and Pressure

Shown in Figure 4.6 and 4.8, the solubility of Duomeen TTM in the CO_2-rich phase was measured at two temperatures (40 and 60°C) and at a range of pressures from 1500 to 2800 psig. The error bars represent general error from the experimental procedure and LCMS analysis as well as the reproducibility of the data.

As expected, when temperature decreases or pressure increases, the surfactant solubility in CO_2 increases. When temperature rises at constant pressure, intermolecular interactions amongst surfactant-surfactant and surfactant-CO_2 become weaker resulting in lower solubility levels (Shi et al., 2015; McClain et al., 1996). Conversely, as pressure increases at constant temperature, interactions between surfactant-CO_2 become stronger therefore enhancing solubility (Ren et al., 2014; Shi et al., 2015). Ultimately, the intensification of surfactant-CO_2 interactions, also known as solvation strength or capacity, positively correlates with CO_2 density, which is a function of temperature and pressure in

the system, and surfactant solubility in CO_2 (Adkins et al, 2010). For this reason, it is assumed that CO_2 solvation is the dominant factor followed by intermolecular interactions (tail-tail, surfactant-surfactant, etc.) and surfactant volatility in altering surfactant solubility (Liu et al., 2004; Adkins et al., 2010).

Taking a further look at Figure 4.6 and 4.8, the solubility of Duomeen TTM in CO_2 increases and stabilizes around 1 wt.% at 40°C, while the solubility drops down to 0.65 wt.% at 60°C due to a loss in CO_2 solvation from rising temperatures. Moderate-high solubility in CO_2 can be attributed to Duomeen TTM's highly methylated structure. The terminal methyl groups are bulky and generate large steric hindrance (lack surfactant-surfactant interaction), thereby allowing the CO_2 and methyl groups to interact and form hydrogen bonds between the oxygen atom of the CO_2 and hydrogen atom of the methyl group thus enhancing solubility (Shervani et al., 2004).

Furthermore, Figure 4.7 and 4.9 displays the carbon tail group distribution (CTD) of the surfactant solubilized in CO_2. These figures can provide information about the degradation and selectivity of the tail groups exposed to various temperatures, pressures, and CO_2 conditions. The CTD of calibrated samples can be referred to in Appendix A or by the red-dotted lines denoted on the CTD figures. It is shown that after exposure to conditions stated above, Duomeen TTM at 40 and 60°C appear to have similar CTD distributions compared to the calibrated samples, but differ in magnitude. When thermally exposed, the distribution for the C18-20 tail groups reduced while the smaller tail groups increased. As anticipated, CO_2 preferentially dissolves shorter tail groups at low temperatures, due to its lower molecular weight and weaker tail-tail interactions compared to longer tail groups. This preferential demise as temperature increases. Furthermore, the pressure of the system has negligible impact on general spreading of the distribution (+/- 5%), since liquids show little to no dependence on pressure unlike gaseous substances.

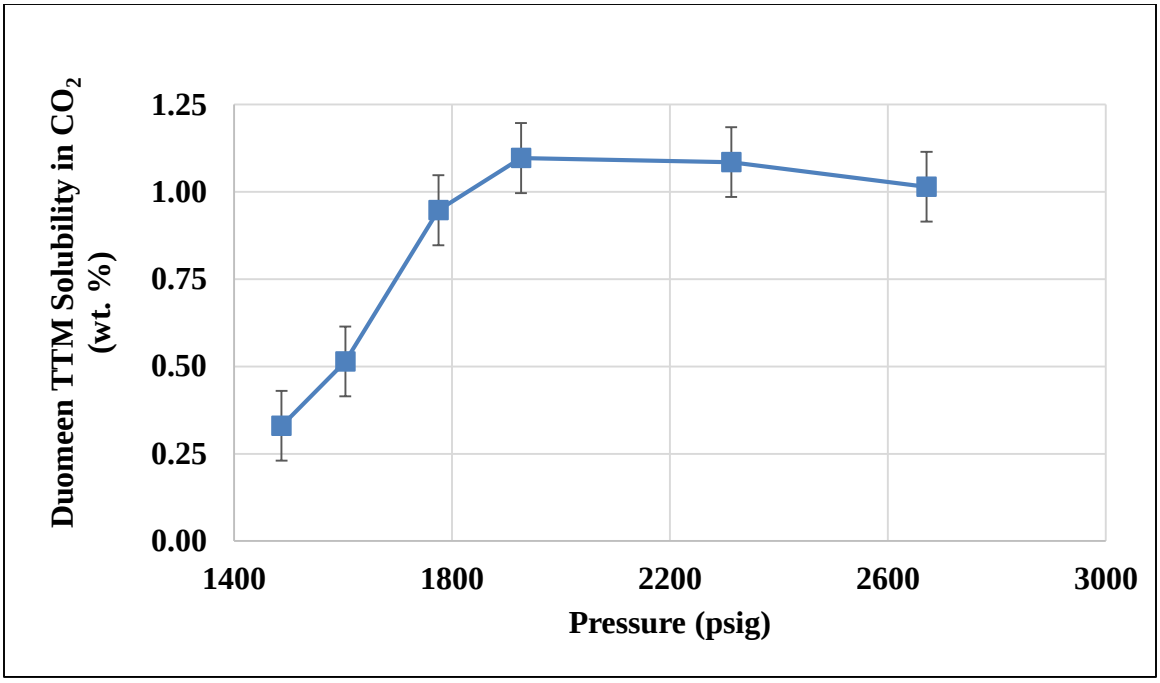

Figure 4.6: Duomeen TTM solubility in CO_2 at 40°C

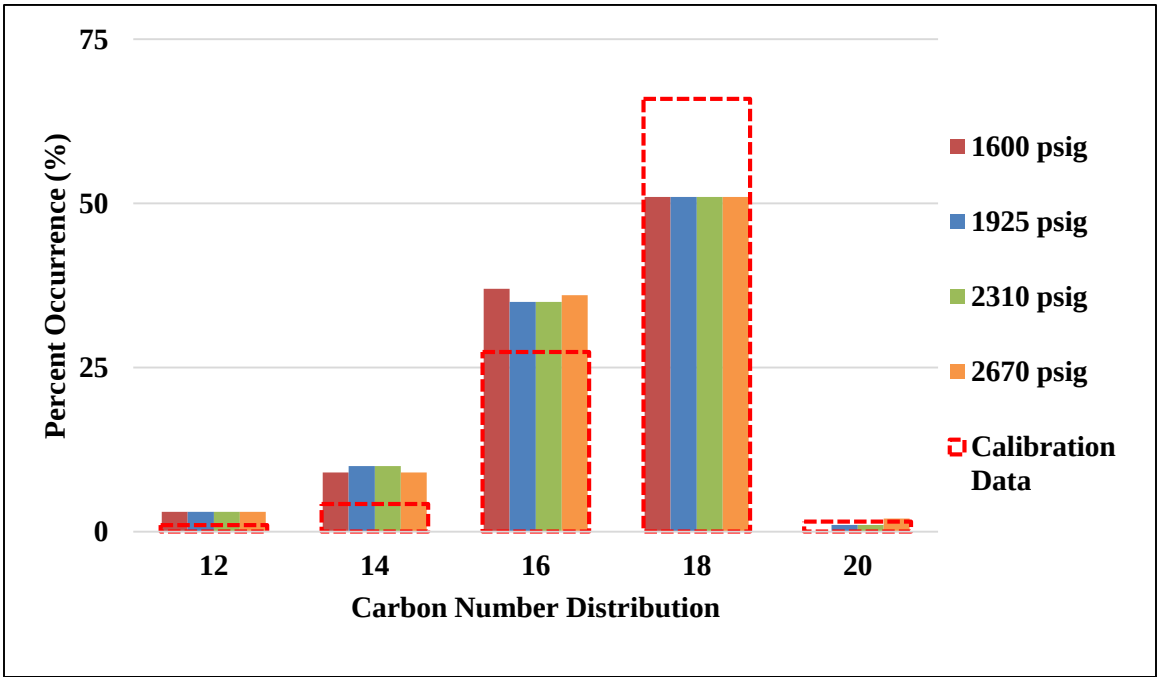

Figure 4.7: Duomeen TTM carbon number tail distribution in CO_2 at a given pressure (40ºC)

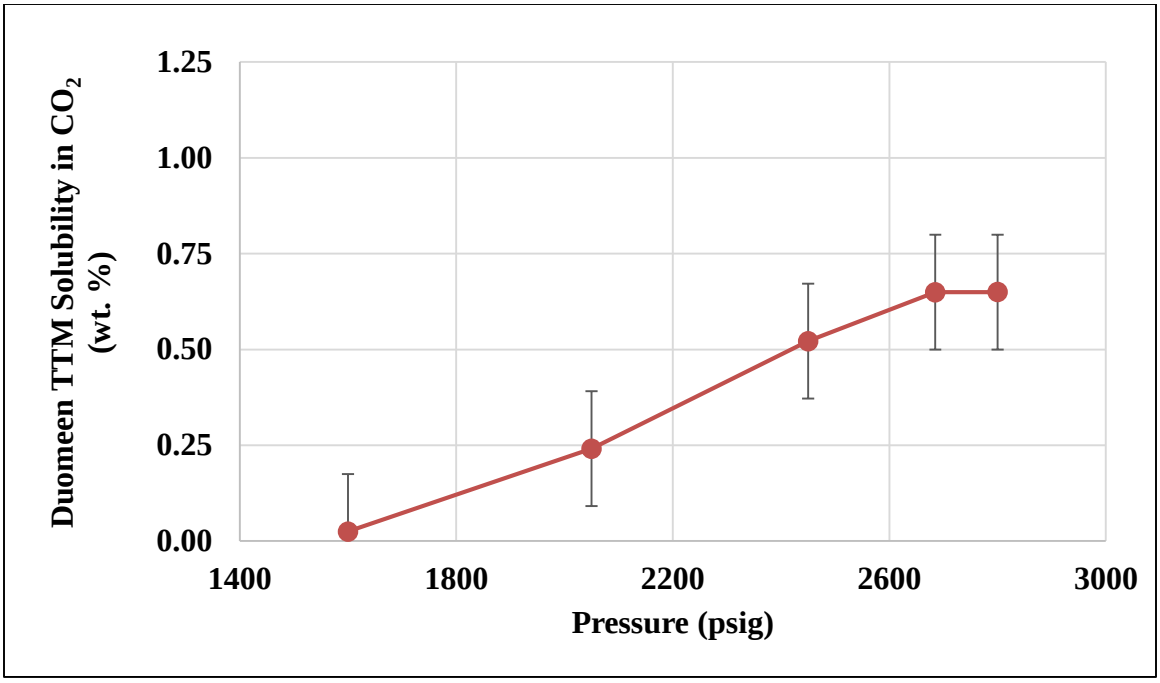

Figure 4.8: Duomeen TTM solubility in CO_2 at 60°C.

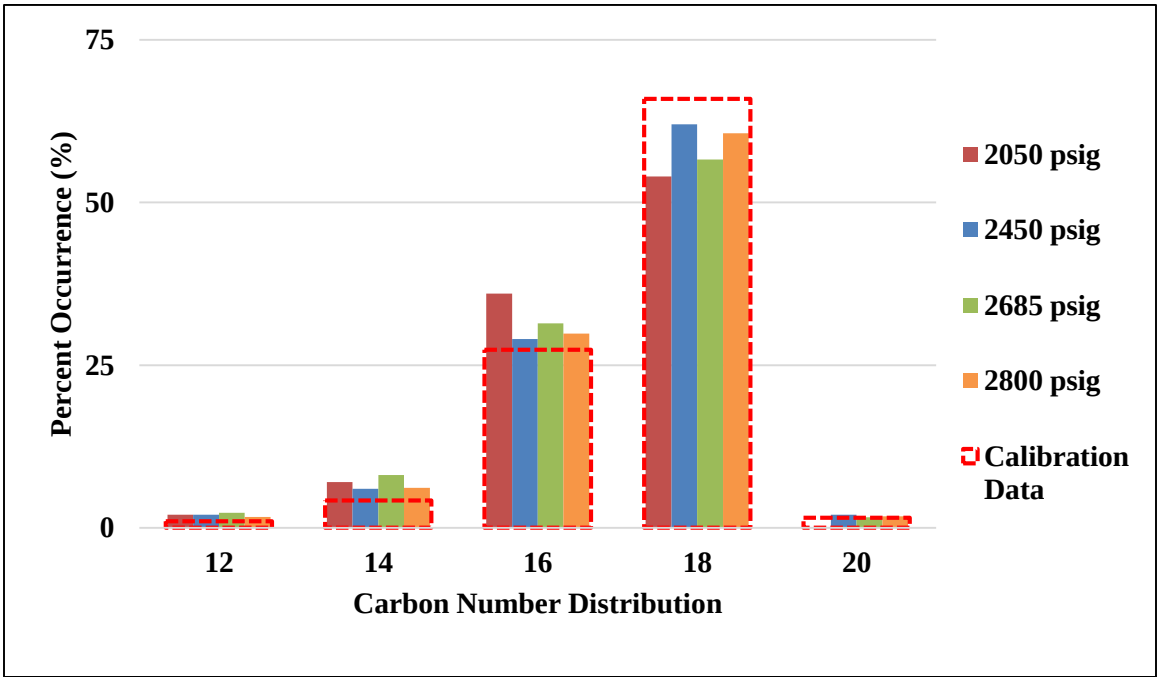

Figure 4.9: Duomeen TTM carbon number tail distribution in CO_2 at a given pressure (60ºC)

Effect of Chemical Structure

Ethoduomeen T13, Armeen DMCD, and Duomeen TTM are presented in Figure 4.10. It can be shown that Ethoduomeen T13 has significantly lower solubility in CO_2 than Armeen DMCD and Duomeen TTM due to changes in terminal functional groups and having the highest molecular weight.

Ethoduomeen T13 consists of terminal hydroxyethyl functional groups, which have polar and hydrophilic properties. This group hydrogen bonds amongst other surfactant molecules resulting in an increase in surfactant-surfactant interactions and weaker surfactant-CO_2 interactions, especially at lower temperatures (Shervani et al., 2004). This means that additional solvation power, typically from the rise in CO_2 density, is required to solubilize these hydrophilic compounds compared to CO_2-philic compounds (Shi et al., 2015). For instance, at higher pressures, the solubility of Ethoduomeen T13 rises and stabilizes due to enhanced CO_2 solvation strength.

For the highly methylated surfactant structures, the solubility of Armeen DMCD in CO_2, 0.9 wt.%, is analogous to the solubility of Duomeen TTM, 1 wt.%, at the same temperature. From the results, Armeen DMCD attains maximum solubility before Duomeen TTM, due to its molecular weight being smaller and having a shorter tail allowing CO_2 to pick it up at a lower solvation strength. Some factors that can cause differences in solubility values can be attributed to Armeen DMCD's coco-based tail group being less branched and unsaturated, as well as length differences compared to tallow-based tails, i.e. Duomeen TTM. In addition, diamine surfactants, such as Duomeen TTM, act as alcohols and contain an additional terminal methyl group, which can improve CO_2 solubility, while compromising weight.

The tail distributions for Armeen DMCD and Ethoduomeen T13 are illustrated in Figure 4.11 and 4.12, respectively. Armeen DMCD tail distribution shows a rather clear

case of selectivity and degradation of the surfactant dissolved in CO_2. Compared to the calibration results, the C12 tail group increased, while C16-18 tail groups dropped off. In addition, Armeen DMCD also shows unaffected tail distribution with pressure, a similar response to Duomeen TTM.

Moreover, Ethoduomeen T13 had three tail lengths analyzed (C14-18). This surfactant displays similar trends with the two other amine surfactants, the C14-16 tails increased in frequency, while C18 decreased compared to the calibration CTD.

In all, Armeen DMCD has the most significant alteration in tail distribution compared to the diamine surfactants. It can be concluded that C12 is the most common tail for Armeen DMCD and C16-18 are most prevalent for both diamine chemicals.

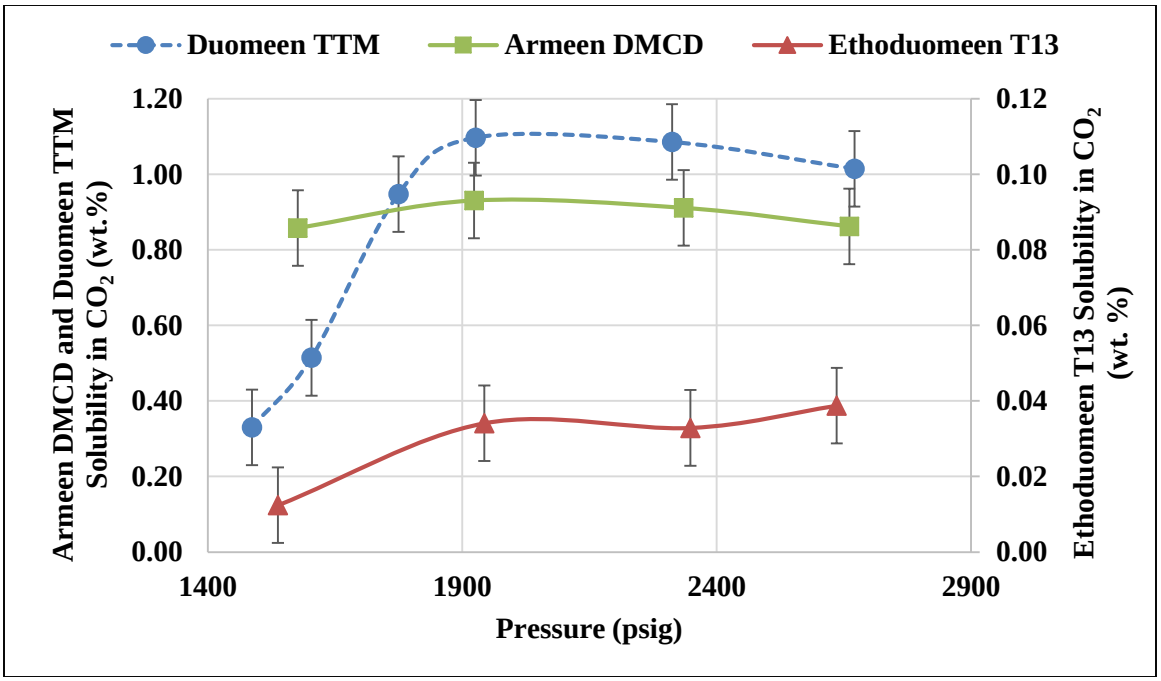

Figure 4.10: Armeen DMCD, Duomeen TTM and Ethoduomeen T13 solubility in CO_2 at 40°C.

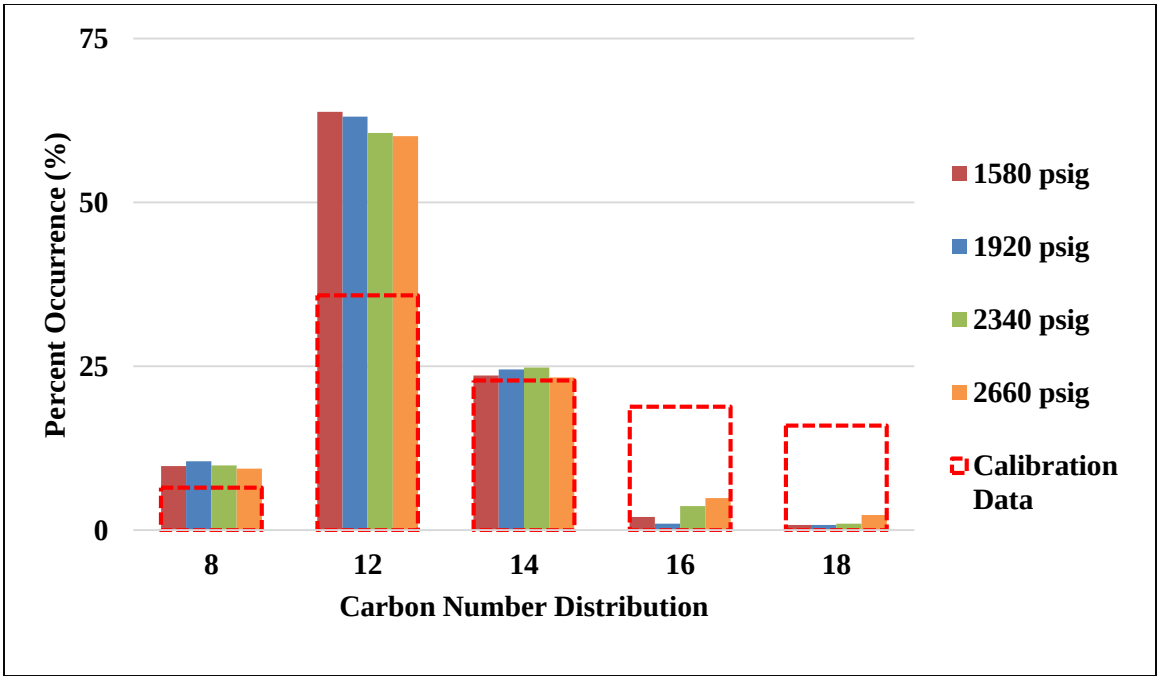

Figure 4.11: Armeen DMCD carbon number tail distribution in CO_2 at a given pressure (40ºC)

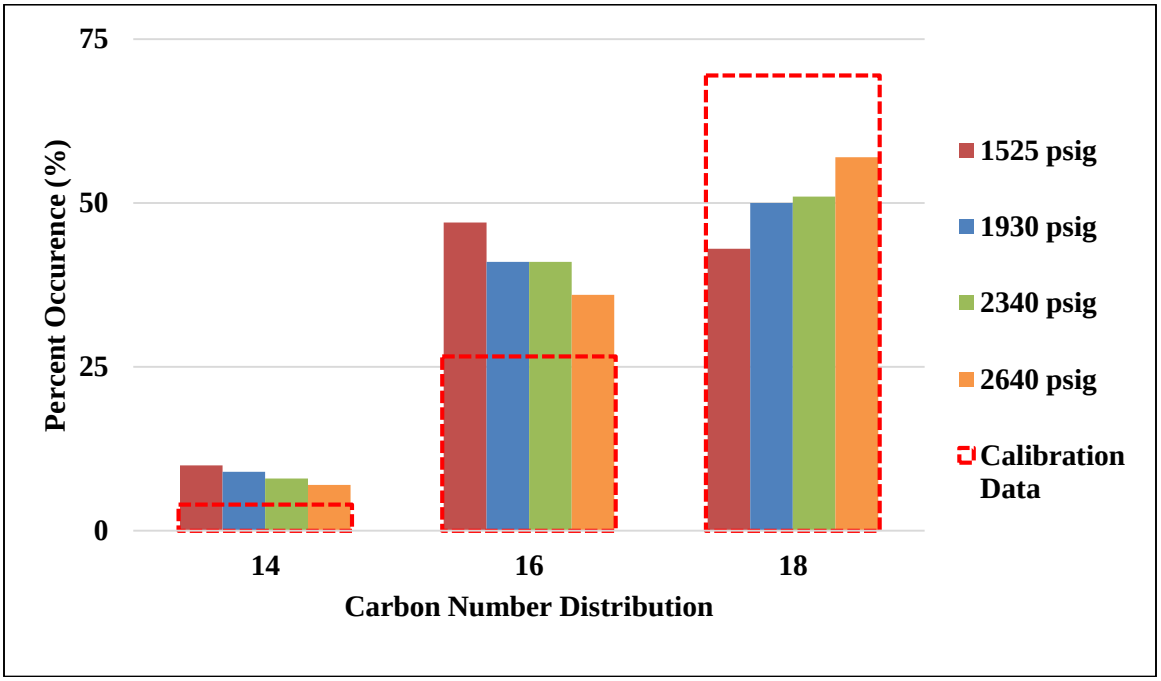

Figure 4.12: Ethoduomeen T13 carbon number tail distribution in CO_2 at a given pressure (40ºC).

4.3.2 Surfactant Solubility in the Mixture of CO_2 and CH_4

Effects of Temperature and Pressure

Methane is a main component of solution gas in hydrocarbon formations. Surfactant transport in the CO_2 phase can be influenced by the in-situ mixing of CO_2 and methane. The presence of methane reduces the solvation strength and CO_2-philicty of the system (Zheng et al., 2015). At the temperatures and pressures analyzed, methane is a gas with densities spanning 0.061 to 0.138 g/cc, therefore it cannot dissolve materials with liquid-like properties compared to supercritical CO_2 that has densities similar to water at high pressures. It can be seen from Figure 4.13 that the presence of methane interferes with solvation at high pressures around 2650 psig. For both temperatures, the solubility of Duomeen TTM drops off significantly as methane is supplemented into the system. Interestingly, the solubility reduces by 50% at around 16-17% methane dilution for both temperatures.

On another note, the CTD for Duomeen TTM is also impacted by the changes in gas composition. It can be seen in Figure 4.14 and 4.15 that methane preferentially dissolves smaller tail groups, even more than with pure CO_2. This is due to methane having weaker solvation strength than CO_2 (Zheng et al., 2015). Conclusively, all gas compositions display the same CTD spread but at different magnitudes.

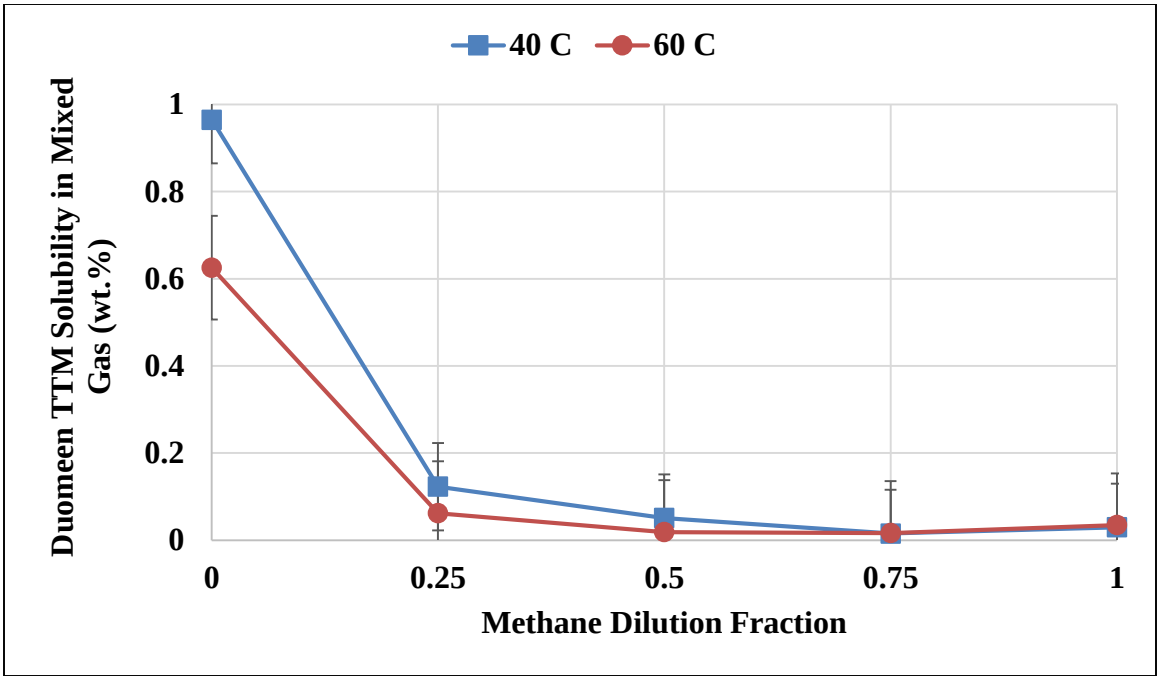

Figure 4.13: Duomeen TTM solubility in different CO_2/CH_4 ratios at 40°C and 60°C. 0 is pure carbon dioxide and 1 represents methane.

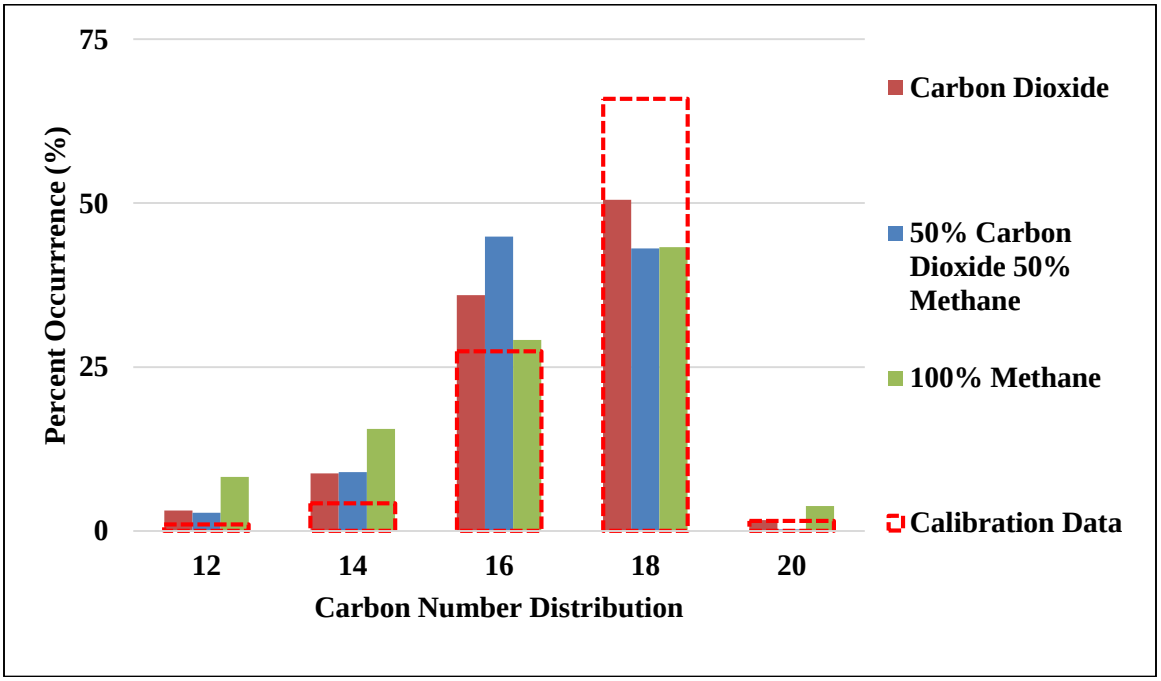

Figure 4.14: Duomeen TTM carbon number tail distribution at different mixed gas fractions at 2650 psig and 40ºC.

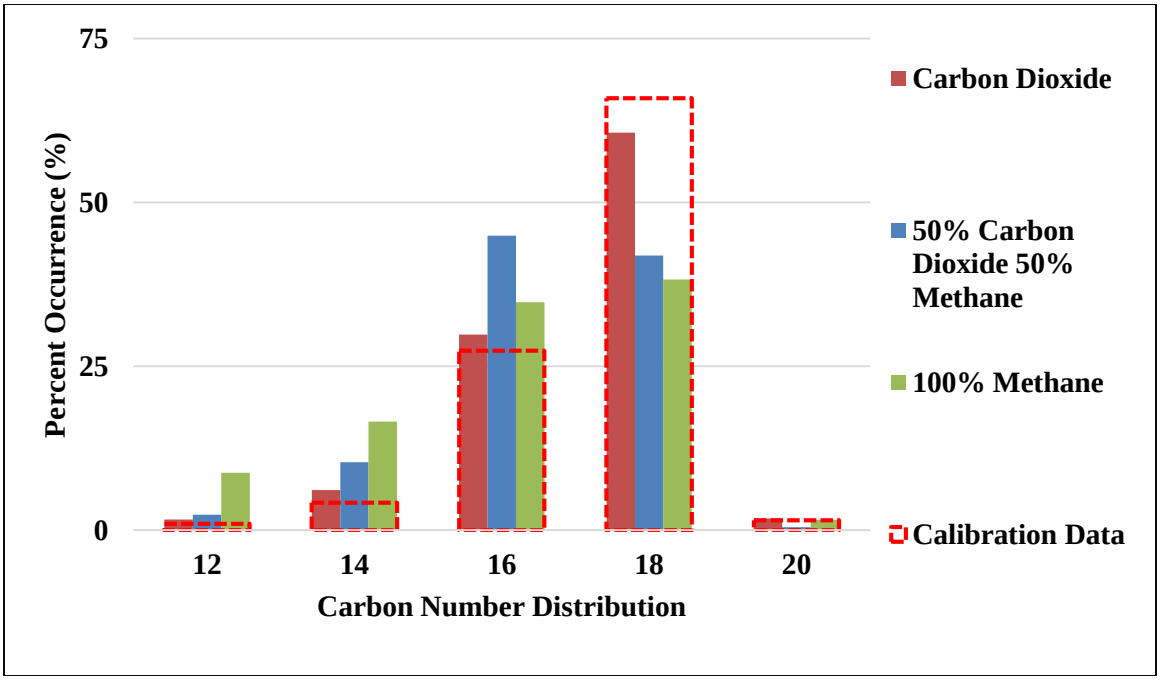

Figure 4.15: Duomeen TTM carbon number tail distribution at different mixed gas fractions at 2650 psig and 60ºC.

Effect of Chemical Structure

The solubility of Armeen DMCD, Duomeen TTM and Ethoduomeen T13 in CO_2 at different methane molar fractions are displayed in Figure 4.16. It can be shown that Armeen DMCD has the best solubility with methane dilution. The solubility reduces by 50% at 35% methane dilution. In addition, Armeen TTM sustains a solubility of 0.2 wt.% in pure methane, while the solubility of Duomeen TTM dwindles to 0.03 wt.%. One possible reason is that Armeen DMCD is smaller in terms of molecular weight and tail size compared to Duomeen TTM (AkzoNobel, 2010).

On the other hand, Ethoduomeen T13 experiences a slight increase when exposed to methane. It still remains more insoluble than Armeen DMCD, but achieves the same solubility as Duomeen TTM. Since there are only three data points for Ethoduomeen T13 further investigation should be conducted for this chemical.

Figure 4.17 and 4.18 represent the CTD of Armeen DMCD and Ethoduomeen T13, respectively. Both show that methane has a higher frequency of occurrence with smaller tail groups than other gas compositions, similar to Duomeen TTM. Again, this is due to methane having weaker solvation strength, therefore preferentially picking up surfactant molecules with the lowest molecular weight and tail group.

Some discussion points to bring up is the reason for Armeen DMCD maintaining higher solubility levels than Duomeen TTM when exposed to methane, and why Ethoduomeen T13's solubility remained unaltered at different gas fractions. Essentially, it is all based on the intermolecular, solubility and steric effects of the surfactant's functional groups and its interactions towards the gas mixture. The chemistry and interaction energies is beyond the scope of this thesis, but be a topic to look further into.

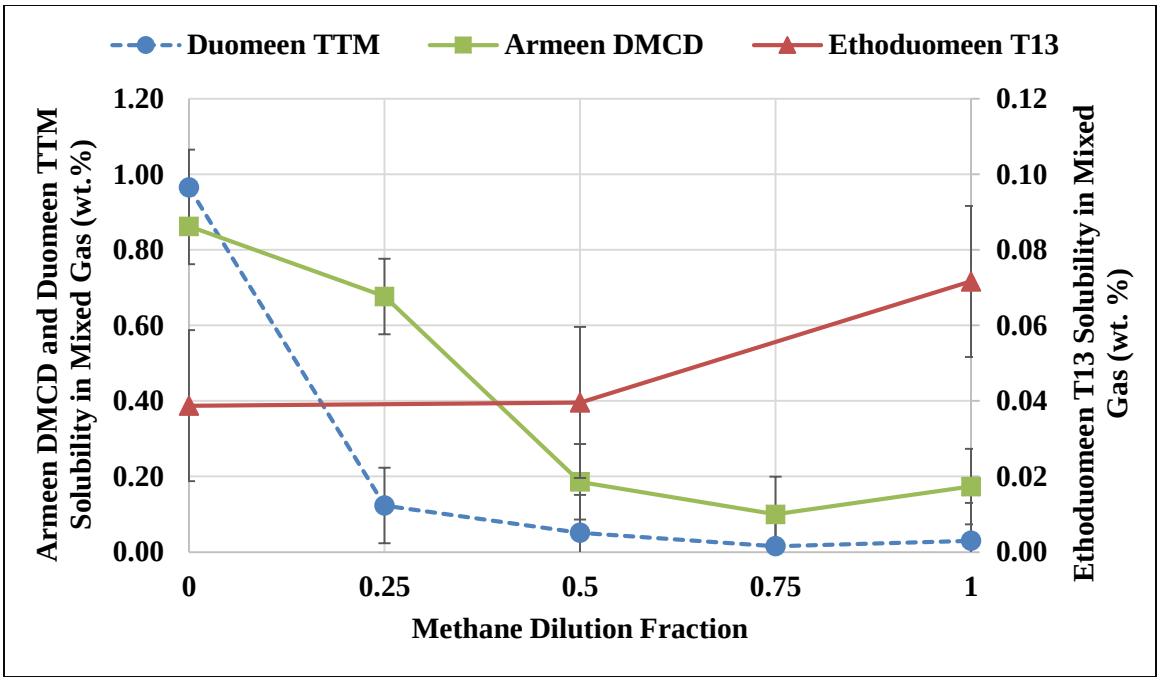

Figure 4.16: Armeen DMCD, Duomeen TTM and Ethoduomeen T13 solubility in different CO_2/CH_4 ratios at 40°C. 0 is pure carbon dioxide and 1 represents methane.

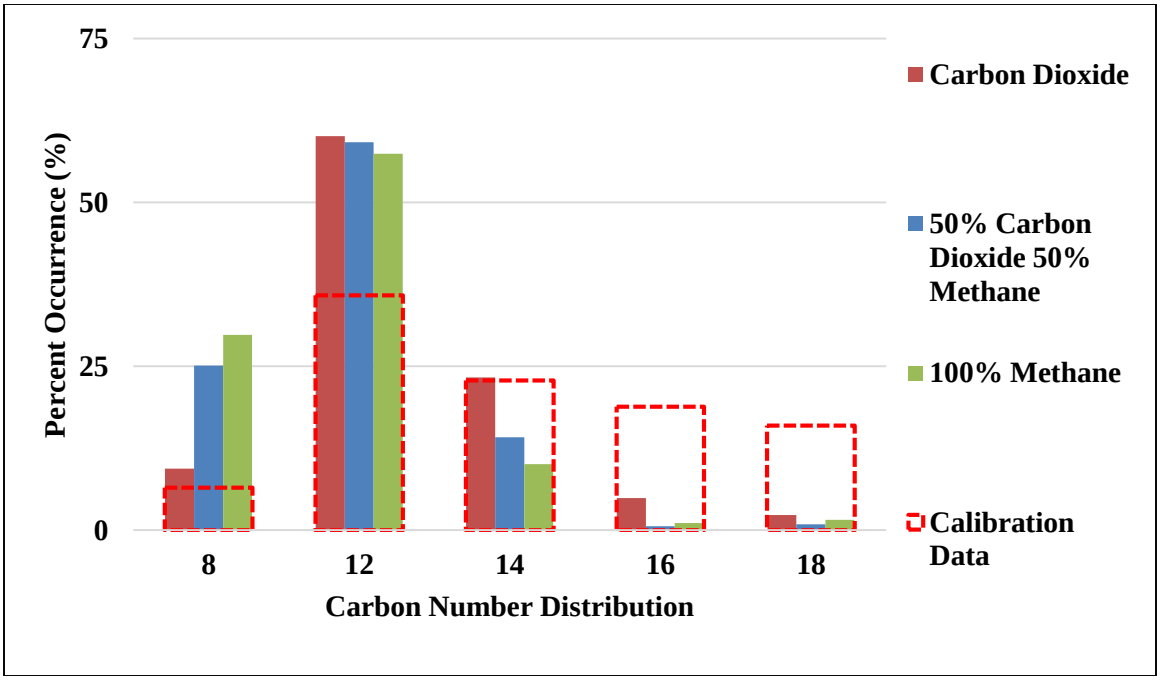

Figure 4.17: Armeen DMCD carbon number tail distribution at different mixed gas fractions at 2650 psig and 40ºC.

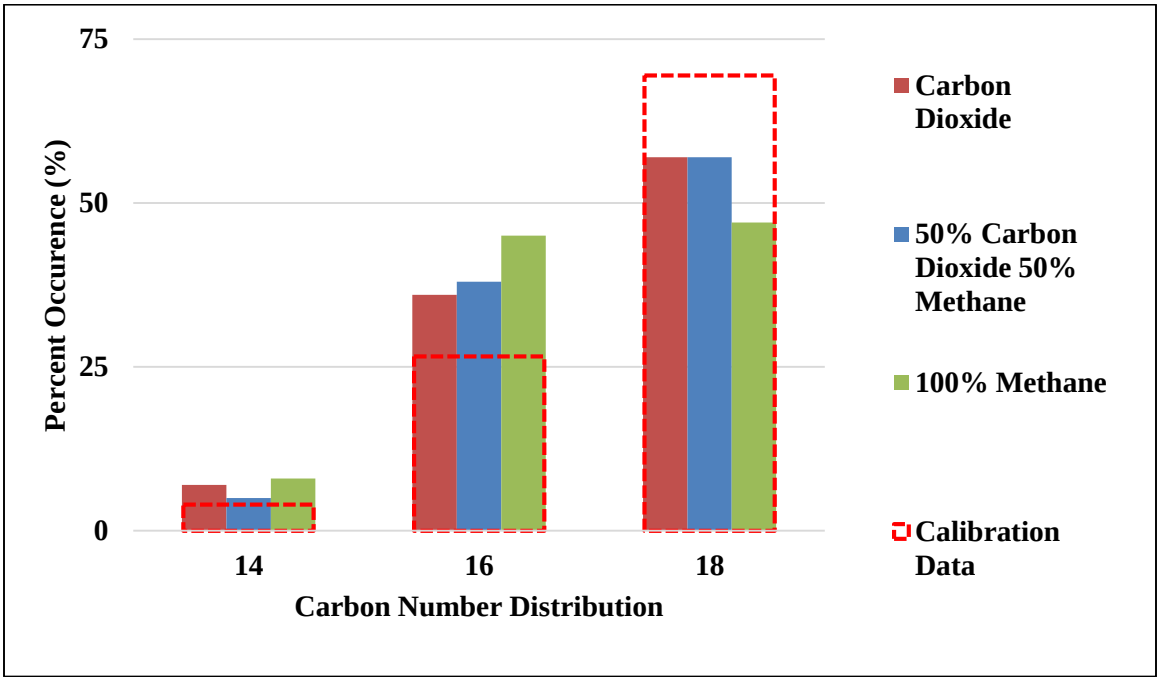

Figure 4.18: Ethoduomeen T13 carbon number tail distribution at different mixed gas fractions at 2650 psig and 40ºC.

4.3.3 Partition Results

Partition experiments were employed to determine if Duomeen TTM is hydrophilic and water-soluble under acidic conditions with 1 wt.% NaCl added into the solution. Salt and pH promotes micellar aggregation and hydrophilicity of the amine surfactant solution. The surfactant will protonate and prefer the aqueous phase at low pH. From the results, it was found that for 0.2 wt.% Duomeen TTM solution at temperatures of 60 and 80°C, the partition coefficient was less than 0.05, the weight ratio of surfactant in CO_2 to water. The surfactant solubility in water should decrease as temperature increases, due to loss in hydrogen bonding, therefore increasing the partition coefficient as temperature rises. This partition coefficient value implies that Duomeen TTM is water-soluble under acidic conditions, in agreement with the general behavior of amine surfactants. The amine head group is solvated in the water by ion-dipole interactions while the hydrocarbon tail solvates weakly in CO_2 therefore promoting a lower partition coefficient (Zheng et al., 2015).

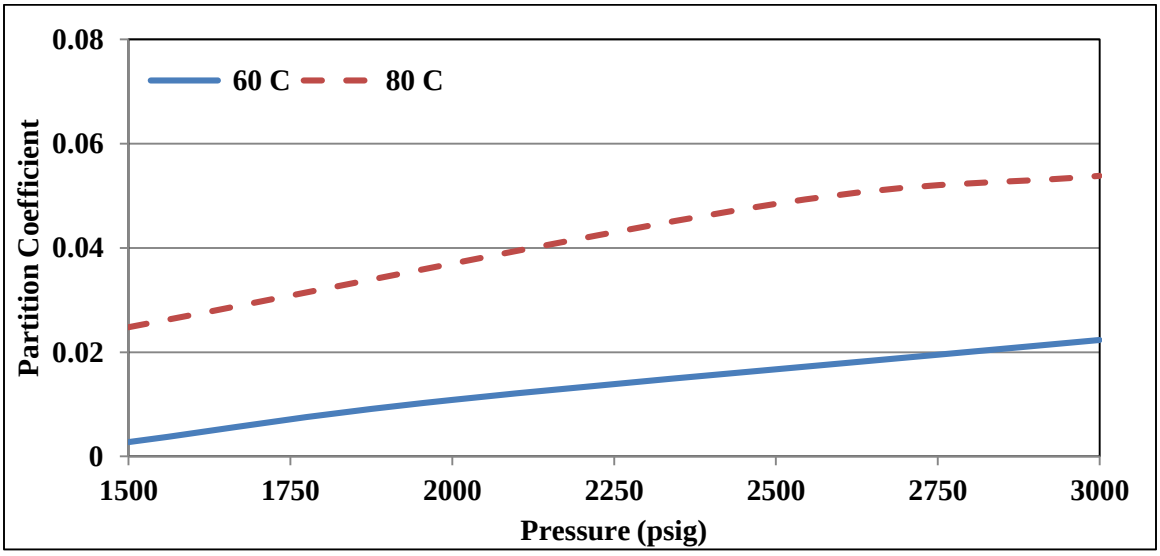

Figure 4.19: Partition coefficient (mass of surfactant in CO_2 to water) results for Duomeen TTM at different pressures and temperatures.

4.4 CONCLUSION

Solubility

- When unprotonated, Duomeen TTM is very soluble in CO_2, up to 1 wt.% at 40°C. The solubility decreases as temperature increases or pressure decreases, since these two parameters alter the solvation strength and density of CO_2.
- For Duomeen TTM and Armeen DMCD, terminal methyl groups are bulky and have large steric hindrance resulting in less surfactant-surfactant interaction and stronger surfactant-CO_2 interactions from hydrogen bonding.
- For Ethoduomeen T13, hydroxyethyl groups require a higher solvent strength to directly solubilize due to the hydrophilic nature of the head group. The -OH terminals hydrogen bond with other surfactant molecules thereby increasing surfactant-surfactant interactions while weakening surfactant-CO_2 interactions.
- Exposure to methane is detrimental to the solubility of Duomeen TTM in the CO_2 phase. The solubility decreased by 33 times at 2650 psig and 40°C when CO_2 was replaced by pure methane.
- The carbon tail distribution (CTD) remained constant at various pressures, but altered slightly with changes gas composition. Methane tended to dissolved smaller carbon tail groups than other gas mixtures due to methane's weak solvation strength compared to CO_2.
- Armeen DMCD displays the highest solubility with the presence of methane compared to Duomeen TTM and Ethoduomeen T13. If the head group composition remains fixed, as molecular weight or tail length decreases, solubility increases since the surfactant can be picked up easier at lower solvation strengths.

Partition

- Duomeen TTM has a very low partition coefficient of less than 0.05, insinuating this surfactant prefers the continuous phase at a pH of 3. Low pH results in protonation of the amine head group promoting water solubility of the surfactant, even with the high degree of hydrophobicity from the terminal and tail groups of Duomeen TTM.

Chapter 5: Rheological Characterization of Alkyl Amine Surfactants[2]

5.1 INTRODUCTION

This chapter reflects the work completed to advance and control viscoelastic properties of N, N, N' trimethyl-N'-tallow-1,3-diaminopropane, Duomeen TTM. This chemical has the capability of transitioning into a viscoelastic surfactant (VES) at concentrations above 0.2 wt.% Duomeen TTM with the addition of NaCl. The main mechanism for inducing viscoelasticity is by altering salinity, while fine-tuning pH, temperature and surfactant concentration can adjust viscosity to a desirable condition. Modifying pH changes the protonation level of the molecules; temperature controls the minimization of free energy by breaking, reformation, and branching of micellar networks, while surfactant concentration controls the aggregation density. As surfactant concentration increases, the distance between surfactant molecules decrease leading to entanglement of flexible chains and an increase in van der Waal force making it difficult for molecules to deform under stress (Sheng, 2011).

The steady-state shear rate analysis confines samples ranging from 0.2 to 2 wt.% Duomeen TTM and 5 to 25 wt.% NaCl under typical reservoir conditions and injective concentrations for flow in porous media. Rheological measurements insinuate changes in the macroscopic and microscopic behavior of the solution, as well as indicate critical degrees of freedom to prompt viscoelasticity. Along with Duomeen TTM results, investigation of three similar chemical structures will be studied to see how viscosity changes with alterations in tail and head group composition at high salinities. In all, the

[2] This chapter is adopted from the March 2016 SPE manuscript "Salt-Induced Viscoelastic Response of Alkyl Amine Surfactant", Manuscript ID: SJ-0316-0062, Status: Pending. Journal article written by Madalyn M. Liebum and co-authored by Dr. Quoc P. Nguyen. Dr. Nguyen's contribution included peer reviewing article before submission and providing resources to conduct this research.

ability to fine-tune viscoelasticity and rheological behavior is an engineering novelty, optimizing performance and efficiency for subsurface application.

5.2 MATERIALS AND PROCEDURE

Duomeen TTM (N, N, N' trimethyl-N'-tallow-1,3- diaminopropane, 95% activity) from AkzoNobel was used as received. Samples were prepared using bulk solutions composed of deionized water, pH-adjusted 11 wt.% Duomeen TTM solution, 27.5 wt.% sodium chloride (NaCl), and 2N hydrochloric acid (HCl) from Fischer Scientific. A Santorius Scale ED623S, Eppendorf Repeater Plus, and Hanna Instruments pH meter were used to weigh, prepare, and identify the pH of the samples, respectively. A TA instrument AR-G2 rheometer with smart swap analyzed all samples. The Couette concentric cylinder was selected based on the samples' fluid behavior ranging from Newtonian to viscoelastic. Relating geometry of the Couette cylinder and rotational velocity provides effective shear rate. This method is used for all results (Schramm and Wassmuth, 1994).

In the TA instrument computer program, the settings were adjusted to the following:

- Conditioning Step:
    - Equilibration time: 60 seconds
    - Selected desired temperature: most experiments were at 40°C
- Steady-State Step:
    - Selected steady-state shear rate option
    - Sample time: 30 seconds
    - Total time: 2:30 minutes
    - Equilibrium attained after three consecutive sample times had less than 5% change in shear stress and torque

5.3 RESULTS AND DISCUSSION

This section entails the effects of salinity, pH, temperature and chemical structure on the viscoelasticity of the solution. Appendix B will provide additional results encompassing the relaxation time, G' and G" of seven viscoelastic Duomeen TTM solutions.

5.3.1 Effects of Salinity for Duomeen TTM

The type and amount of salt portrays a significant role in developing viscoelastic solutions. The Cl^- ions shrink the double layer around each head group and screen electrostatic repulsion allowing surfactant molecules to aggregate and gradually transform into various micellar structures. To attain viscoelasticity, a higher concentration is required if using a weak, non-binding salt, such as NaCl, since this type of salt shields the surface of the micelles unlike strong hydrotropic salts that penetrate into the micellar structure initiating viscoelasticity at lower concentrations. (Hoffmann, 1994; Calabrese et al., 2015; Trickett and Eastoe, 2008).

In general, applying the packing parameter relationship, as salt concentration increases in the solution, the effective head group size shrinks leading to a rise in the packing parameter value. This increase can facilitate micellar growth from spherical to cylindrical thereupon entangle and elongate to form worm-like structures (Kalur and Raghavan, 2005). In other words, the addition of salt reduces the critical micelle concentration, allowing lower surfactant concentrations to transform into a viscoelastic state (Lee et al., 2010). In addition, Truong (2001) pointed out that high NaCl concentrations promote micellar flexibility of the system providing a favorable environment for the growth of worm-like micelles (Maeda et al., 2001).

Shown in Figure 5.1, the addition of NaCl significantly affects viscosity, notably for solutions encompassing high surfactant concentrations. For each surfactant

concentration at a typical reservoir shear rate of 10 s^{-1}, the transition slope implies that the fluid behavior changes from Newtonian to pseudo-plasticity at a fixed range of salinities. This means that the onset of the transition slope shifts to higher salinities ranges when surfactant concentrations decreases, therefore delaying viscoelasticity. It can be seen that all the curves converge at the lowest salinity analyzed; meaning that even with changes in surfactant concentration at 5 to 10 wt.% NaCl, the concentration does not seemingly alter the Newtonian behavior due to low scission energy (the difference in end cap energy and electrostatic energy of the micelle), but becomes a pivotal factor after surpassing a critical salt concentration near the beginning of the transition region. Principally, this figure displays how salinity triggers the growth of micellar structures thereby increasing the apparent viscosity of the solution, while the surfactant concentration magnifies and enhances the salinity's impact on viscosity. It is important to note that at high salinities, the viscosity appears to approach a plateau, supposedly resulting in maximum entanglement or growth of the micelles due to thermodynamic and hydrodynamic limitations or micellar branching (Mu and Li, 2001). Calabrese et al. (2015) mentions at high salt environments, branching becomes more energetically favorable as scission energy increases leading to larger micellar formations due to the weakening in electrostatic repulsion from the salt.

Figure 5.2 displays how shear rate imposes significant changes in viscosity. Four surfactant concentrations were selected to visualize viscosity profiles against shear rate at three different salinities: 20 wt.%, 15 wt.%, and 10 wt.% NaCl. At a shear rate of 1 s^{-1}, the viscosity drops nearly a magnitude when the surfactant concentrations are halved at 20 wt.% NaCl. This observation suggest that micellar growth and viscosity depends on the aggregation density and micellar size, which is associated with surfactant concentration. As surfactant concentration increases, the micelles are more prone to overlap and entangle

into a transient network due to a larger presence of surfactant molecules in the solution (Collura et al., 2001).

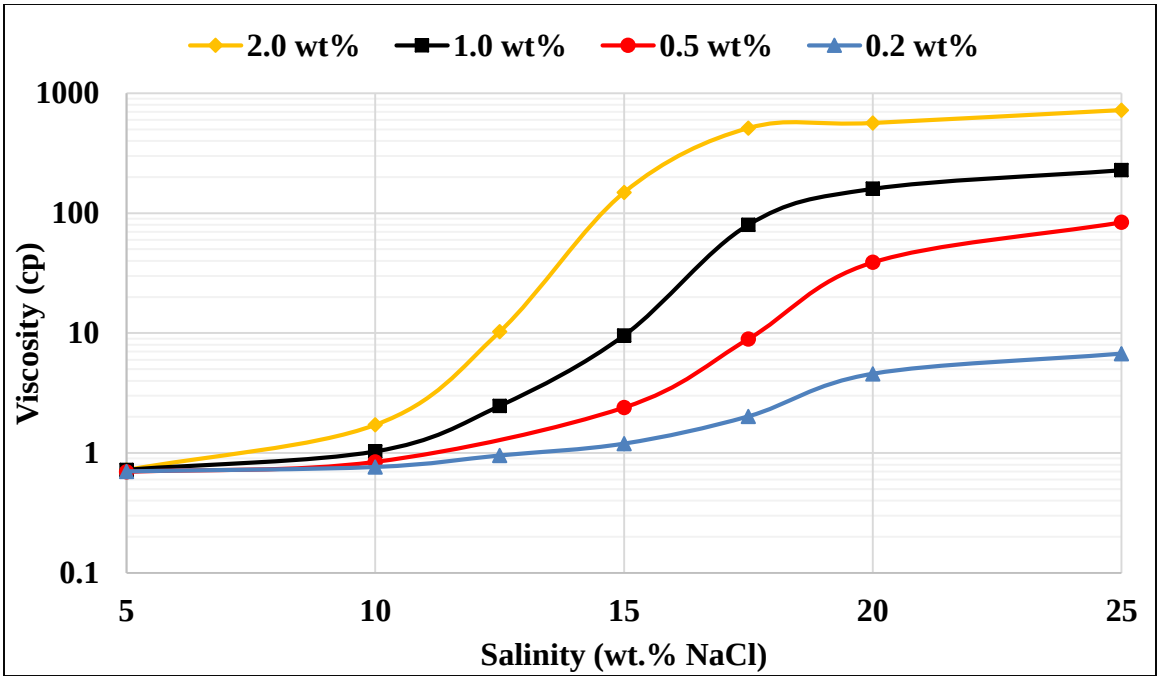

Figure 5.1: Changes in Duomeen TTM concentration (wt.%) at a fixed shear rate (10 s^{-1}) conducted at 40°C. Viscosities at low salinity behave Newtonian then exhibit a transition region and plateaus when solution becomes viscoelastic with pseudo-plastic behavior.

In addition, shear thinning or pseudo-plasticity shown at high salt concentrations suggests disentanglement of the system and alignment of the wormlike micelles under shear flow (Acharya, 2006; Shchipunov and Hoffmann, 2000; Trickett and Eastoe, 2008). This alignment causes viscosity degradation since the micellar structure orients in a way that minimizes resistance to flow and friction causing the solution to move as a single object (Lin et al., 2001). Furthermore, a slight degree of shear thickening occurs at low salt concentrations and dilute solutions leading to a fractional viscosity increase of 0.2 cp from 1 to 100 s^{-1}. This many indicate hydrodynamic instabilities in the solution above a critical

shear rate, most likely attributed to the formation of non-equilibrium shear-induced micellar phase transitions (Barentin, 2001; Berret, 1998; Hu et al., 1998). In addition, Koehler (2000) states that shear thickening under steady shear can occur when the solutions' surfactant concentration is close to the critical micelle concentration.

It has been reported that numerable viscoelastic surfactant solutions display shear banding in which the micellar solution becomes unstable and splits into shear bands with spatial heterogeneities consisting of different viscosities, velocities and/or internal structure (Cates, 1994; Rehage and Hoffmann, 1991). The occurrence of velocity gradient or vorticity banding depends on the orientation of the band stratification. For velocity gradient banding, a non-monotonic relation between shear stress and shear rate occur where stress remains constant at a range of shear rates typically under extreme shear thinning conditions (Anderson, 2006). According to Kalur and Raghavan (2005), shear banding and shear thinning behavior allude to the existence of worm-like micelles due the dynamics of relaxation, breakage and recombination of the micellar structure as well as the alignment of the chains and disentanglement with respect to the flow gradient (Hu and Lips, 2005). These listed references provide more information about the relation between shear banding and worm-like micelle structures (Cappelaere and Cressely, 1997; Calabrese et al., 2015; Britton, 1999; Miller and Rothstein, 2007; Dhont and Briels, 2008; Manneville, 2008; Delgado et al., 2009; Pipe et al., 2010; Fardin et al., 2015; Thareja et al., 2011; Helgeson et al., 2009; Liberatore, 2009; Hu and Lips, 2005; Hu et al., 2008; Yesilata et al., 2006).

It can be seen in Figure 5.2 that Duomeen TTM at certain concentrations at 1 and 2 wt.% Duomeen TTM and salinities at 20 and 25 wt.% NaCl could display a stress plateau and perhaps the presence of wormlike micelles. In this regime, the flow becomes strongly time-dependent as stress fluctuates between a maximum and minimum value at a given shear rate (Yesilata et al., 2006). The time for stress to equilibrate in the plateau region

can be two or more magnitudes higher than the viscoelastic relaxation time of the fluid, causing uncertainty of the plateau's slope, curvature and reproducibility of the data (Yesilata et al., 2006). Moreover, no apparent stress plateau is detected at lower salt and surfactant concentrations, as stress remains linear representing Newtonian behavior. In addition, at shear rates above or below the shear banding or stress plateau regime, the stress coincides linearly with the changes in shear rate.

Nonetheless, a stress plateau can represent other causes rather than shear banding when interpreting solely shear rate rheological measurements, for instance wall and stick slip, elastic instabilities, shear induced phase separation (SIPS) (Thareja et al., 2011), Taylor-instabilities at high shear rates (Dhont and Briels, 2008), geometry, uncertainty from stress measurements, and inherent stress gradient from device can cause similar responses (Hu et al., 2008). According to Manneville (2008), a plateau in shear stress provides insufficient evidence of the shear banding presence since the Couette geometry only measures global measurements and shear banding requires more localized characterization tools to measure the organization and microstructure of the bands. Further investigation to confirm the presence of shear banding (gradient or vorticity) at a wider range of shear rates (10^{-2} to 1000 s^{-1}) and using other techniques, such as particle velocimetry (Hu et al., 2008), NMR (Dhont and Briels, 2008), SANS (Dhont and Briels, 2008), SAXS (Manneville, 2008), SALS (Dhont and Briels, 2008), photon correlation spectroscopy (Manneville, 2008), ultrasonic velocimetry (Dhont and Briels, 2008), bifringence (Dhont and Briels, 2008), and turbidity measurements (Manneville, 2008) shall be conducted.

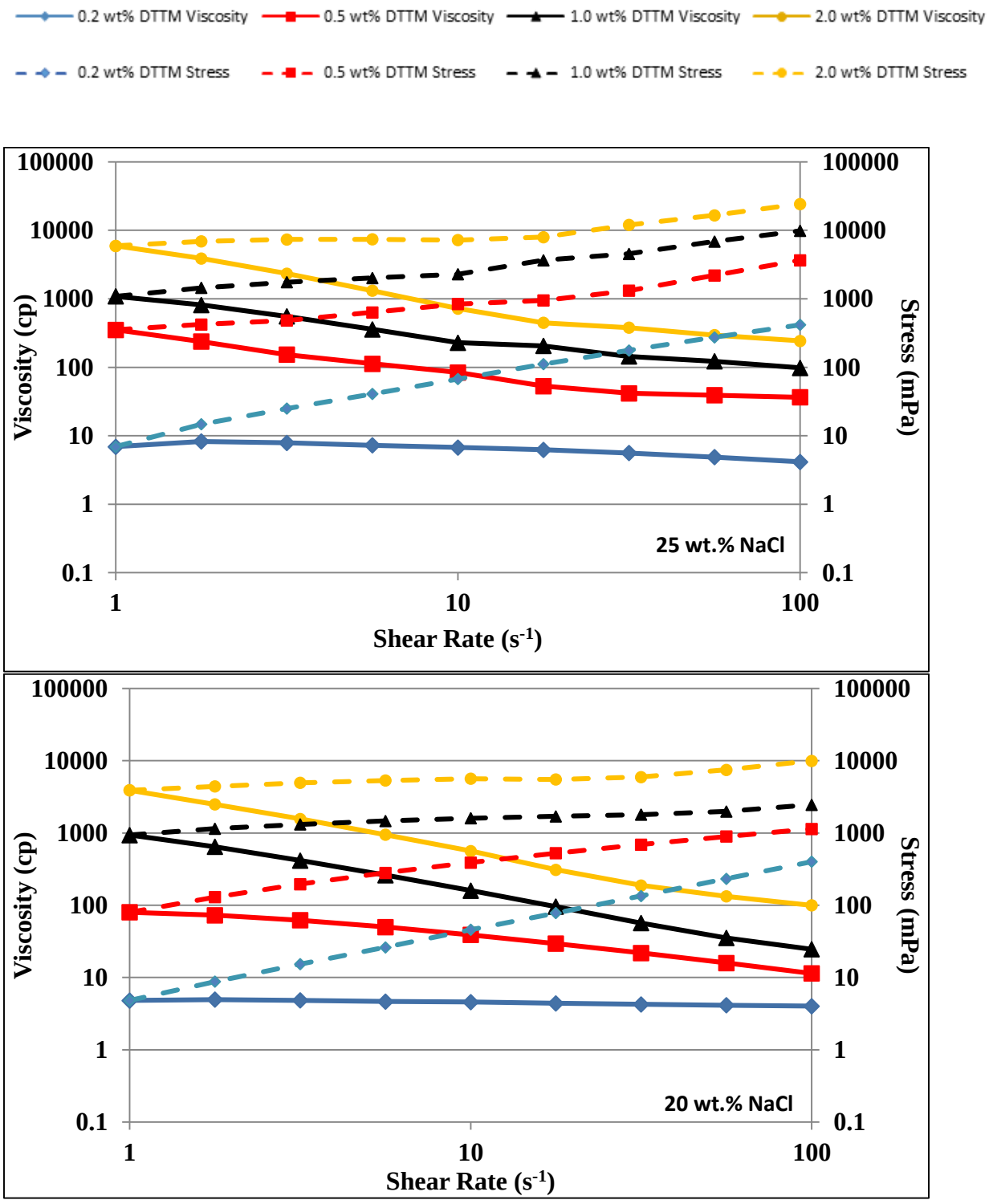

Figure 5.2: Steady-state shear rate at 40°C at 25 and 20 wt.% NaCl.

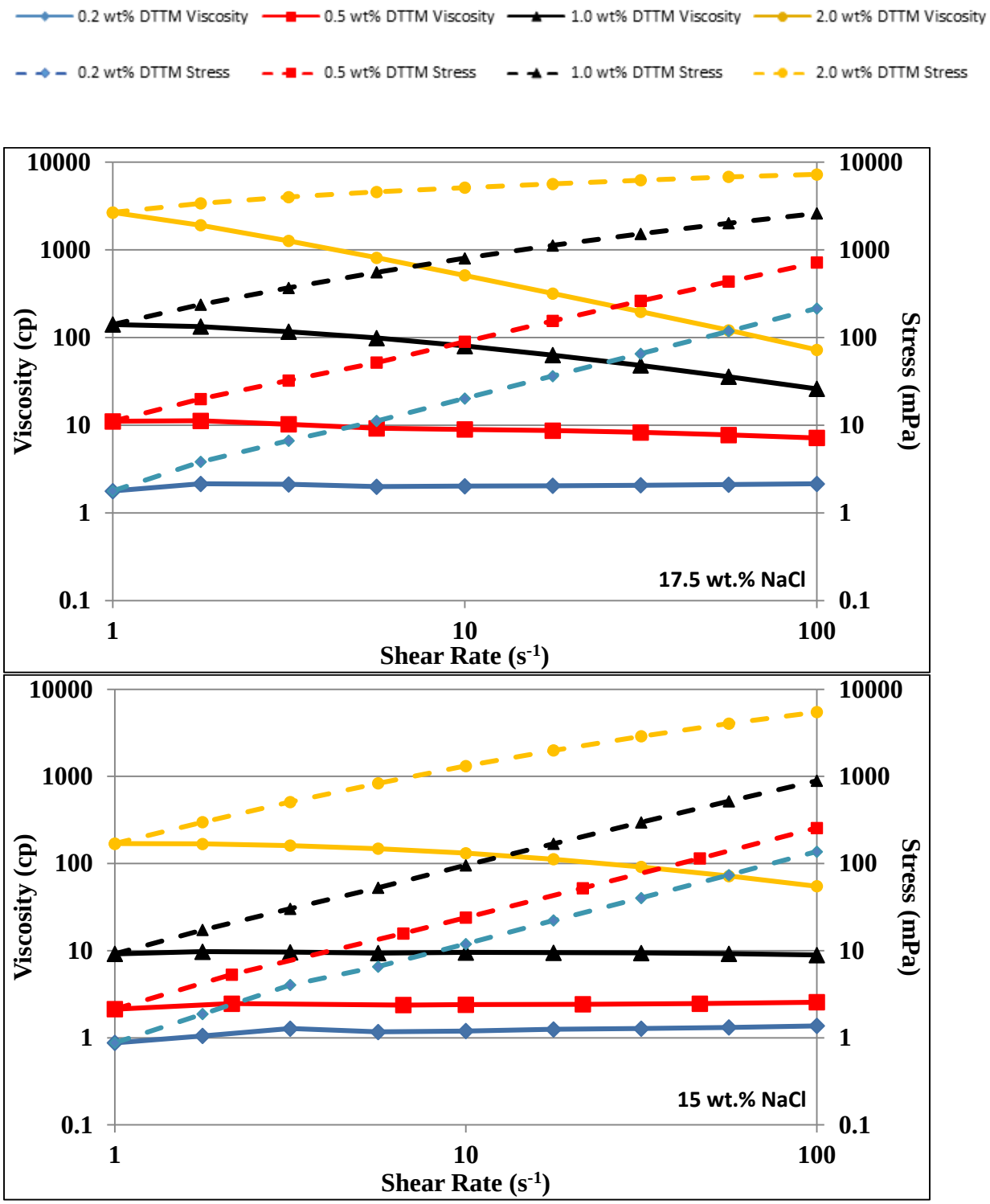

Figure 5.2 Cont.: Steady-state shear rate at 40°C at 17.5 and 15 wt.% NaCl.

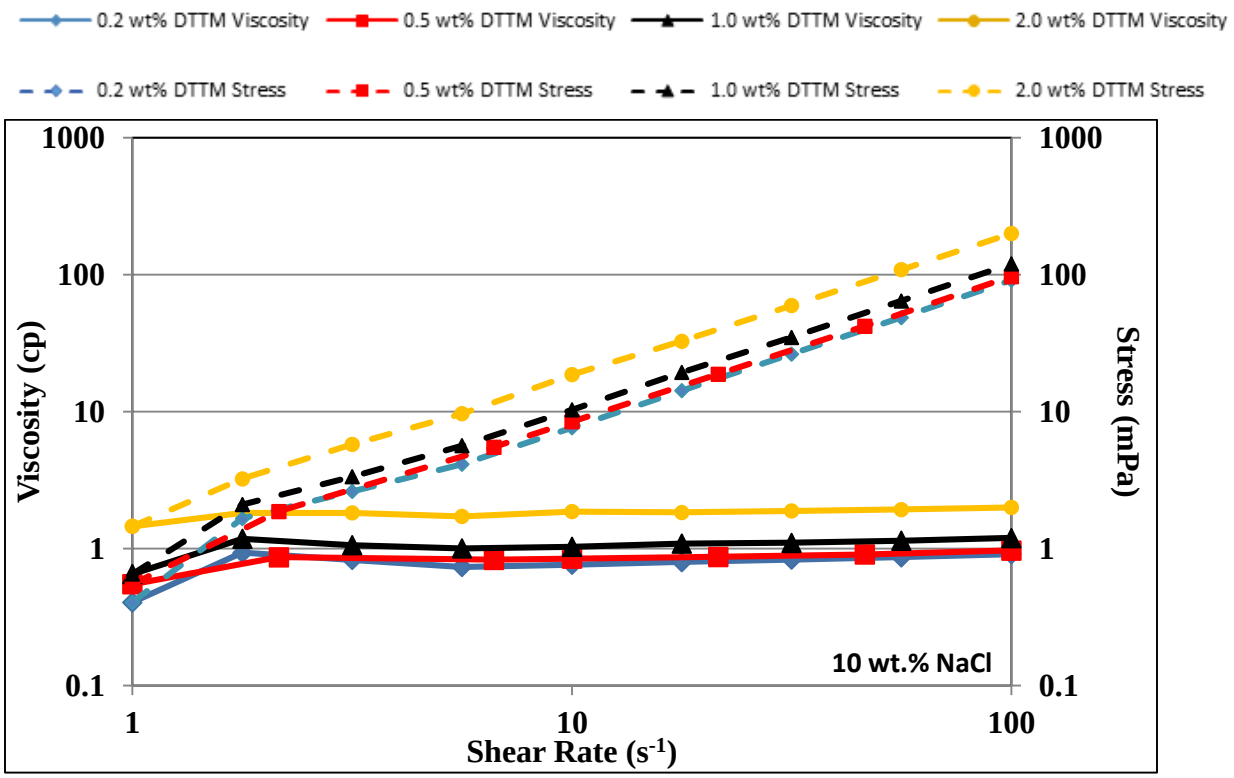

Figure 5.2 Cont.: Steady-state shear rate at 40°C and pH around 5 to 7. Each plot has a different salinity value ranging from 10 wt.% to 25 wt.% NaCl, the solid lines represent the viscosity profile and dotted lines signify shear stress at various surfactant concentrations from 0.2 wt.% to 2 wt.% Duomeen TTM. Shear stress can indicate the presence of shear banding in a solution and viscosity specifies Newtonian and non-Newtonian (notably pseudo-plasticity) behavior.

5.3.2 Effects of pH for Duomeen TTM

Duomeen TTM is characterized as a nonionic compound at high pH, but protonates into a cationic surfactant under acidic conditions. Effects of protonation on viscosity are well established for amine cationic surfactants and discussed in this section (Maeda et al., 2001; Wang et al., 2008). According to the packing parameter model, as the head group enlarges from amine protonation from the addition of hydrogen ions, the "a" parameter from Eq. 2.17 increases leading to smaller micellar structures. However, when pH rises,

the effective head group becomes smaller due to the reduction of ionic repulsion causing micelles to tightly compact and transform into cylindrical, vesicles, or lamellar structures.

To support this relationship, Maeda et al. (2001) stated for tetradecyldimethylamine oxides, the half-ionized state (α=0.5) can have viscosities magnitudes greater than solutions at other protonation states since the micelle size exhibits a maximum and the CMC of the solution is at a minimum. Wang et al. (2008) contributed by describing the pH and protonation effects of a surfactant containing multi-amine head groups, bis (amidoethyl-carbamoylethyl)-octadecylamine. It was concluded that at the full ionized state (α=1), the surfactant solution forms small micelles due to an increase in repulsion between same-charged head groups at low pH, and the micelles transforms to a globular vesicle morphology at neutral pH since deprotonation decreases repulsion leading to large micellar aggregates.

Figure 5.3 displays how viscosity evolves with shear rate (1 to 100 s^{-1}) based on the addition of HCl from 3 wt.% to 30 wt.% From the results, after a shear rate of 10 s^{-1}, the curves start to overlap and converge to a single viscosity of 34 cp at 100 s^{-1}. Additionally, at shear rates of 1 s^{-1}, the viscosity profiles are widely distributed than at high shear rates, suggesting the impact of pH on flow is limited to a finite range of shear rates.

In terms of viscoelasticity, all solutions observed to be polymer-like to some degree before conducting the experiment, even at a pH levels near zero. One reason can be attributed to the amount of Cl^- ions from the 20 wt.% NaCl salt solution and added HCl providing enough electrostatic screening to reduce repulsion amongst surfactant molecules. This effect is offset by the amount of H+ ions present in the solution that push to form smaller micelles because of hydrogen bonding and hydration of the solution.

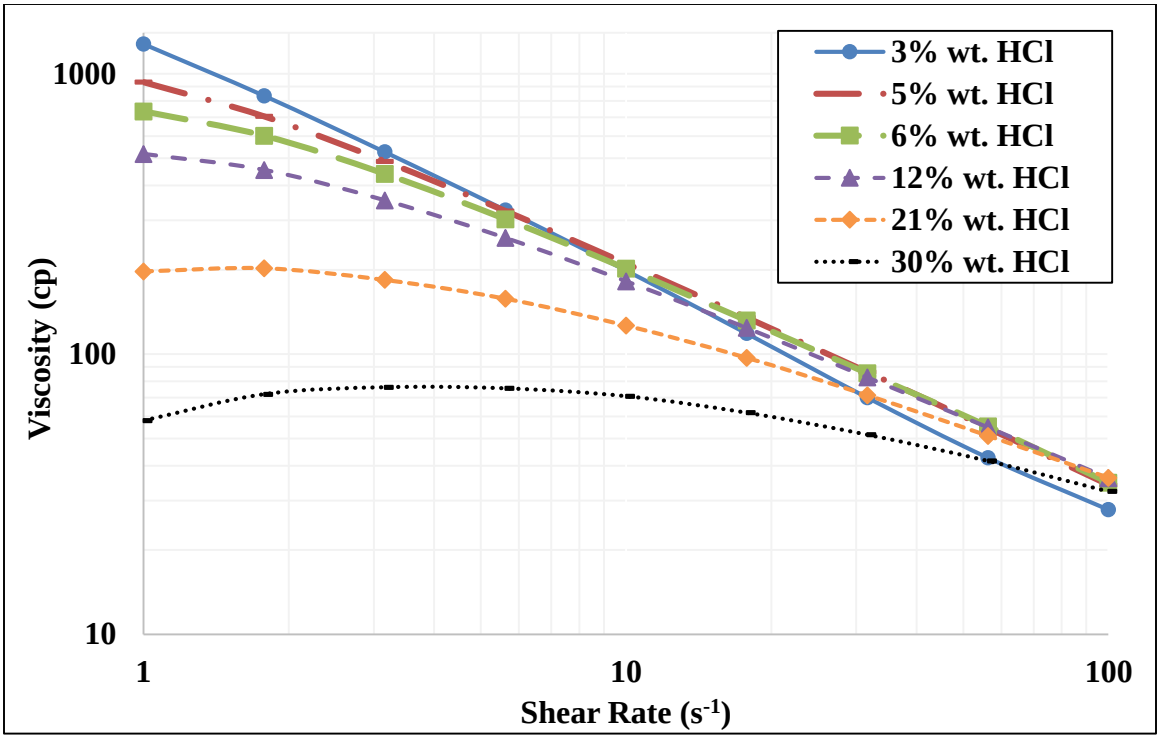

Figure 5.3: Steady shear rheology with various amounts of HCl added for pH adjustment conducted at 1 wt.% Duomeen TTM solution, 20 wt.% NaCl, and 40°C. Acidic viscosity distribution apparent at low shear rates, but merge to a characteristic viscosity value at higher shear rates. All viscosity profiles show a degree of viscoelasticity and pseudo-plasticity behavior.

5.3.3 Effects of Temperature for Duomeen TTM

For this surfactant, unusual temperature behavior was observed, where viscosity initially rises until reaching an inflection or critical temperature point in which viscosity begins decreasing afterwards with temperature. Three prominent factors alter the location of the turning point and viscosity profile of a solution; surfactant concentration, salinity and shear rate. According to Raghavan and Kaler (2001), this "enhancement" in viscosity suggests that not all of the micelles entangled to form wormlike micelles at low temperatures. In addition, Zhao et al. (2015) and Kalur et al. (2005) stated that when

temperature increases the salt ions can desorb from the micelles leading to a decline in surface charge and a promotion in viscoelasticity. In addition, Zhang et al. (2016) reported that at high salinities, thermo-induced thickening behavior due to hydrogen bonding and thermal stability of the viscoelastic solution increases the viscosity. Trickett and Eastoe (2008), Koehler (2000) and Calabrese et al. (2015) noted micelles grow and entangle before the inflection point due to the minimization of free energy, but after the turning point the onset of micellar branching occurs (decreases the effective entanglement micellar length to distance between breaking points) leading to a decrease in viscosity. In addition, Trickett and Eastoe (2008) observed only a range of surfactant concentrations display this viscosity enhancement phenomenon and the critical temperature where the turning point exists is a function of surfactant concentration and shear rate. Thus, in general, as the temperature increases, micelles elongate and entangle into chains until the competing effect of temperature surpasses the entanglement process and initiates micellar branching. When this happens, the inflection point occurs and viscosity starts to decline.

Figure 5.4 characterizes how temperature changes with steady state shear rate at 1 wt.% Duomeen TTM solution and 20 wt.% NaCl. It can be seen that at low shear rates, the viscosity is more dispersed with temperatures ranging from 1076 cp at 50°C to 109.4 cp at 80°C, then as shear rate increases, solutions display shear thinning behavior resulting in a concentrated viscosity range at all temperatures. This suggests that temperature plays an important role in altering apparent viscosity in low shear environments, which according to Kalur et al. (2005) displays representative behavior of wormlike micelles.

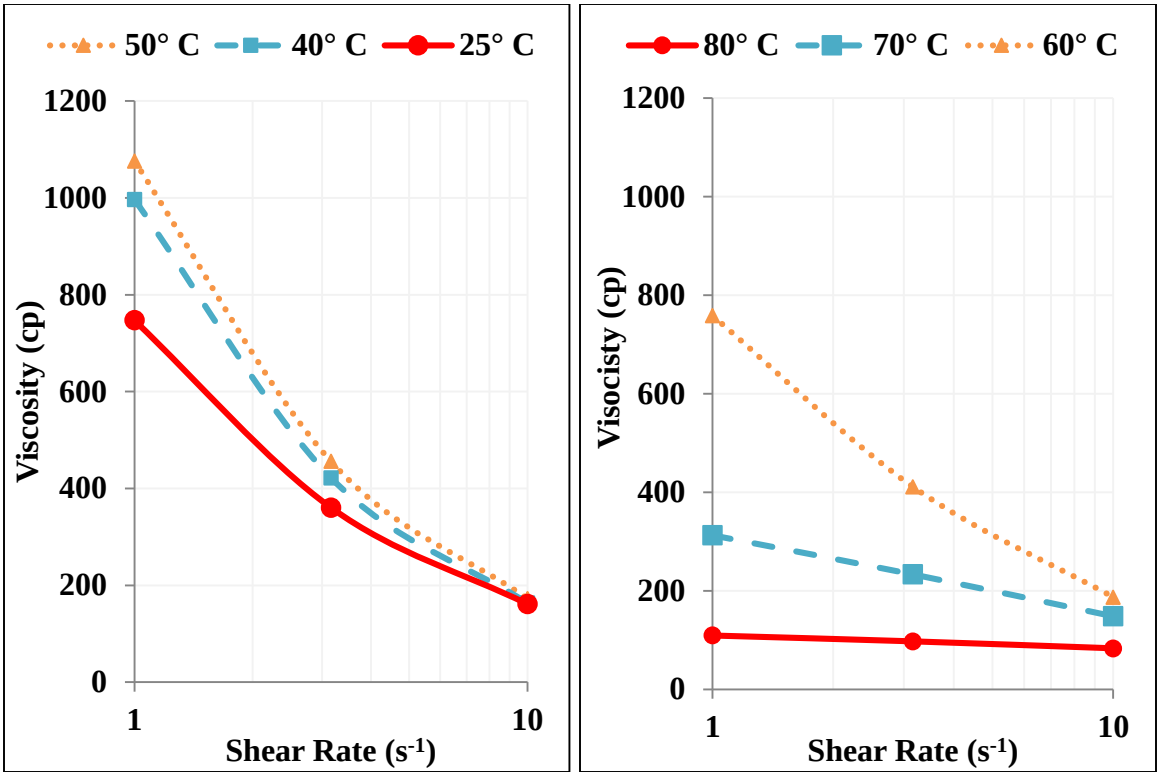

Figure 5.4: Steady-State shear rheology at 1 wt.% Duomeen TTM, 20 wt.% NaCl solution at temperatures ranging from 25°C to 80°C with pH around 5 to 7. The first plot on the left side represents how viscosity increases with temperature and from the right plot, the viscosity of Duomeen TTM begins to decline at a smaller degree of shear thinning.

From another perspective in Figure 5.5, with fixed shear rates of 1 s^{-1} and 10 s^{-1} at 1 and 0.5 wt.% Duomeen TTM, the viscosity increase at low temperatures can be visually seen for all three curves followed by the inflection point then a viscosity drop-off afterwards. The inflection point occurs at different critical temperature points for each curve. First, at a fixed surfactant concentration at two different shear rates, the inflection point shifts to higher temperature as shear rate increases. The difference in temperature is around 10°C, but higher shear rates display a lower margin of viscosity enhancement as mentioned above. Second, comparing surfactant concentrations at a rate of 10 s^{-1}, as surfactant concentration decreases the inflection point translates to a lower temperature for

the 0.5 wt.% surfactant solution, it is conceivable that the inflection point will disappear at a low surfactant concentration concluding that viscosity enhancement is limited to a fixed surfactant concentration range for a given salinity. Further test to explore the impact of salinity and surfactant concentration for this type of chemical is advisable.

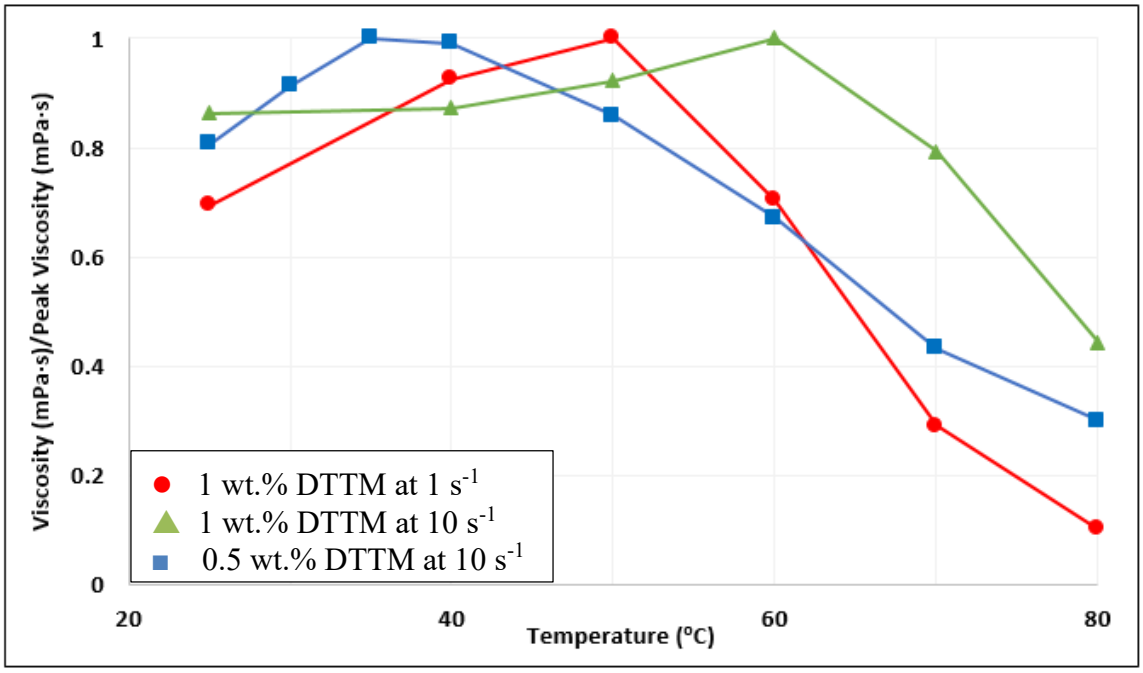

Figure 5.5: Fixed shear rate of 1 s^{-1} and 10 s^{-1} for 1 wt.% and 0.5 wt.% Duomeen TTM at 20 wt.% NaCl Solution with pH around 5 to 7. Viscosity values were normalized to the peak viscosity for each curve in order to more clearly analyze the turning points and critical temperature values.

5.3.4 Effects of Chemical Structure

Rheological properties were conducted for four cationic surfactants: Armeen DMCD, Duomeen TTM, Ethomeen C12, and Ethoduomeen T13. Structures are shown in Figure 5.6.

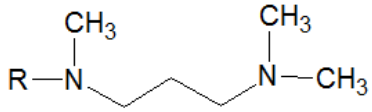

Duomeen TTM:
N, N, N' trimethyl-N'-tallow-1,3-diaminopropane

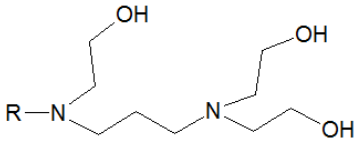

Ethoduomeen T13:
Tris(2-hydroxyethyl)-N-tallowalkyl-1,3-diaminopropane

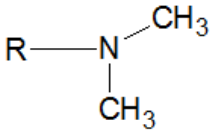

Armeen DMCD:
Distilled dimethyl, cocoalkylamine

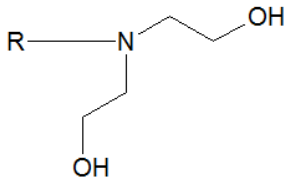

Ethomeen C12:
Hydroxyethyl cocoalkylamine

Figure 5.6: Chemical Structures analyzed for viscoelasticity

With diverse combinations of hydrophobic tail lengths, functional groups, and quantity of nitrogen ions available, it is apparent that each surfactant will behave differently with changes in surfactant concentration and interact uniquely in the presence of salt. This section will analyze all four chemicals at two different salinities, 20 wt.% and 25 wt.% NaCl, to investigate the onset of viscoelastic behavior, if any, for each chemical composition. Figure 5.7 illustrates the viscosity and fluid profile of each surfactant as salinity changes from 20 wt.% to 25 wt.% NaCl. Each chemical was tested at 1 wt.% and 40°C with pH around 6. It can be shown that strong viscoelasticity only occurs with Duomeen TTM at both salinities, while Ethoduomeen T13 and Armeen DMCD are weakly

viscoelastic at 25 wt.% NaCl. Ethomeen C12 does not show signs of shear thinning or containing viscoelastic properties, which agrees with recent literature about this chemical.

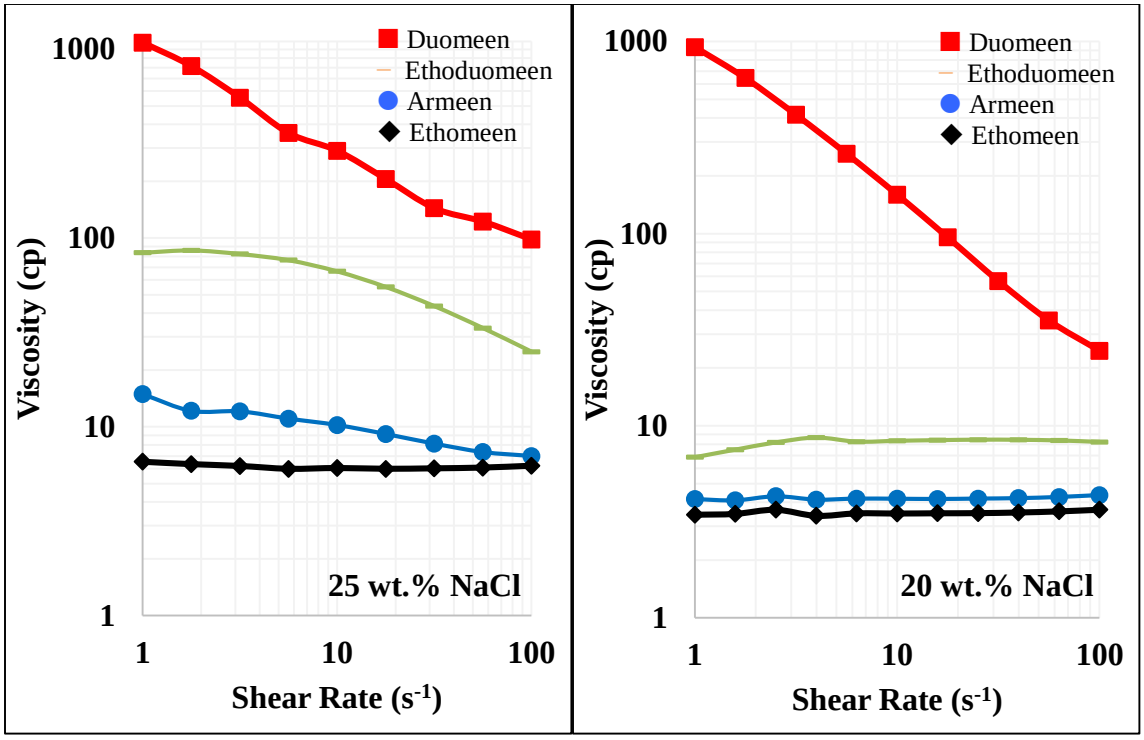

Figure 5.7: Viscoelastic comparison amongst chemical structures: 25 and 20 wt.% NaCl with 1 wt.% surfactant concentration at 40°C. Duomeen TTM had the highest viscosity under both salt concentrations while Ethomeen performed the poorest not showing any signs of viscoelasticity.

Some reasons behind the changes in viscoelastic response due to modifications of the chemical structure is discussed below:

Hydrophobic Tail Group

The length and composition of the tail is of primary importance when it comes to altering rheological properties of the solution (Raghavan and Kaler, 2001). In this case, chemicals with coco-based tails, such as Armeen DMCD and Ethomeen C12 typically

contain 12 to 16 carbon atoms while the Duomeen TTM and Ethoduomeen T13 tallow tails consist of 14 to 18 carbons. According to Raghavan et al. (2002), as the alkyl tail length lessens, synergism in self-assembly decreases, leading to weak micellar growth and a small rise in viscosity. When the tail length increases, the interaction among the tail groups becomes stronger and more entangled causing a dramatic growth of micellar chains and a rise in viscosity (Raghavan et al., 2002).

Terminal Functional Group Structure in Head-Group

In addition, terminal head group branches can also attribute to the alterations in rheological properties. Branches consisting of hydroxides or ethoxylates are more hydrophilic compared to methyl branches. The hydrophilicity induces a more hydrating atmosphere for the surfactant molecule and aids its dissolution in water. The presence of hydrophobic branches, such as methyl groups found in Duomeen TTM and Armeen DMCD, can dehydrate the surfactant molecules with excess salt in the aqueous solution. This hydrophobicity favors the growth of long micelles, since according to Raghavan et al. (2002), hydrophobic molecules have higher end-cap energy, in which end-cap energy is exponentially proportional to the micellar length (Raghavan and Kaler, 2001; Berret, 1997).

Hydrophilic Nitrogen Ions in Head Group

Furthermore, the amount of nitrogen ions present in the head group can contribute to the growth of micellar structure due to changes in molecular interactions based on the degree of protonation. As stated in the pH results section, the protonation process ionizes each nitrogen one-by-one in a two-step process for diamines, while monoamines occur in a one-step process. This means surfactants with a single nitrogen ion will fully protonate at a higher pH than molecules with two nitrogen ions due to the amount of H^+ ions required.

Since monoamines are at a more protonated state than diamines at a higher pH, the micellar structures for each type should be dissimilar due to differences in ionic repulsion amongst molecules. When the surfactant molecules are fully protonated the micelles tend to self-assembled into smaller spherical aggregates since they all possess the same ionic charge resulting in an increase in electrostatic repulsion and effective head group size of the molecules. On the other hand, molecules that are partially protonated have mix ionic charge making them prone to self-assemble into larger micellar aggregates, such as cylindrical to globular, due to the hindrance of electrostatic repulsion among the surfactant molecules.

CMC and Critical Salt Concentration

Lastly, shown for Duomeen TTM in the next section, the onset of viscoelastic behavior occurs at different salt concentrations for each surfactant concentration. If the transition region in which the fluid transforms from Newtonian to non-Newtonian behavior is called the critical salt concentration (CSC), the CSC should be different for each composition due to changes in electrostatic interaction among salt and surfactant molecules, CMC of the chemical, thermodynamic and hydrodynamic behavior, as well as its degree of protonation. Duomeen TTM has the lowest CSC followed by Ethoduomeen T13, then Armeen DMCD and lastly Ethomeen C12 that showed no presence of viscoelasticity at the set conditions.

In all, chemical structure plays a role in the strength and onset of viscoelasticity, as this is important when screening chemicals for a particular application.

5.4 CONCLUSION

In this work, we have investigated the viscoelastic behavior of Duomeen TTM under typical reservoir conditions. From the decoupled results:

- Salt concentration is the main factor for inducing viscoelasticity since salt triggers the growth of micellar structures by reducing electrostatic repulsion amongst the molecules.
- Surfactant concentrations above the CMC fine-tune viscoelasticity by altering the amount of surfactant molecules present to aggregate and entangle into micellar structures.
- pH effect for Duomeen TTM resembles typical amine-based surfactant behavior by exhibiting a direct relationship of pH and viscosity at low shear rates due to the protonation and deprotonation process of the molecules below critical pH. At higher shear rates, the viscosity profile at all concentrations converge at 34 cp signifying the pH effect is only applicable at low shear rates below 100 s^{-1} for Duomeen TTM.
- For changes in temperature, the viscosity initially increases as the temperature ramps up then decreases after the inflection point (critical temperature). Similar to pH, the temperature effect occurs prominently at low shear rates and lessens at higher shear rates above 10 s^{-1}. This ramp up in viscosity insinuates the entanglement of the worm-like micelles until the competing effect of temperature begins branching the micellar chains.

Three similarly structured alkyl amine surfactants along with Duomeen TTM were studied to analyze how changes in the head and tail group influences the viscoelastic response of a solution. Further investigation to define the main structural component that imparts viscoelastic response of the solution is needed. According to the results:

- Duomeen TTM notably has a larger presence and range of viscoelasticity under typical reservoir conditions. This means that onset of viscoelasticity for Duomeen TTM occurs at a lower NaCl concentration and surfactant concentration. At high salt concentrations, Duomeen TTM can sustain a viscosity 1 to 2 magnitudes higher than the other three chemical structures.
- A longer tail length, such that of Duomeen TTM and Ethoduomeen T13 contributes to the growth of micellar chains and rise in viscoelasticity due to more efficient entanglement abilities.
- There is a viscosity discrepancy between surfactants that only have changes in terminal functional groups of the surfactant. This suggest that branches consisting of hydroxylates have a lower viscosity than that of methyl branches due to the hydration and dehydration of the solution when salt is present and the difference in degrees of hydrophobicity.
- It was observed that a head group consisting of two nitrogen ions resulted in a higher viscosity than surfactants containing a single nitrogen due to the protonation process of the surfactant molecules.

For application in the petroleum industry, Duomeen TTM is promising for mobility control, gel treatment, and matrix acidizing in carbonate reservoirs. Its chemical stability and viscoelastic response at high salinities, variable temperatures, and pH values makes Duomeen TTM adaptable and versatile under numerous conditions.

Chapter 6: Bulk Rheology vs. Rheology in Porous Media[3]

6.1 INTRODUCTION

The use of viscoelastic surfactants is important in applications related to enhanced oil recovery and subsurface conformance control. Viscoelastic surfactants bear a resemblance to polymer where it acts as a mobility control agent by increasing the displacing fluid's viscosity to improve sweep efficiency and recovery in porous media (Pope, 2007). However unlike polymer, viscoelastic surfactants, notably amine-based, are able to sustain viscoelasticity when exposed to high temperatures and saline conditions. (Pope, 2007). For surfactants, the onset and strength of its viscoelastic properties are triggered and fine-tuned namely by changes in salinity, surfactant concentration, pH, and temperature of the solution as discussed in Chapter 5. In all, the objective of this study is to determine if the bulk rheometry data can predict the rheological behavior of a viscoelastic surfactant solution in porous media.

This study was conducted to merely observe the correlation between bulk viscosity and apparent viscosity in porous media (limestone core and glass beads) for Duomeen TTM. Shear rate for both medias were derived from the injection rate, porosity, and permeability to compare bulk and apparent rheology sets at the same shear rates. A packed bed of glass beads provided an idealized case to which permeability and tortuosity can be set and flow can be visually seen, while flow through a limestone core is more difficult to analyze due to consolidation and uncertainty about the exact nature of the media (Rothstein, 2008).

[3] Adopted from a published article in TechConnect 2016, "Rheological Behavior od Novel Switchable Cationic Surfactant in High Salinity Carbonate Reservoirs". Journal article written by Madalyn M. Liebum and co-authored by N. Gurusinghe, G. Ramadhan, and Q.P. Nguyen. Gurusinghe and Ramadhan conducted and compiled data for the limestone core and Nguyen reviewed and provided resources for this article. Liebum conducted bulk rheology and glass bead experiments as well as wrote this article.

From the results, it is shown that the bulk and apparent rheological behavior for a 0.5 wt.% Duomeen TTM and 20 wt.% NaCl solution contradicted one another. Bulk rheology data exhibited shear thinning behavior while apparent viscosity in the porous media revealed a thickening response as shear rate increases. Mathematically, this thickening behavior is from the large pressure drops associated with increasing flow rate. Furthermore, other processes and mechanisms can attribute to this thickening response, this includes permeability reduction, extensional flow, elongation, tortuosity, relaxation time, pore size, surfactant plugging and retention (Sheng, 2011). The observed non-Newtonian rheology of this particular viscoelastic surfactant at high salinity is similar to viscoelastic polymeric solutions for subsurface applications. These findings imply that porous media adds complexity in evaluating rheological behavior for viscoelastic Duomeen TTM solutions.

6.2 MATERIALS AND PROCEDURE

6.2.1 Materials

Custom-fabricated piston accumulators connected to Quizix pumps were used to transfer the 0.5 wt.% Duomeen TTM in 20 wt.% NaCl solution and 20 wt.% NaCl brine to a 1-inch diameter glass column or core holder with working pressures of 60 psid (displacement pressure) and 5000 psi, respectively. Both the column and core holder were mounted vertically with injected fluid flowing upwards through the media. Two Mity Mite backpressure regulators (BPR) were used for the core setup only. The BPR supplied 1500 psi to the system. Pressure taps are present in core holder recording pressure differentials in three evenly spaced sections and two absolute pressure gauges measured the inlet and outlet of the core holder. For the glass beads, a differential pressure transducer was

connected to the inlet and outlet of the column. All transducers were connected to Labview software and voltage readings were converted to pressure readings using a calibration curve.

6.2.2 Preparation

Glass Beads

Glass beads (100-120 mesh) were sieved and packed into the glass column using a shaker. The glass column (1" D, 30" H) with built in mesh had Teflon tape wrapped on the ends securing the inlet and outlet caps from leaking. Leak test was applied after installation.

Estillades Limestone Core

The core was cut according to the core holder dimension and dried at 110 °C in an oven for five days. Then the core was covered using clear plastic wrap, aluminum foil and then inserted into a shrink heat tube mending the cover tightly to the core. Finally, the core was placed in the core holder. Confining pressure was slowly applied using a hydraulic pump, while nitrogen gas was used to pressurize the inside of the core holder (always 500 psi less than the confining pressure). First the confining pressure was set at 1000 psi, then 1500 psi, and repeated until the confining pressure achieves 2100 psi and nitrogen pressure at 1600 psi. Leak test was applied after installation.

6.2.3 Pore Volume Calculations

Glass Beads

Column was initially vacuumed. Mass difference was applied to determine the pore volume of the glass beads setup. The unsaturated column was weighed on a scale, then 20 wt.% NaCl brine was flushed into the column and reweighed for the saturated mass. Dead volume of the plastic tubing was accounted for.

Estillades Limestone Core

The core was initially vacuumed using a vacuum pump to remove air from the core. Brine was pumped into the core at a constant rate until the pressure exceeded the safety pressure of 1550 psi. Trapped air was degassed then the outlet was open for the effluent brine to be calculated. Pore volume was calculated using the volume of injected brine, effluent collected and dead volume of the tubes. Porosity is then calculated as the difference in pore volume to bulk volume.

$$\text{Pore Volume: PV} = \text{Saturated Volume} - \text{Dead Volume} - \text{Bulk Volume} \quad (6.1)$$

$$\text{Porosity: } \phi = \frac{\text{Pore Volume}}{\text{Bulk Volume}} \quad (6.2)$$

6.2.4 Permeability Measurement

Glass Beads

Permeability measurements were carried out at 40°C using 20 wt.% NaCl brine at incremental injection rates. Given the injection rate and pressure drop, Darcy's law was applied to calculate the brine permeability of the system.

Estillades Limestone Core

Two permeability measurements were carried out at room temperature and at 40°C. The core was saturated with 20 wt.% NaCl brine. The injection rates increased step-wise and then decreased. Using Darcy's Law, permeability of the entire media and sections of the core were calculated.

$$Q = \frac{-kA\Delta P}{\mu L} \quad (6.3)$$

where, Q is the flow rate (cm^3/s), k is permeability of the brine solution (cm^2), A is cross-sectional area of the core (cm^2), ΔP is the pressure differential of the core or sections (Pa), μ is the apparent viscosity of the brine (Pa-s), and L is the length of the core (cm).

6.2.5 Glass Beads Setup

This setup, shown in Figure 6.1, comprises of two accumulators that supply brine (20 wt.% NaCl) and surfactant solution (0.5 wt.% Duomeen TTM, 20 wt.% NaCl) to the glass column. The porous media was flushed with brine to characterize the pore volume, porosity and permeability of the column. Mass differences between the bulk versus saturated column defined pore volume and porosity was calculated using the ratio of pore volume to bulk volume. In addition, monitoring the differential pressure drop when the flow rate of the brine varies measures permeability of the porous media. A fraction collector compiles the effluent. Table 6.1 displays holder dimensions, pore volume, porosity and permeability values for the glass beads setup.

Chauveteau and Zaitoun et al. (1981) formulated shear rate relationships for glass beads assuming the porous media contained similar pore shapes (Sun et al., 2012). The equations listed below were used for this study to characterize the apparent shear rate as a function of pore radius and flow rate.

$$r = \left(\frac{8k}{\phi}\right)^{\frac{1}{2}} \tag{6.4}$$

$$\dot{\gamma} = \alpha\left(\frac{4v}{r}\right) \tag{6.5}$$

where k is permeability (cm^2), Φ is porosity, r is the average hydrodynamic pore radius in homogeneous unconsolidated porous media (cm), v is superficial velocity (cm/s) and α is equal to 1.7 for large spheres having the same diameter.

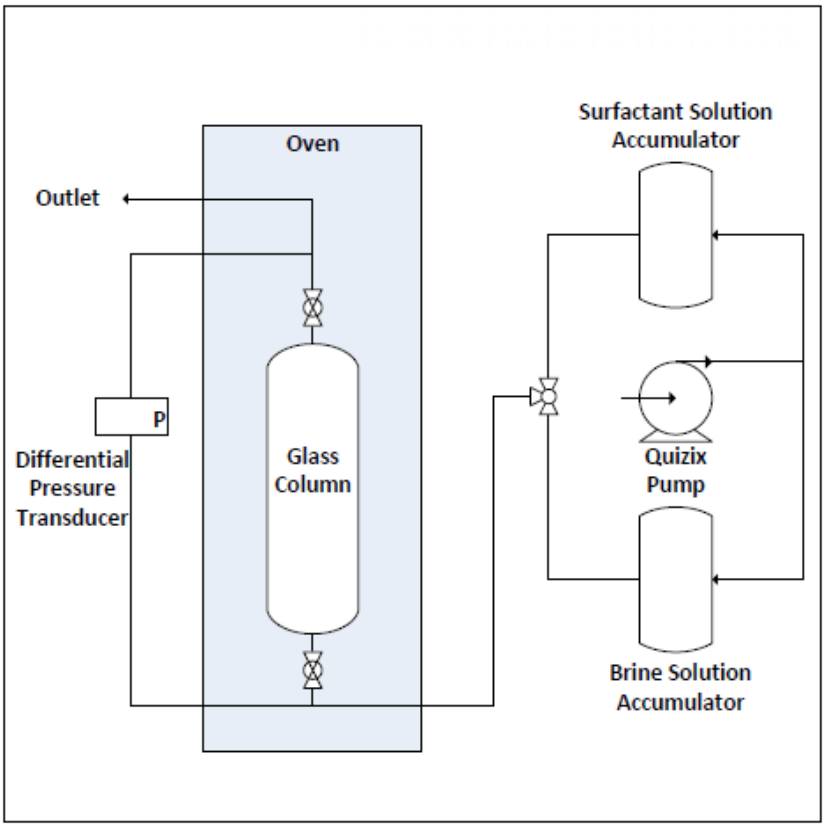

Figure 6.1: Glass Beads Setup

Table 6.1: Intrinsic properties for glass bead setup. Values assumed to remain unchanged during the experiment.

Parameter	Value	Units
Pore Volume	58	cm^3
Porosity	38	%
Permeability	1.1×10^{-7}	cm^2
Glass Column Dimensions	1” D x 30” H	in^2
Glass Bead Size	100-120	mesh

6.2.6 Core Setup

Illustrated in Figure 6.2, the core setup uses two pumps to transfer the brine and surfactant solution to the core. Pressure taps within the core holder provide pressure readings from the influent, intermediate and effluent regions of the limestone core. Pore volume is calculated by the difference of total volume injected to total volume produced. Porosity and permeability measurements were equated the same as stated previously. These results are displayed in Table 6.2.

The main objective of this core flood is to study the shear rate and apparent viscosity dependence in porous media in a non-ideal and less predictable environment. Various literature present models that correlate the injection rate and shear rate in the subsurface. This chapter will analyze the results for four models used to express non-Newtonian and polymeric flows in porous media.

$$\dot{\gamma} = \left(\frac{3n+1}{4n}\right)^{\frac{n}{n-1}} \left(\frac{12Q}{A(150k\phi)^{0.5}}\right) \quad \text{(Hirasaki and Pope, 1974)} \quad (6.6)$$

$$\dot{\gamma} = \left(\frac{4\alpha Q}{A(8k\phi)^{0.5}}\right) \quad \text{(Chauveteau, 2002)} \quad (6.7)$$

$$\dot{\gamma} = \frac{3n+1}{4n}\left(\frac{4Q}{A(8k\phi)^{0.5}}\right) \quad \text{(Veerabhadrappa, 2013)} \quad (6.8)$$

$$\dot{\gamma} = \frac{3n+1}{4n}\left(\frac{12Q}{A(150k\phi)^{0.5}}\right) \quad \text{(Christopher and Middlemen, 1965)} \quad (6.9)$$

where Q is flow rate (cm^3/s), A is cross sectional area of the core (cm^2), k is permeability (cm^2), Φ is porosity, and α is a coefficient in which n is flow behavior index of the bulk solution.

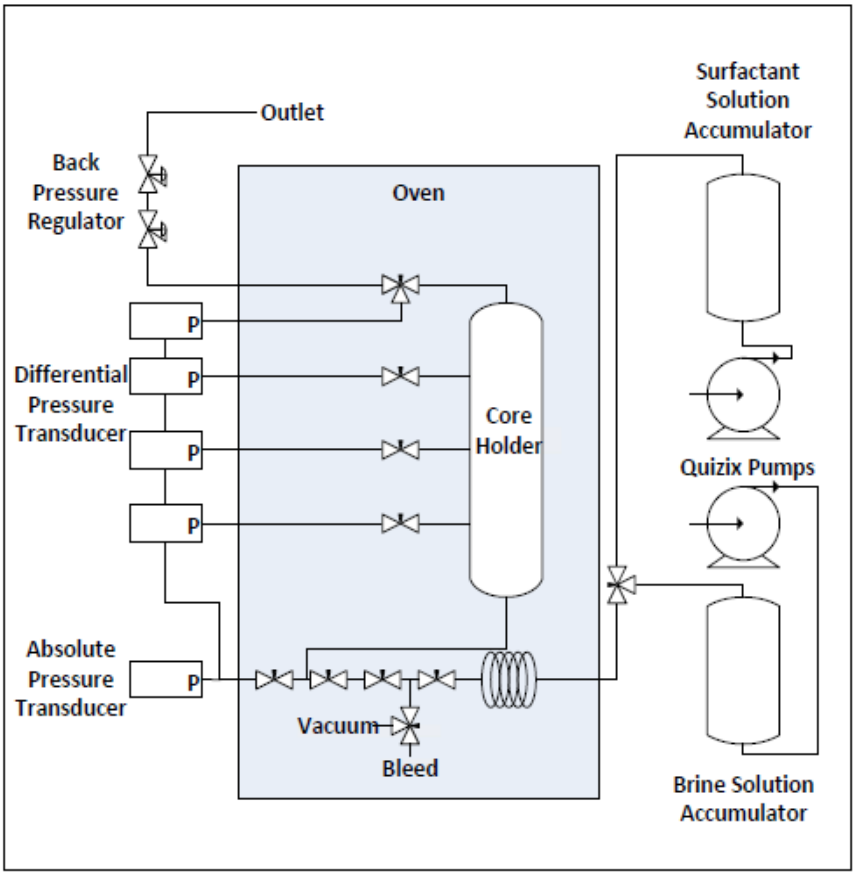

Figure 6.2: Limestone Core Flood Setup

Table 6.2: Intrinsic properties for core flood setup. Values assumed to remain unchanged during the experiment.

Parameter	Value	Units
Pore Volume	52	cm^3
Porosity	36	%
Core Permeability	8.3×10^{-10}	cm^2
Core Flood Dimensions	1” D x 11.5” H	in^2

6.3 RESULTS AND DISCUSSION

This section comprises of bulk and apparent viscosity results followed by a brief discussion of mechanisms influencing the shear thickening response for surfactant floods.

6.3.1 Bulk Rheology Results

The bulk measurement was conducted using a rheometer and will be compared to the apparent viscosity results in porous media. Figure 6.3 displays the viscosity profile for 0.5 wt.% Duomeen TTM in 20 wt.% NaCl solution at steady-state shear rate. This solution has shear thinning properties, which is representative behavior for viscoelastic surfactant solutions. A power law trend line exhibited on the chart will be used for future analysis.

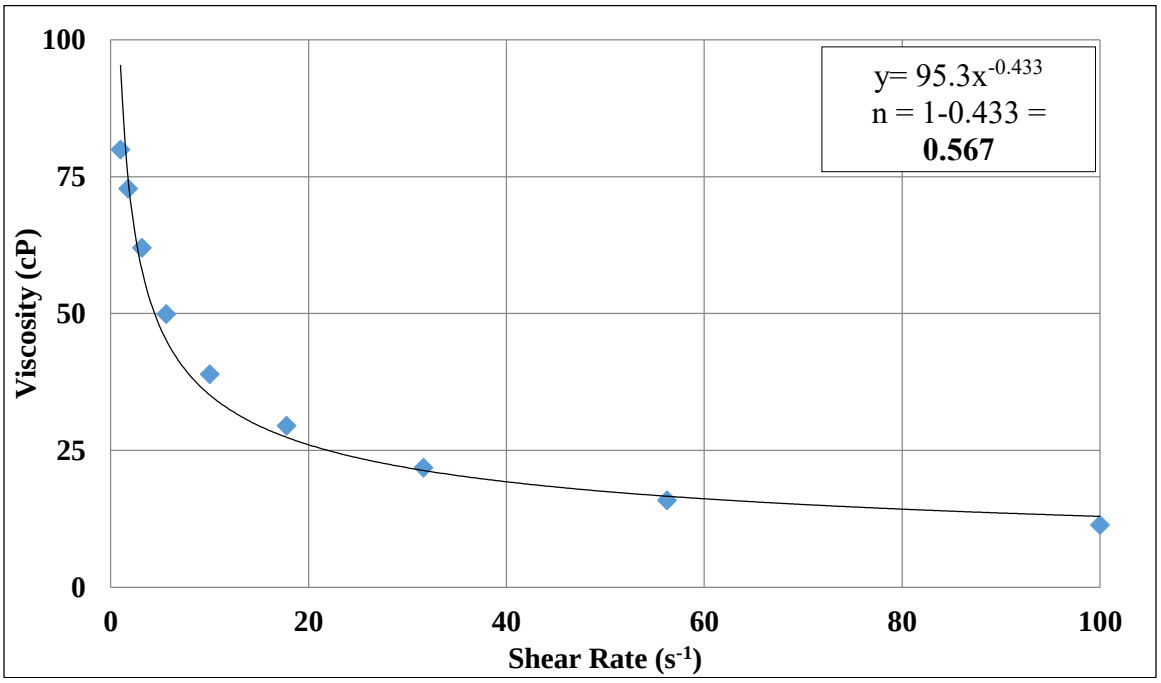

Figure 6.3: Bulk rheology results for 0.5 wt.% Duomeen TTM and 20 wt.% NaCl. Displays pseudo-plasticity and shear thinning trend.

6.3.2 Glass Beads Results

Shear rates from 9 to 1 s^{-1} with corresponding flow rates ranging from 0.61 to 0.07 cm^3/min were applied to analyze the changes in pressure drop amongst the inlet and outlet of the glass bead column. The short range in shear rates is due to the pressure limitations of the glass column (maximum pressure drop assumed 60 psi). At higher shear rates, the pressure drop overshoots and can be 20 psid higher than the equilibrated pressure drop recorded. Shown in Figure 6.4, the apparent viscosity displays shear thickening behavior unlike the bulk viscosity that clearly exhibits shear thinning. At low shear rates, the bulk and apparent viscosities converge. The difference in apparent and bulk viscosities is likely attributed to the elastic contribution of the viscoelastic solution in porous media. In addition, a hysteresis is displayed when flow rate increases and then decreases, viscosity values are higher when flow rate rises, therefore it is important to note the rate dependency of the apparent viscosity in porous media.

Figure 6.5 illustrates the rheological comparison of the bulk and effluent samples from the media. Each flow rate's effluent samples were tested in the rheometer to analyze if viscosity has been compromised from surfactant retention in the porous media. The viscosity of the effluent was divided by the bulk viscosity at a given shear rate and plotted for all flow rates. It is shown that most samples had less than 15% change compared to the bulk solution, with uncertainty involving effluent collection, salt precipitation and calibration of the rheometer. In all, the rheometry results insinuate little to no surfactant retention occurred in this type of media.

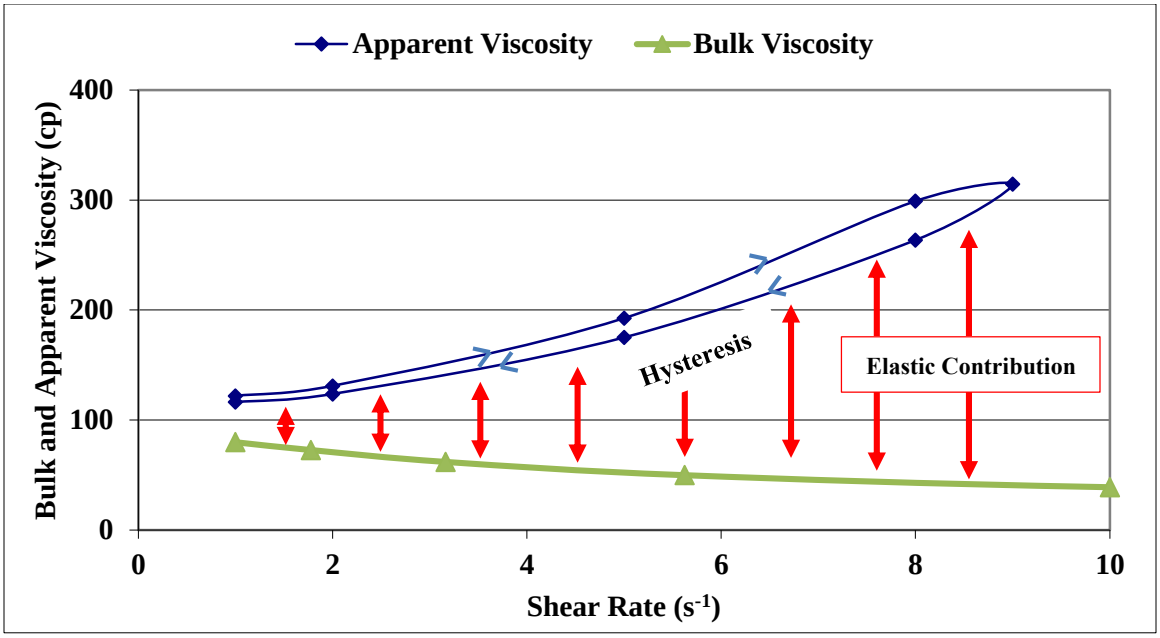

Figure 6.4: Glass Beads Setup results

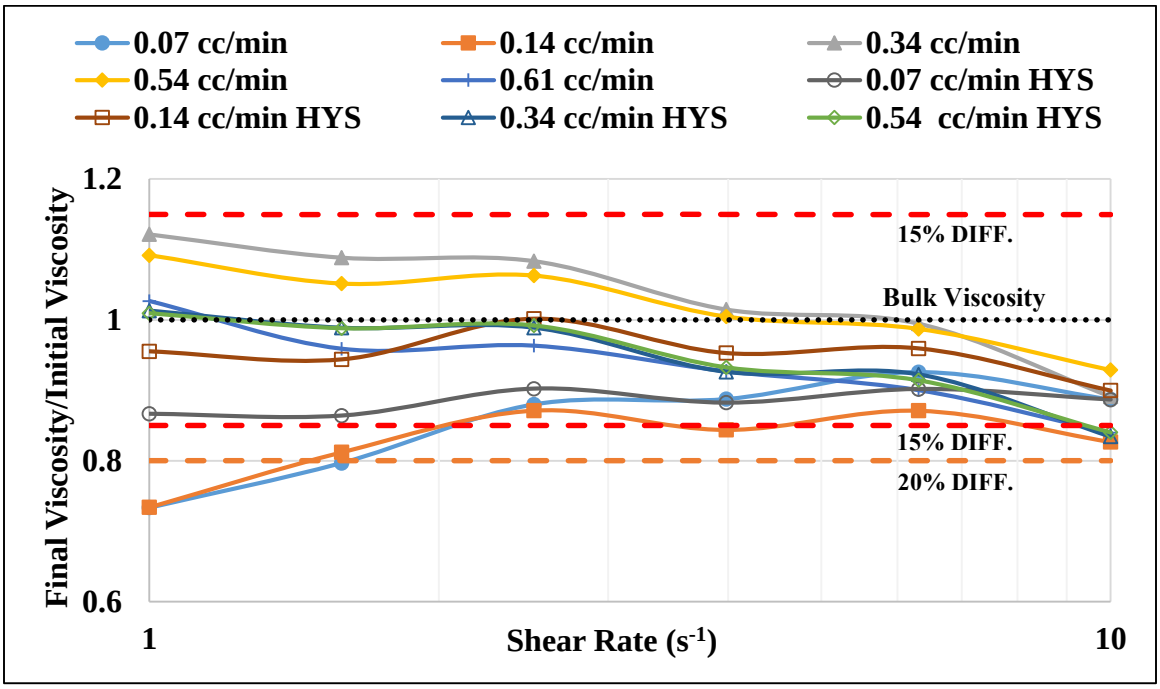

Figure 6.5: Rheology comparison for glass beads setup. Ratio is based on the flow rate's viscosity to the initial bulk viscosity. Flow rates were first ramped up until 0.61 cc/min then ramped down. Ramped down flow rates are labeled HYS.

6.3.3 Limestone Core Results

The same methodology was applied compared to the glass beads experiment, but the shear rates ranged from 33 to 4.75 s^{-1} with flow rates of 0.10 to 0.01 cm^3/min, respectively. As seen in Figure 6.6, a similar thickening trend was observed throughout the core, but at a lower response than the glass beads experiment. Furthermore, the models mentioned previously are shown in Figure 6.6. This chart illustrates how different models shift the calculated shear rate and thickening response based on the constants and structure of the expression.

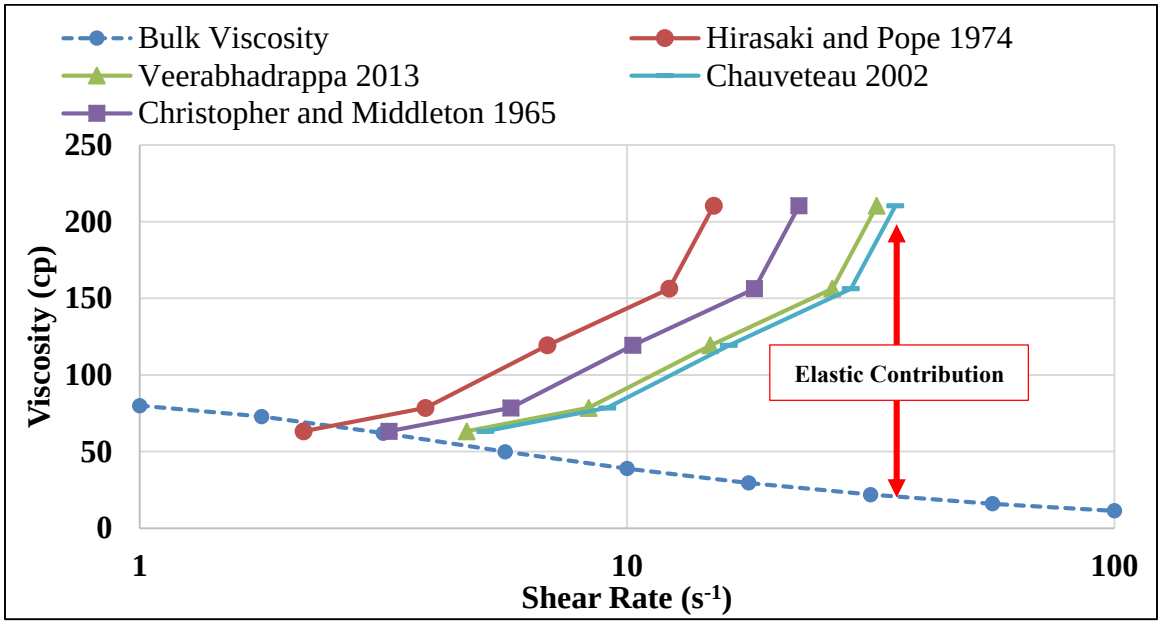

Figure 6.6: Limestone Core flood results

6.2.4 Discussion

According to Savins (1969), there are several claimed mechanisms to explain the shear thickening behavior observed in porous media and shear thinning response in a viscometric flow device for micellar or polymer viscoelastic solutions. These include: temporary network formations of the viscoelastic solute, bridging, chain unwinding and

intensification of intermolecular interactions, tortuosity of the path, extensional flow, elastic flow, pore blocking, adsorption, and plugging. In addition, at dilute to moderate concentrated solutions, flow destabilization and departure from laminar flow causes abnormal pressure differentials producing the shear thickening response (Savins, 1969).

Moreover, shear viscosity dominates at low shear rates while elongation viscosity is the principal factor at higher shear rates. The elastic portion of the viscoelastic surfactant is controlled by the relaxation time of the surfactant solution. If the relaxation time is comparable or larger than the transit time, Deborahs number, the elastic effects become more significant. However, for this solution, the relaxation time is less than a minute, shown in Figure 6.7, while the transit time can span hours, so the solution has the time to readjust to the changing flow conditions in porous media (Savins, 1969; Garrouch and Gharbi, 1999).

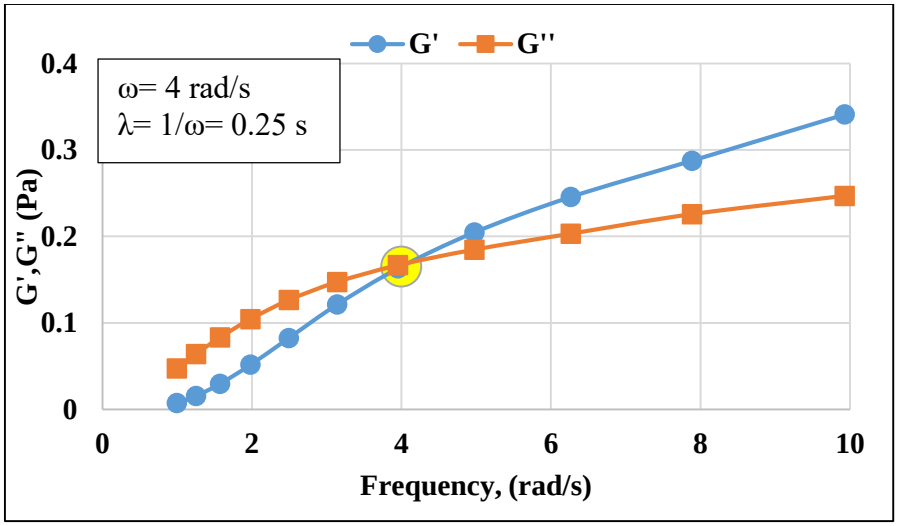

Figure 6.7: Relaxation time at 0.5 wt.% Duomeen TTM and 20 wt.% NaCl.

Similar results were obtained for other wormlike micelle solutions containing CTAT/SDS at low shear rates below 10 s^{-1}. Rojas et al. (2008) mentioned the apparent

viscosity increased significantly in porous media and did not solely abide by the shear viscosity results from the rheometer. This trend can be contributed to the formation of entanglement networks of wormlike micelles that favor the elongation component of flow (Rojas et al., 2008). Unlike the relaxation time stated above, this component increases the relaxation time for entanglement formation (Rojas et al., 2008). Furthermore, at higher shear rates, it is expected that micelles will break and flow with less resistance resulting in viscosity degradation (Rojas et al., 2008). In all, Rojas et al. (2008) concluded that extensional and elastic components of the solution from the interaction of wormlike micelles play a significant role in altering the resistance and viscosity of flow through porous media.

Additionally, for both cases, plugging can cause shear thickening in porous media as a function of tortuosity of the pathways and molecular weight of the micellar structures (Muller et al., 2004). Correspondingly, in the limestone core only, surfactant adsorption can add to the shear thickening response due to the micelles being retained within the pore structure therefore lowering permeability of the core.

6.4 CONCLUSION

An amine switchable surfactant was studied that displayed shear-dependent thickening behavior through porous media and exhibited shear thinning flow using a rheometer. While many mechanisms have been documented throughout the years, the exact reasons explaining these results are speculated from previous claims. Further investigation is warranted in determining the principal effects of the shear thickening response in porous media to better characterize how viscoelastic micellar solutions will engage in subsurface processes prone to changes in shear rates and heterogeneity.

Chapter 7: Surfactant In-Situ Viscosification during Single -Phase Flow in Limestone Cores

This chapter introduces a series of core floods for Duomeen TTM at 40°C. It comprises of single phase in-situ viscosification experiments to test gel-treatment capabilities for conformance control purposes.

The purpose is to trigger Duomeen TTM to transition from a Newtonian to a viscoelastic fluid in-situ by the presence of a salinity gradient. At low salt concentrations, the surfactant solution behaves Newtonian, but at higher salt concentrations the solution becomes more viscoelastic then strengthens to a gel-like consistency. Therefore, the goal is to see if Duomeen TTM solutions can viscosify at the salt mixing zone between the injected solution and 25 wt.% NaCl resident brine. As shown in the last chapter, injecting a viscoelastic fluid is undesirable due to the surge in pressure drop and surfactant retention/blocking experienced near the inlet of the core.

7.1 MATERIALS AND PROCEDURE

7.1.1 Materials

Fluid Injection System:

Two Quizix pumps were used to inject brine and surfactant solution (Duomeen TTM in brine) into the core. Both pumps were calibrated to ensure accuracy for all experiments. Brine and surfactant solutions are loaded into designated high-pressure piston accumulators.

Core Holder and Pressure Transducers:

A Phoenix Hassler type core holder (1” D x 12” L) with a working pressure of 5000 psi was mounted vertically and fluids were injected bottom-up. Hydraulic oil was pumped

between the core holder and core, which compressed and sealed the system to assure the axial flow of the injection fluids and to prevent leaks.

For the holder, the top and bottom end-caps were connected to two Rosemount absolute pressure transducers. Evenly-spaced pressure taps in the holders were used to measure pressure drops along three sections of the core using differential pressure transducers. Moreover, two transducers measured absolute pressures at the inlet and outlet of the core up to 2500 psi and the three differential transducers measure pressure differences up to 300 psi.

Backpressure Regulators and Effluent Collector:

Two Mity Mite BPRs in series maintained constant back pressure of 1500 psi during the floods. The first BPR was set to 1500 psi while the second BPR at 1450 psi. Automatic sample collector obtained effluent from the flood.

7.1.2 Preparation and Procedure

Core and the Core Holder Preparation:

"Estillades Limestone" cores were cut according to specific dimensions and placed in the oven at 110°C to dry out for two weeks. The dried core was wrapped using clear plastic wrap, aluminum foil and then inserted into a heat shrink tube. Then, the tube was heated and mended to the core. The core was then slowly loaded into the core holder and the top and bottom end-caps were tightly secured.

The core holder was mounted then the inlet, outlet, and pressure transducer lines were securely connected. Next, confining pressure was applied step by step to minimize any possible rock or equipment. First, 1000 psi of confining pressure was applied using a hydraulic pump and then inside the core holder was pressurized to 500 psi with N_2 gas using the inlet port. This gauge pressure was monitored for 15 min for any possible leaks.

This procedure was repeated every 500 psi until the confining pressure was set to the desired value while always increasing the N_2 pressure 500 psi less than the confining pressure. The pressure gauge was monitored until the pressure stabilizes at the desired value. The overburden pressure value was maintained constant throughout the experiment. Final N_2 pressure was used to leak test the core holder and transducer lines.

Pore Volume and Porosity Calculation:

After leak testing, the pressure was relieved from the holders and the core was vacuumed for about 12 hours. After vacuuming, the brine was bled to a point close to the core entrance and the brine pump cumulative volume was zeroed. Brine was pumped into the core at a constant rate until reaching a preset safety pressure while keeping the outlet valve closed. After several degassing steps to remove trapped air from the system, the outlet valve was opened to allow the effluent to be collected into graduated tubes until continuous flow of brine occurred. The mass of the collected liquid was measured using a scale and the density of the liquid was used to calculate the volume. Pore volume is calculated from the difference in the volume of brine injected, collected and dead volume. Using this pore volume value and bulk volume, porosity of the core can be computed.

Permeability Measurement:

Permeability of the core was measured using resident brine at room temperature and 40°C. The core is initially saturated with brine, then flow rates sequentially increased step-wise then decreased step-wise under steady-state conditions. The absolute pressure values and the pressure differential between the sections were recorded at each injection rate. The pressure readings and injection flow rate were applied in Darcy's law to calculate the brine permeability of the entire and sections of the core.

Surfactant Flooding:

After brine saturation, the surfactant flood \was flowed at 0.0784 cc/min or 2 PV/day. The rate was maintained for the entire experiment. All pressure readings were recorded. At the end of the experiment, the core is flushed with DI or low saline brine to recover the permeability and porosity, so it can be reused.

Schematic

Schematic of experimental setup is shown in Figure 7.1. Appendix C illustrates the in-situ viscosification in the core with a salinity gradient.

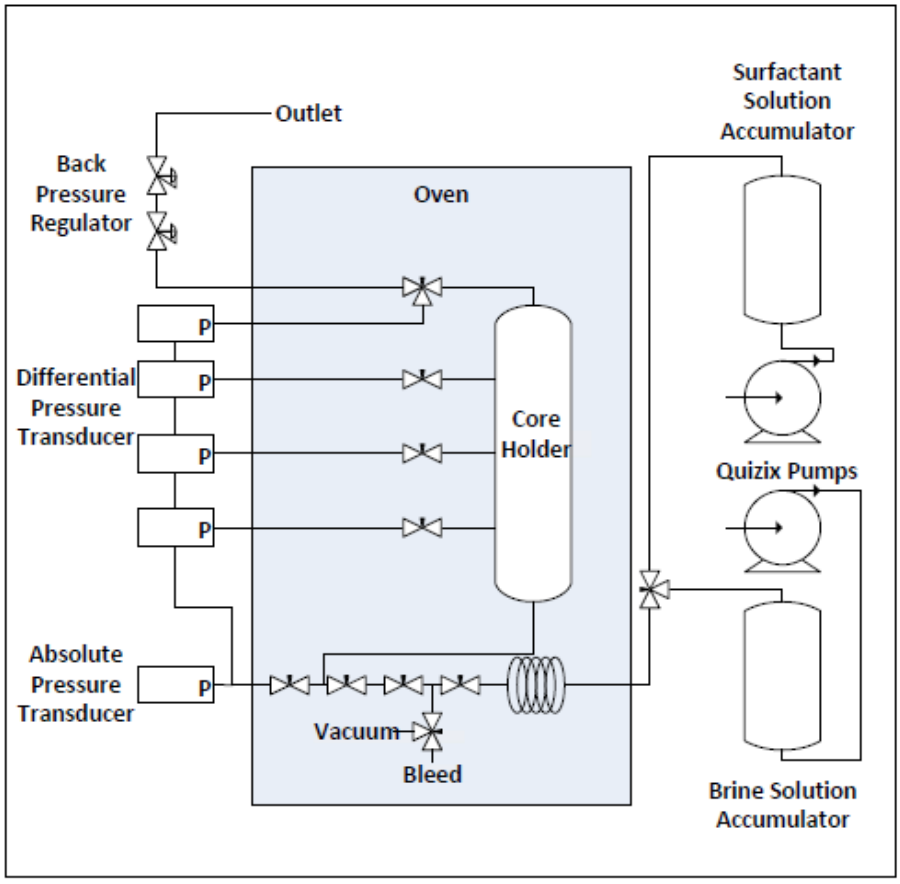

Figure 7.1: Schematic of the core flood. Surfactant solution accumulator consist of 0.5 wt.% Duomeen TTM and brine for salinity gradient experiments.

7.2 RESULTS

7.2.1 Salinity Gradient Experimental Series

Since the "switchable" surfactant is noted to become viscous with changes in salt concentration, the methodology of these types of experiments is to understand if gel can form in-situ when a low-salt surfactant solution mixes with very saline resident brine. Injecting surfactant in a high salt solution is not advisable due to large pressure drops encountered within the core due to the solution's viscous and elastic behavior.

Three runs were conducted at 0.5 wt.% Duomeen TTM with different injective salinities of 5 (Run 1), 10 (Run 2) and 15 wt.% NaCl (Run 3). The resident brine remained at 25 wt.% NaCl for all runs. The following figure has been transcribed from earlier sections of the thesis to illustrate the surfactant solution's behavior at different concentrations of NaCl at 10 s^{-1}. The dotted horizontal lines represent the expected viscosification at the "salt-mixing" zone for each run. The mixing zone is assumed the average of the injected solution and resident brine salt concentrations. For instance, it can be seen that Run 3 achieves higher viscosification in the salt mixing zone thereby it is expected that this run will have a higher-pressure drop response than the other two runs.

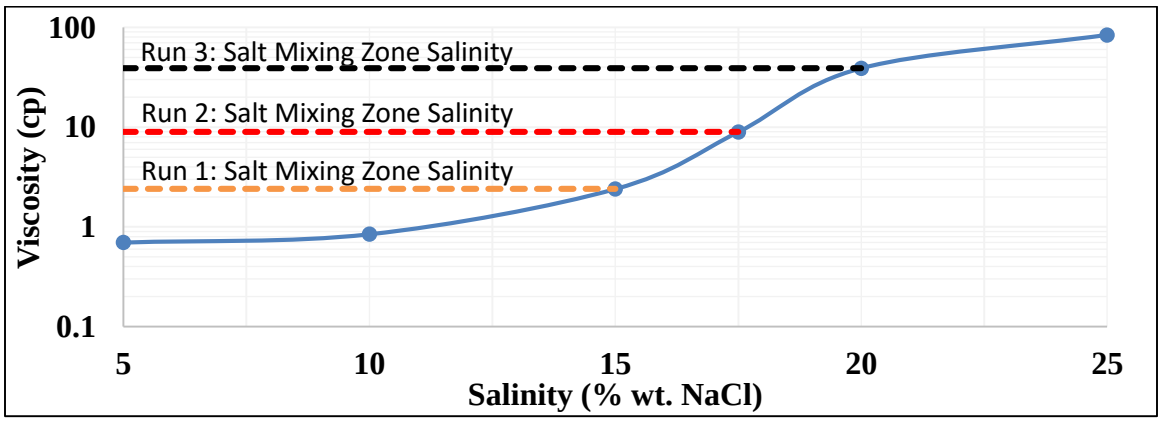

Figure 7.2: Viscosity profile of 0.5 wt. % Duomeen TTM solution at different salinities. The dotted horizontal lines display the anticipated viscosification at each run's salt mixing zone (the mix between the injected and resident solutions).

Run 1: 0.5 wt.% Duomeen TTM with 5 wt.% NaCl and 25 wt.% NaCl resident brine

This section discusses the results for Run 1. It consists of injecting the surfactant solution at the lowest salinity conditions into a core saturated with 25 wt.% NaCl. The following table presents the core properties and experimental conditions for this run.

Table 7.1: Parameters for Run 1: 0.5 wt.% Duomeen TTM with 5 wt.% NaCl

Parameters		**Values**
Surfactant Solution Salinity (wt.% NaCl)		5
Pore Volume (cm^3)		51.18
Porosity (%)		36
Permeability at 40°C (md)	*Overall Core*	71.46
	Section 1	60.87
	Section 2	66.67
	Section 3	43.05

From Figure 7.3, it can be seen that the mix between the injected and resident solutions were not sufficient in obtaining in-situ viscosification of the surfactant solution or gel development. For one, the injected fluid has a similar viscosity to water at 0.7 cp and the resident brine has a higher viscosity of about 1.2 cp at 40°C. Therefore, according to Darcy's Law, the pressure drop should decrease as the surfactant solution front propagates through the core. This is identifiable in the figure by the first section's pressure drop decreasing initially followed by the second and third section. In all, due to no rise in pressure drop, this injected fluid profile indicates low flow resistance by viscous surfactant in high saline conditions.

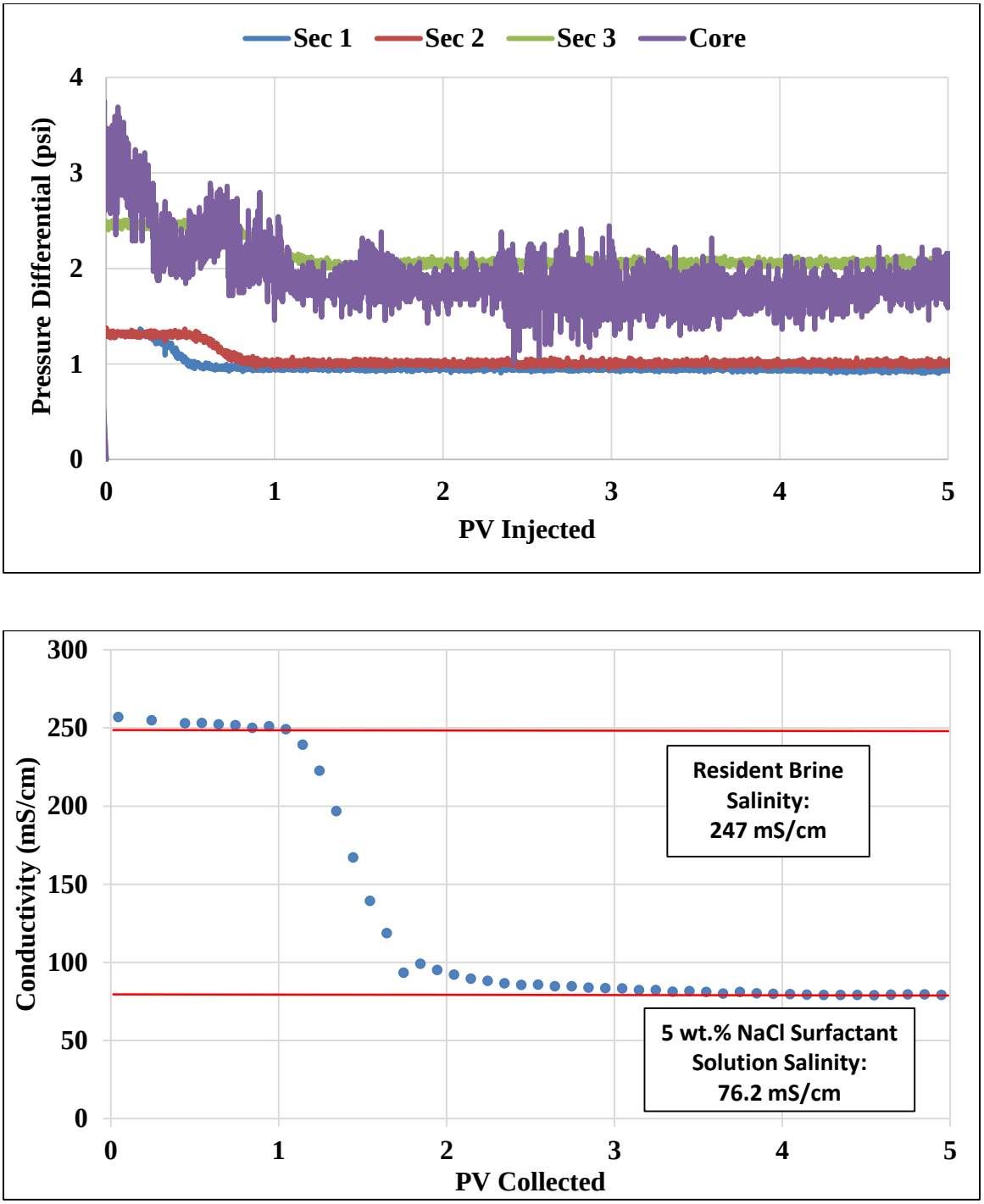

Figure 7.3: Core flood results for 0.5 wt.% Duomeen TTM and 5 wt.% NaCl brine solution. Pressure drop was decreasing for each section and for the entire core. Salinity gradient transitioned around 1.45 PV.

Run 2: 0.5 wt.% Duomeen TTM with 10 wt.% NaCl and 25 wt.% NaCl resident brine

This section discusses the results for Run 2. It consists of injecting the surfactant solution at 10 wt.% NaCl into a core saturated with 25 wt.% NaCl. The following table presents the core properties and experimental conditions for this run.

Table 7.2: Parameters for Run 2: 0.5 wt.% Duomeen TTM with 10 wt.% NaCl

Parameters		**Values**
Surfactant Solution Salinity (wt.% NaCl)		10
Pore Volume (cm^3)		53.76
Porosity (%)		38
Permeability at 40°C (md)	*Overall Core*	51.17
	Section 1	88.26
	Section 2	48.90
	Section 3	43.87

Figure 7.4 displays the pressure profile for an injected salt concentration at 10 wt.% NaCl. The rise in salt concentration increases the viscosity of the injected solution to about 1 cp at 40°C. From the figure, distinguishable propagation is illustrated, where section 1 has the lowest pressure drop, however the pressure drop progressively enhances for each section afterwards. The maximum pressure drop was achieved at about 6 psi in the core section. Moreover, higher-pressure drops in the later sections signify gel formation as it propagates through the core (Le et al., 2008). In addition, the final steady-state pressure drop did not reach its respective initial pressure drop value for section 2 and 3 suggesting residual gel in the core (Le et al., 2008).

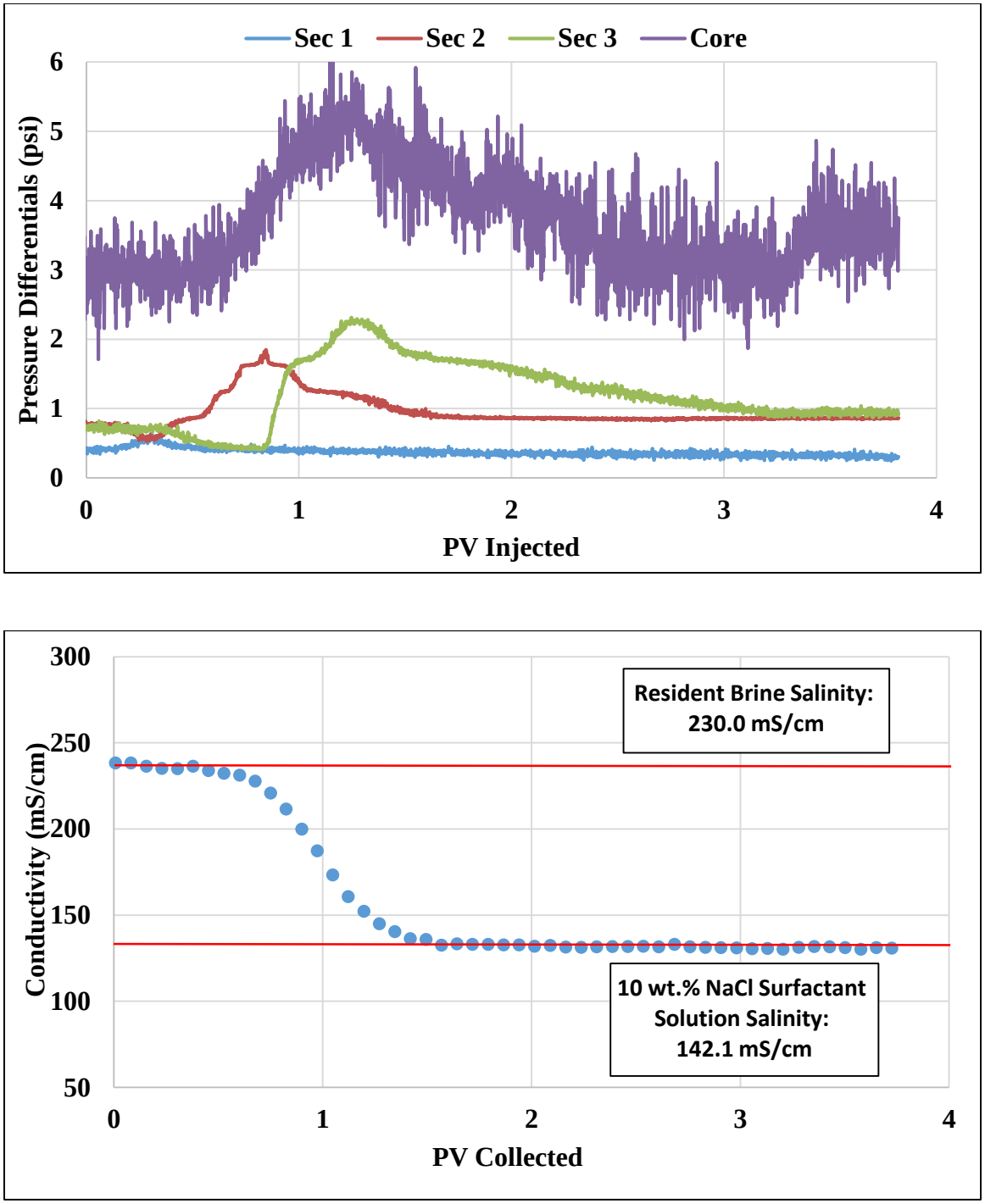

Figure 7.4: Core flood results for 0.5 wt.% Duomeen TTM and 10 wt.% NaCl brine solution. Maximum pressure drop was less than 2 psi for each section and 3 psi for the entire core. Salinity gradient transitioned around 1 PV.

Run 3: 0.5 wt.% Duomeen TTM with 15 wt.% NaCl and 25 wt.% NaCl resident brine

This section discusses the results for Run 3. It consists of injecting the surfactant solution at 15 wt.% NaCl into a core saturated with 25 wt.% NaCl. The following table presents the core properties and experimental conditions for this run.

Table 7.3: Parameters for Run 3: 0.5 wt.% Duomeen TTM with 15 wt.% NaCl

Parameters		**Values**
Surfactant Solution Salinity (wt.% NaCl)		15
Pore Volume (cm^3)		51.18
Porosity (%)		36
Permeability at 40°C (md)	*Overall Core*	57.38
	Section 1	60.92
	Section 2	45.00
	Section 3	71.97

The same conclusions as in Run 2 can be transcribed to in Run 3. In this run, the salinity of the injected fluid was raised to 15 wt.% NaCl thereby increasing the solution's viscosity to about 2.3 cp at 40°C. From Figure 7.5, the pressure drops are significantly higher compared to Run 2 reaching over 20 psi drop in the core. This strong pressure response can be attributed to viscosification of the surfactant solution increasing flow resistance. In other words, as the injected salinity increases, the propagation rate decreases resulting in an improved sweep efficiency and transport of the surfactant solution. Moreover, as the injected fluid propagates through the core, each section's pressure drop progressively increases inferring strong gel development, however the pressure drop in each section did not level off to its initial value suggesting some degree of retention and plugging.

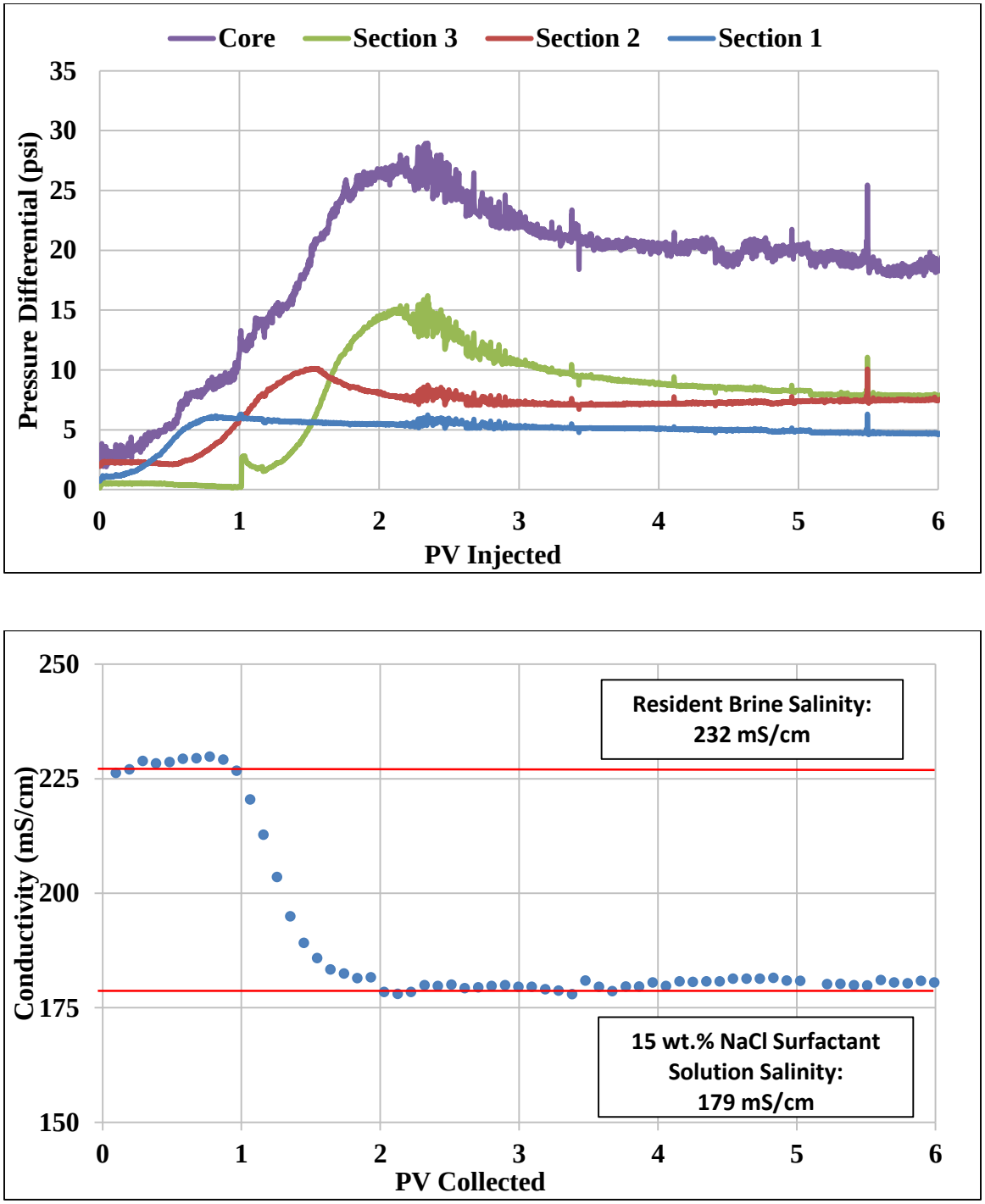

Figure 7.5: Core flood results for 0.5 wt.% Duomeen TTM and 15 wt.% NaCl brine solution. Maximum pressure drop was less than 15 psi for each section and 20 psi for the entire core. Salinity gradient transitioned around 1.3 PV.

7.3 CONCLUSION AND DISCUSSION

The following remarks summarize and discuss the results from this chapter.

- Formation of gel is dependent on the salt type, salt concentration, surfactant concentration, chemical structure, temperature, and pH of the solution. In these experiments, changes in NaCl concentration was the focus, while the other parameters listed remained fixed. In general, Duomeen TTM can form gel in moderate-high salinity conditions depending on surfactant concentration. The gel strength is predominately governed by salt concentration, where gel strengthens as salinity increases.
- In-situ salinity gradients from the mixing of the resident brine and the injective solution at different salinities were applied to analyze the pressure drop response in porous media. As the salinity of the mixing zone increases, then viscosification of the surfactant solution increases resulting in stronger gel development and retention.
- For the injected solutions, low salt concentrations at 5 wt.% NaCl perform poorly showing insignificant in-situ viscosification, while salt concentrations at 15 wt.% NaCl produced strong gel development (greater than 20 psid in core) in porous media. The middle option of 10 wt.% NaCl showed moderate pressure drop responses (2-3 psid in core) related to weak gel development.
- Run 2 and 3 both have a degree of gel retention and plugging, likely in the high permeability regions of the core. This was representative of the final steady-state pressure drop not returning to its initial state. It is assumed that higher differences between the final and initial imply greater development and/or strength of gel.
- As the injected solution's salinity increases, the viscosity increased as well. By increasing viscosity, the fluid mobility decreases leading to slower propagation through the core.

Chapter 8: Conclusion and Recommendations

This thesis details the recent work and results for Duomeen TTM, an amine-based surfactant, that is capable of switching from a nonionic to a cationic state under changing pH conditions. It was established that this chemical is stable under a large array of salinities, temperatures, and pH along with having viscoelastic properties under a certain set of environmental conditions. In addition, solubility analysis indicated that Duomeen TTM has relatively high solubility in CO_2 and deteriorates with the presence of methane. With being soluble in CO_2 in its nonionic state, this surfactant can transform to a water-soluble surfactant when exposed to acidic water due to its low partition coefficient and head group protonation process. From the bulk rheological properties of the surfactant, core floods were performed to test whether Duomeen TTM can viscosify within the core when injecting a low viscous solution into a core saturated with high saline brine.

Summary and conclusion of this thesis is deliberated in this chapter followed by recommendations of future work for this surfactant and of its kind.

8.1 CONCLUSION

8.1.1 Aqueous Stability and Critical pH

Duomeen TTM is soluble at a high range of salinities, temperatures, and pH. It is known that this surfactant is insoluble with no pH adjustments in the aqueous phase, but becomes water-soluble as pH declines due to protonation of the nitrogen ions located in the hydrophilic head. Critical pH analyzed where the insoluble-soluble boundary of the surfactant lies when environmental conditions change. For instance, as temperature increases or salinity decreases then critical pH decreases. In terms of viscoelasticity, the onset of this fluid behavior is near the critical pH boundary for the solution at hand. This solution tolerated high temperatures of 80 and 120°C when proper pH adjustments were

employed. Some solutions experienced phase separation or discoloration due to the water-soluble pH range lessens as temperature increases.

8.1.2 Solubility and Partition

Duomeen TTM and two comparable surfactants, Armeen DMCD and Ethoduomeen T13 have different solubilities in pure CO_2 and gas mixtures with different percentages of methane. For pure CO_2, Duomeen TTM and Armeen DMCD have solubilities around 1 wt.%, while Ethoduomeen T13 was only slightly-soluble in the same temperature and pressure conditions. With the presence of methane, the solubilities in Duomeen TTM and Armeen DMCD experienced a decay as methane content increased, while the solubility in Ethoduomeen T13 remained unaltered.

This surfactant behaves similarly to other nonionic surfactants, in which as temperature increases or pressure decreases then solubility decreases due to changes in tail-tail interactions and solvation strength of CO_2 or gas mixture. In addition, Duomeen TTM has a very low partition coefficient, meaning it is water-soluble especially in low pH environments. Since the chemical structure contains two nitrogen ions, these ions become very hydrophilic when protonated and act as anchors to retain the surfactant in the aqueous phase.

8.1.3 Bulk Rheology

Salinity, surfactant concentration, temperature, and pH play a role in the viscoelasticity and micellar formation of the solution. Salinity triggers the induction of viscoelasticity when the pH is below critical and sufficient surfactant molecules are present in the system. In general, salt reduces electrostatic repulsion, surfactant concentration limits aggregation density, pH controls the protonation process of the molecules, and temperature can delay the onset of micellar growth.

It was also found that changes in the chemical structure influences the viscoelastic properties of the surfactant. Modifications in tail length, functional groups, and amount of nitrogen ions in the head group are the three main topics discussed in the thesis. Essentially, as tail length, degree of hydrophobicity or nitrogen ions increase then the strength and onset of viscoelasticity is improved.

8.1.4 Core Flooding

A series of core floods were tested using limestone cores. These floods analyzed the in-situ viscosification that develops when a salinity gradient is present in the core. The results exhibit that runs with 10 or 15 wt.% NaCl injected surfactant solutions mixed with 25 wt.% NaCl resident brine provided reasonable viscosification compared to surfactant solutions with lower salinity.

8.2 RECOMMENDATIONS

8.2.1 Bulk Characterization

- Phase behavior, solubility, partition, and rheology test should be employed with the presence of oil at different carbon numbers.
- Interfacial tension and surface adsorption experiments have been proposed for future characterization with or without oil.

8.2.2 Foam Flooding

- Future experiments should consist of two-phase flow with brine and CO_2 using injection methods such as co-injection, foam-assisted WAG and SAG. Additionally, studies should be conducted on the effects of foam quality with and without the

presence of oil. These experiments will use the information from Chapter 4 to optimize the injection scheme.

- Similar to bulk solubility test, the core floods should be performed with different gas mixtures and compositions.
- Core flood experiments in the thesis were conducted at 40°C, so future test should be conducted at higher temperatures in very saline reservoirs in order to characterize the behavior of this surfactant under extreme conditions.
- Finally, future core floods should demonstrate how Duomeen TTM can be injected into the CO_2 phase therefore reducing the reliance of injected brine for propagation and foam development. These floods should analyze how changes in salinity, foam quality and injection scheme alters the foam generation and stability in porous media.

Appendices

APPENDIX A: ADDITIONAL INFORMATION FOR CHAPTER 4

The following charts are the calibration carbon tail distributions (CTD) for three surfactants tested in Chapter 4: Duomeen TTM, Armeen DMCD, and Ethoduomeen T13. The calibrated samples were prepared by adding pure surfactant at different concentrations in the same acidic water used for the solubility experiments. Then the calibrated samples were analyzed in the LCMS along with the other solubility samples tested.

These "calibration" charts will be used to compare how the carbon tail distribution changes with temperature, pressure and exposure to CO_2/CH_4. To simplify, red dotted lines were transcribed in all CTD charts in Chapter 4 to represent the average frequency of all concentrations for each carbon number. This provides quick 'before and after' interpretation while reading.

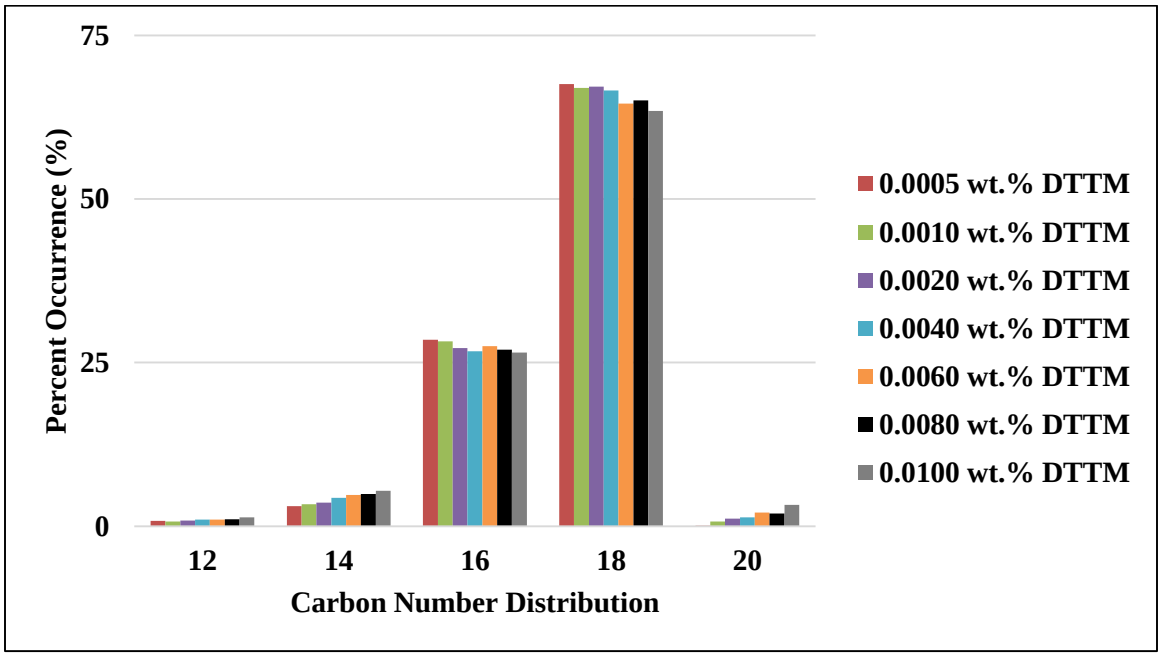

Figure A.1: Duomeen TTM calibration carbon tail distribution. Weight percentages are based on amount of Duomeen TTM present in the acidic water (pH 2).

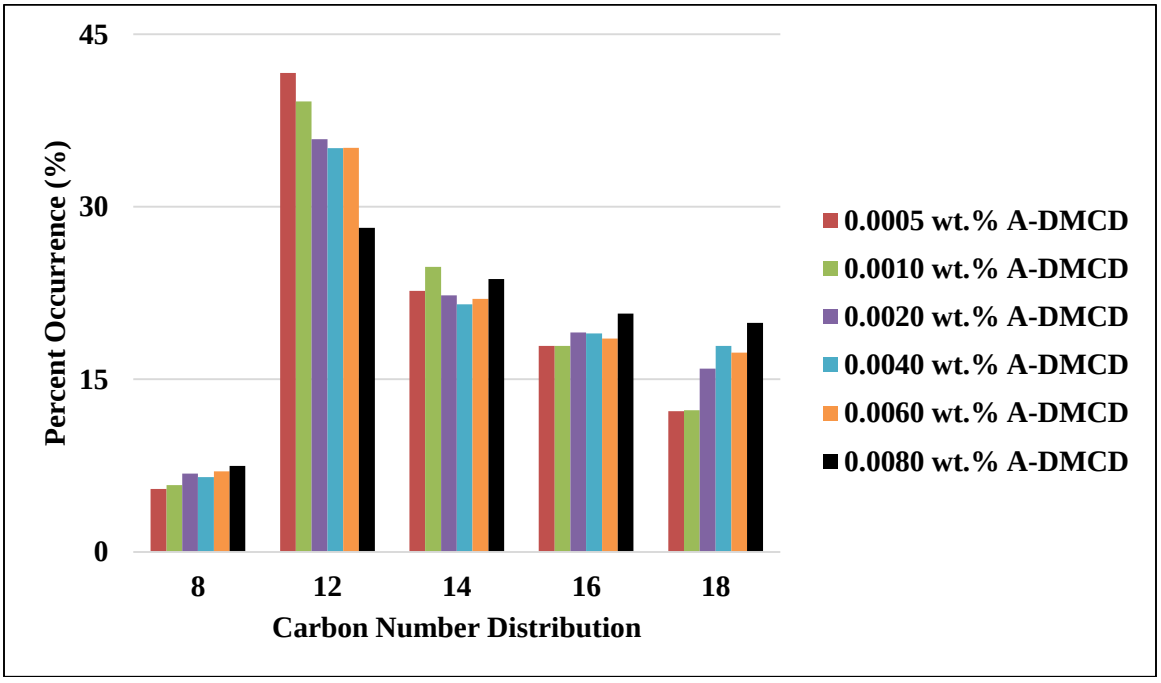

Figure A.2: Armeen DMCD calibration carbon tail distribution.

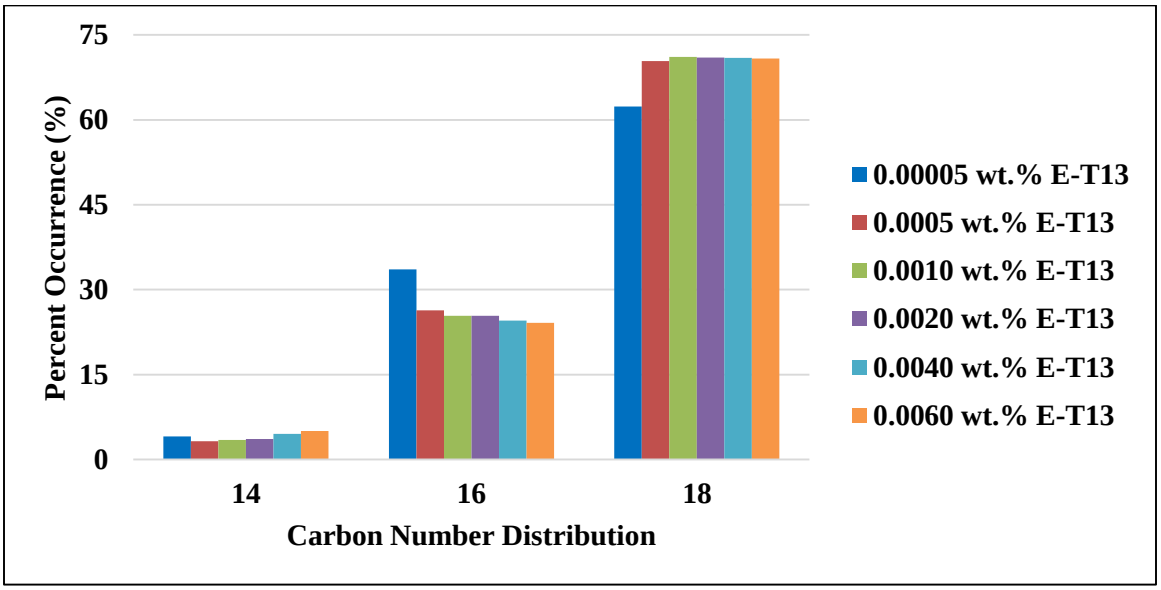

Figure A.3: Ethoduomeen T13 calibration carbon tail distribution.

APPENDIX B: RELAXATION TIMES FOR DUOMEEN TTM VISCOELASTIC SOLUTIONS

B.1 Dynamic Rheological Response

This section is dedicated for the dynamic rheological results for seven viscoelastic Duomeen TTM solutions for future references. All experiments were conducted with 2° cone-plate geometry at 25°C. A stress test was first applied at a constant frequency to identify linear viscoelastic region (LVR) for each solution. Choose a constant stress value in the LVR region for the frequency sweep test. The following equations were defined in the literature review section of the thesis and will be important when analyzing these sets of data.

$$G'(\omega) = \sum_k G_k \left(\frac{\omega^2 \lambda_k^2}{1+\omega^2 \lambda_k^2}\right) \tag{B.1}$$

$$G''(\omega) = \sum_k G_k \left(\frac{\omega \lambda_k}{1+\omega^2 \lambda_k^2}\right) \tag{B.2}$$

From these equations, relaxation time can be calculated from the inverse frequency, ω_c, at the crossover between G' and G". The following is notation of the relaxation time expression.

$$\lambda = 1/\omega_c \tag{B.3}$$

The remainder of the appendix will display frequency sweep results for all seven solutions ranging from 0.2 to 2 wt.% Duomeen TTM in 15 to 20 wt.% NaCl. If there is no crossover between G' and G", the solution is termed to be fully elastic or gel-like. However, most crossover at different frequencies signifying the presence of cylindrical or wormlike micelles and the changes in relaxation time making each solution unique.

At the end, Table B.1 list all the relaxation times to its corresponding surfactant solution.

B.1.1 Relaxation Time of Duomeen TTM Solutions

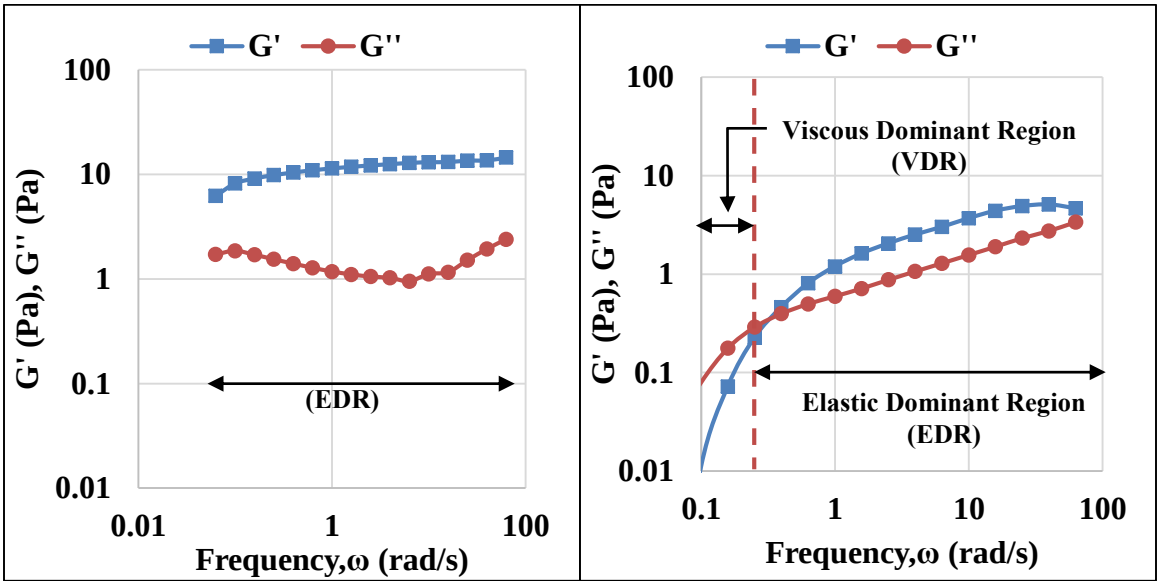

Figure B.1: Left: 2 wt.% Duomeen TTM in 20 wt.% NaCl Brine at 20°C. Right: 2 wt.% Duomeen TTM in 15 wt.% NaCl Brine at 20°C

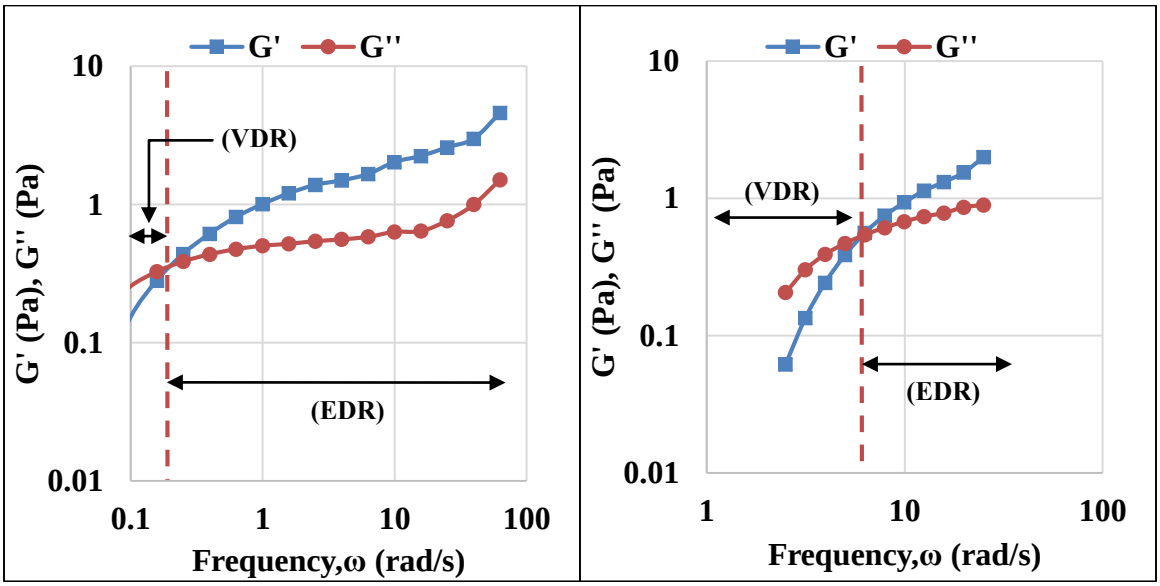

Figure B.2: Left: 1 wt.% Duomeen TTM in 20 wt.% NaCl Brine at 20°C. Right: 1 wt.% Duomeen TTM in 15 wt.% NaCl Brine at 20°C

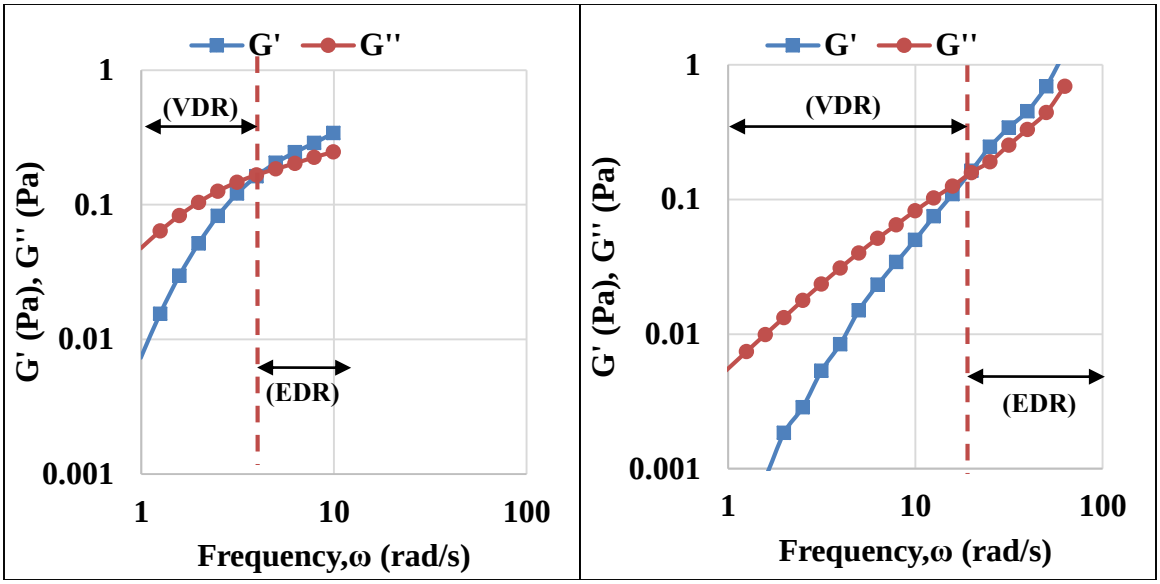

Figure B.3: Left: 0.5 wt.% Duomeen TTM in 20 wt.% NaCl Brine at 20°C. Right: 0.5 wt.% Duomeen TTM in 15 wt.% NaCl Brine at 20°C

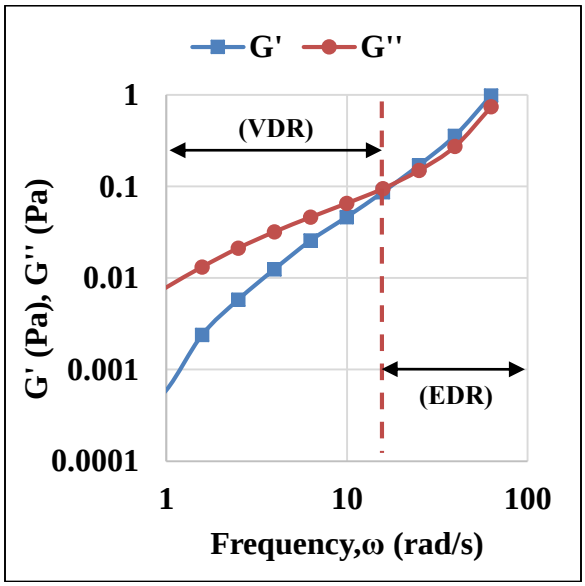

Figure B.4: 0.2 wt.% Duomeen TTM in 20 wt.% NaCl Brine at 20°C

Table B.1: List of Relaxation Times for Each Solution

Duomeen TTM Concentration (wt.% DTTM)	**Brine Concentration (wt.% NaCl)**	**Shear Rate Viscosity at 1; 10 s^{-1} (cp)***	**Crossover Frequency, ω (rad/s)**	**Relaxation Time, 1/ω (s)**
2	20	3905.0; 563.0	N/A	N/A
2	15	169.2; 131.7	0.32	3.114
1	20	935.6; 159.6	0.25	4.000
1	15	9.7; 9.5	10.44	0.095
0.5	20	80.0; 39.0	2.82	0.354
0.5	15	2.5; 2.4	18.88	0.052
0.2	20	6.9; 6.7	18.36	0.054

*Results from Chapter 4

From the table, it can be seen that the relaxation time is associated with the viscoelasticity of the solution. The time for the solution to adjust to changing conditions is lower for less viscous surfactant solutions than ones with a high degree of viscoelasticity due to having a larger viscous region. Furthermore, the surfactant solution with the highest viscosity showed the strongest elastic behavior and had no viscous region present. Therefore, no crossover was observed resulting in no relaxation time.

APPENDIX C: DIAGRAM OF IN-SITU VISCOSIFICATION

The following figure simulates the occurrence of in-situ viscosification of Duomeen TTM when a salinity gradient is present. As the surfactant solution is injected into the core, the injected and resident salinities mix forming a salt mixing zone, in which Duomeen TTM can viscosify due to the rise in salinity of the surfactant solution. The in-situ viscosification generates gel when high salinity is present and blocks permeable pathways in the core. Once all the resident brine has been displaced, the majority of the gel reverts back to its initial state after flushing with the injected surfactant solution, but some gel remains trapped within the media, which is considered residual gel.

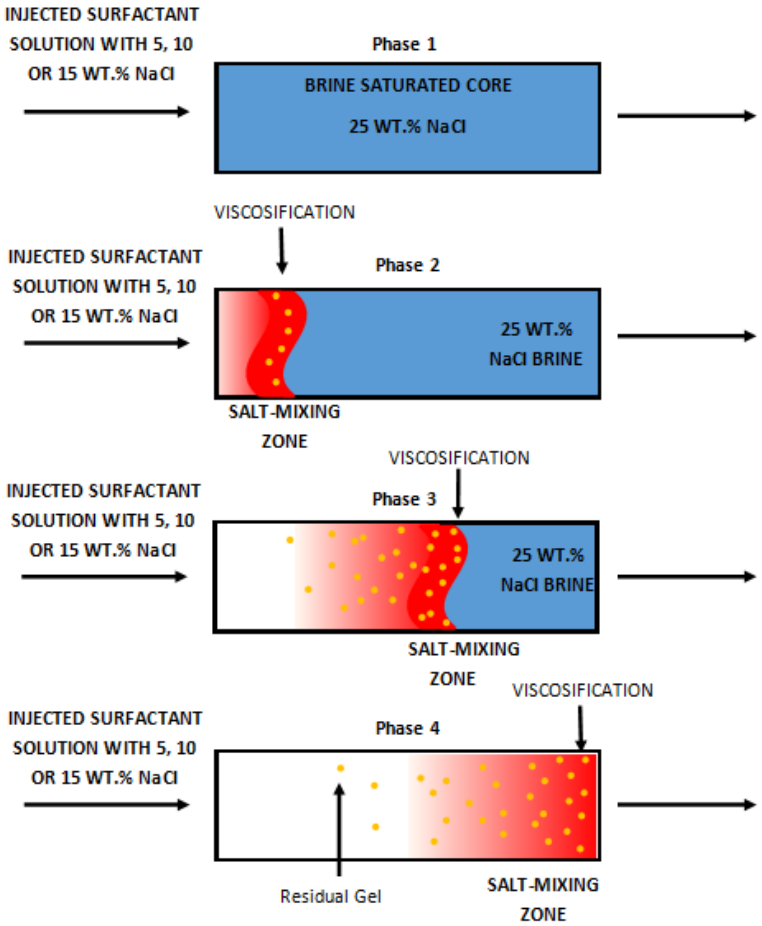

Figure C.1: Diagram of in-situ viscosification for Chapter 7. The phases illustrate the successive steps of gel development.

References

Chapter 1 and 2: Introduction and Literature Review

Adkins, S., Chen, X., Chan, I., Nguyen, Q., Sanders, A., Johnston, K. (2010) Effects of Branching on the Interfacial Properties of Nonionic Hydrocarbon Surfactants at the Air-Water and Carbon Dioxide-Water Interfaces. *Journal of Colloid and Interface Science*, doi: 10.1016/j.jcis.2009.12.059.

Adkins, S., Chen, X., Chan, I., Torino, E., Nguyen, Q., Sanders, A., Johnston, K. (2010b) Morphology and Stability of CO_2 – in- Water Foams with Nonionic Hydrocarbon Surfactants. *Langmuir,* 26(8), 5335-5348.

AkzoNobel. (2010) Surface Chemistry Catalog.

Anderson, V. (2006) The Rheology of Worm-like Micellar Fluids. *The British Society of Rheology: Rheology Review* 2006, 217-253.

Aryanpanah, S. and Nasr-El-Din, H. (2014) Rheological Properties of an Amine Oxide Viscoelastic Surfactant with Application in Well Stimulation. *SPE-169242-MS.*

Barentin, C. (2001) Shear Thickening in Dilute Solutions of Wormlike Micelles. *Europhysics Letters,* 55 (3), 432-438.

Brinchi, L., Germani, R., Di Profio, P., Marte, L., Savelli, G., Oda, R., Berti, D. (2010) Viscoelastic Solutions Formed by Worm-like Micelles of Amine Oxide Surfactant. *J. Colloid Interface Sci.*, 346(1), 100-106.

Cates, M. E. and Candau, S. J. (1990) Statics and Dynamics of Worm-like Surfactant Micelles. *J. Phs.: Condens. Matter,* 2, 6869-6892.

Chen, Y., Elhag, A., Palayangoda, S., Ren, G., Balan, O., Zhang, H., Yerramilli, R., Nguyen, Q., Seay, T., Liao, S., Biswal, L., Ma, K., Cui, L., Puerto, M., Amini, A., Jian, G., Chen, H., Falls, A., and Skurner, J. (2015) Novel CO_2 Foam Concepts and Injection Schemes for Improving CO_2 Sweep Efficiency in Sandstone and Carbonate Hydrocarbon Formations. *DE-FE0005902*.

Collura, J. S., Harrison, D.E., Richards, C.J., Kole, T.K., Fisch, M.R. (2001) The Effects of Concentration, Pressure, and Temperature on the Diffusion Coefficient and Correlation Length of SDS Micelles. *J. Phys. Chem. B,* 105, 4846-4852.

Consani, K.A., and Smith, R. (1990) Observation on the Solubility of Surfactants and Related Molecules in Carbon Dioxide at 50°C. *J. Supercrit. Fluids*, 3(2), 51-65.

Cui, L. (2014) Application of Foam for Mobility Control in Enhanced Oil Recovery. *Rice University Dissertation*.

Davies, J.T. (1957) A Quantitative Kinetic Theory of Emulsion Type, I. Physical Chemistry of the Emulsifying Agent., Gas/Liquid and Liquid/Liquid Interface. *Proceedings of the International Congress of Surface Activity,* 426-438.

Delshad, M., Kim, D.H., Magbagbeola, O.A., Huh, C., Pope, G.A., Tarahhom, F. (2008) Mechanistic Interpretation and Utilization of Viscoelastic Behavior of Polymer Solutions for Improved Polymer-Flood Efficiency. *SPE-113620*.

Eastoe, J., Dupont, A., Paul, A., Steytler, D., Rumsey, E. (2003) Design and Performance of Surfactants for Carbon Dioxide. *Supercritical Carbon Dioxide; ACS Symposium Series*, Chapter 19, 285-308.

Eastoe, J., Paul, A., Nave, S., Steytler, D.C., Robinson, B.H., Rumsey, E., Thorpe, M., Heenan, R.K. (2001) Micellization of Hydrocarbon Surfactants in Supercritical Carbon Dioxide. *J. Am. Chem. Soc.*, 123 (5), 988-989.

Elhag, A., Chen, Y., Reddy, P., Noguera, J., Ou, A.M., Hirasaki, G., Nguyen, Q., Biswal, S., Johnston, K. (2014) Switchable Diamine Surfactants for CO_2 Mobility Control in Enhanced Oil Recovery and Sequestration. *Energy Procedia*, 63, 7709-7716.

Eckert, C.A., Knutson, B.L., Debenedetti, P.G. (1996) Supercritical Fluids as Solvents for Chemical and Material Processing. *Nature*, 383, 313-318.

Enick, R.M. (2012) Mobility and Conformance Control for Carbon Dioxide Enhanced Oil Recovery (CO_2-EOR) via Thickeners, Foams, and Gels - A Detailed Literature Review of 40 Years of Research. *National Technology Laboratory.*

Ergun, S. (1952) Fluid Flow Through Packed Columns. *Chem. Eng. Prog.*, 48, 89-94.

Fan, X., Potluri, V.K., McLeod, M.C., Wang, Y., Liu, J., Enick, R.M., Hamilton, A.D., Roberts, C.B., Johnson, J.K., Beckman, E.J. (2005) Oxygenated Hydrocarbon Ionic Surfactants Exhibit CO_2 Solubility. *J. Am. Chem. Soc.*, 127 (33), 11754-11762.

Farn, R. (2006) Chemistry and Technology of Surfactants. *Wiley-Blackwell*, ISBN: 9781405126960.

Gaudino, D., Pasquino, R., Grizzuti, N. (2015) Adding Salt to a Surfactant Solution: Linear Rheological Response of the Resulting Morphologies. *Journal of Rheology,* 59, 1363-1375.

Girard, E., Tassaing, T., Marty, J.D., and Destarac, M. (2016) Structure-Property Relationships in CO_2-philic (Co)polymers: Phase Behavior, Self-Assembly, and Stabilization of Water/CO_2 Emulsions. *Chemical Reviews*.

Ghaicha, L., Leblanc, R.M., Chattopadhyay, A.K. (1992) Ellipsometric Study of Surfactants Comprising Linear and Branched Hydrocarbon Chains at the Air-Water Interface. *J. Phys. Chem.*, 96 (26), 10948-10953.

Heller J.P. (1994) CO_2 Foams in Enhanced Oil Recovery. In Foams: Fundamentals and Applications in the Petroleum Industry, *Advances in Chemistry, American Chemical Society* 242 (5), 201-234.

Hirasaki, G.J. and Pope, G.A. (1974) Analysis of Factors Influencing Mobility and Adsorption in the Flow of Polymer Solution Through Porous Media. SPE, 337-346.

Hoefling, T.A., Beitle, R.R., Enick, R.M., Beckman, E.J. (1993) Design and Synthesis of Highly CO_2-solbule Surfactants and Chelating Agents. *Fluid Phase Equilibria*, 83, 203-212.

Howe, A.M., Clarke, A., Giernalczyk, D. (2015) Flow of Concentrated Viscoelastic Polymer Solutions in Porous Media: Effect of M_w and Concentration on Elastic Turbulence Onset in Various Geometries. *Soft Matter*, 11, 6419.

Hull, K.L, Sayed, M., Al-Muntasheri, G.A. (2015) Recent Advances in Viscoelastic Surfactant for Improved Production from Hydrocarbon Reservoirs. SPE-173776-MS.

Kalur, G.C. and Raghavan, S.R (2005) Anionic Wormlike Micellar Fluids that Display Cloud Points: Rheology and Phase Behavior. *J. Phys. Chem. B,* 109, 8599-8604.

Kilic, S., Wang, Y., Johnson, J.K., Beckman, E., Enick, R. (2009) Influence of Tert-Amine Groups on the Solubility of Polymers in CO_2. *Polymer*, 50, 2436-2444.

Koehler, R. (2000) Microstructure and Dynamics of Wormlike Micellar Solutions Formed by Mixing Cationic and Anionic Surfactants. *J. Phys. Chem. B,* 104,11035-11044.

Kovscek, A.R. and Radke, C.J. (1994) Fundamentals of Foam Transport in Porous Media. *Foams: Fundamentals and Applications in the Petroleum Industry Advances in Chemistry*, ACS, 115-163.

Kuperkar, K., Mata, J.P, Bahadur, P. (2011) Effect of 1-Alkanols/Salt on the Cationic Surfactant Micellar Aqueous Solutions- A Dynamic Light Scattering Study. *Colloids and Surfaces A: Physiochemical and Engineering Aspects,* 380, 60-65.

Lake, L. (1989) Enhanced Oil Recovery. *Prentice Hall*.

Lapaumier, H.; Picq, D.; Carrette, P. (2009) New Amines for CO_2 Capture. I. Mechanisms of Amine Degradation in the Presence of CO_2. *Ind. Eng. Chem. Res.*, 48, 9061-9067.

Lapaumier, H.; Martin, S.; Picq, D.; Delfort, B.; Carrette, P. (2010) New Amines for CO_2 Capture. III. Effect of Alkyl Chain Length between Amine Functions on Polyamines Degradation. *Ind. Eng. Chem. Res.*, 49, 4553-4560.

Le, V., Nguyen, Q., Sanders, A. (2008) A Novel Foam Concept with CO_2 Dissolved Surfactants. SPE 113370.

Lee, H., Heller, J., Hoefer, A. (1991) Changes in Apparent Viscosity of CO_2 Foam with Rock Permeability. *SPE Reservoir Engineering*.

Lequex, F. (1996) Structure and Rheology of Wormlike Micelles. *Current Opinion in Colloid and Interface Science,* 1, 341-344.

Li, L., Nasr-El-Din, H., Cawiezel, K.E. (2010) Rheological Properties of a New Class of Viscoelastic Surfactant. SPE-121716-PA.

Maeda, H., Yamamoto, A., Souda, M., Kawasaki, H., Hossain, K.S., Nemoto, N., Almgren, M. (2001) Effects of Protonation on the Viscoelastic Properties of Tetradecyldimethylamine Oxide Micelles. *J. Phys. Chem. B,* 105,5411-5418.

McHugh, M.A., Rindfleisch, F., Kuntz, P.T., Schmaltz, C., Buback, M. (1998) Cosolvent Effect of Alkyl Acrylates on the Phase Behavior of Poly (alky acrylates)-Supercritical CO_2 Mixtures. *Polymer*, 39, 6049-6052.

McKinley, G.H., Pakdel, P., ad Oztekin, A. (1996) Rheological and Geometric Scaling of Purely Elastic Flow Instabilities. *J. Non-Newtonian Fluid Mech.*, 67, 19-47.

Miller, E. (2007) The Dynamics and Rheology of Shear-Banding Wormlike Micelles and Other Non-Newtonian Fluids. *Dissertation at University of Massachusetts Amherst*.

Mohamed, A. Sagisaka, M., Guittard, F., Cummings, S., Paul A., Rogers, S., Heenan, R., Dyer, R., Eastoe, J. (2011) Low Fluorine Content CO_2-philic Surfactants. *Langmuir,* 27, 10562-10569.

Nasr-El-Din, H., Al-Nakhli, A.R., Al-Driweesh, S.M., Welton, T.D., Sierra, L.,vam Domelen, M.S. (2009) Application of Cationic Surfactant-Based Fluids for Acid Diversion. SPE 107687.

Nagarajan, R. (2014) One Hundred Years of Micelles: Evolution of the Theory of Micellization. *Surfactant Science and Technology: Retrospects and Prospects*, CRC Press, ISBN 9781439882955.

Raghavan, S. (2009) Distinct Character of Surfactant Gels: A Smooth Progression from Micelles to Fibrillar Networks. *Langmuir,* 25(15), 8382-8385.

Raghavan, S. and Kaler, E.W. (2001) Highly Viscoelastic Wormlike Micellar Solutions Formed by Cationic Surfactants with Long Unsaturated Tails. *Langmuir,* 17, 300-306.

Rehage. H and Hoffmann, H. (1991) Viscoelastic Surfactant Solutions, Model Systems for Rheological Research, *Mol. Phys*. 74(5), 933-973.

Ren, G., Sanders, A., Nguyen, Q. (2014) New Method for the Determination of Surfactant Solubility and Partitioning Between CO_2 and Brine. *Journal of Supercritical Fluids,* 91, 77-83.

Rojas, M.R., Muller, A.J., and Saez, A.E. (2008) Shear Rheology and Porous Media Flow of Wormlike Micelle Solutions formed by Mixtures of Surfactants of Opposite Charge. *Journal of Colloid and Interface Science*, 326 (1), 221-226.

Rounds, R. S. (1994) Shear Effects in Surfactant Solutions. In: *ACS Symposium Series: In Structure and Flow in Surfactant Solutions.* Washington, DC: American Chemical Society, pp. 260-277.

Ryoo, W., Webber, S., Johnston, K. (2003) Water-in-Carbon Dioxide Microemulsions with Methylated Branched Hydrocarbon Surfactants. *Ind. Eng. Chem. Res.,*42, 6348-6358.

Sagisaka, M.; Yoda, S.; Takebayashi, Y.; Otake, K.; Kondo, Y.; Yoshino, N.; Sakai, H.; Abe, M. (2003) Effects of CO_2-philic Tail Structure on Phase Behavior of Fluorinated Aerosol-OT Analogue Surfactant/Water/Supercritical CO_2 Systems. *Langmuir,* 19, 8161-8167.

Sanders, A.W., Nguyen Q.P., Nguyen, N.M., Adkins, S.S., Johnston, K.P. (2010) Twin-Tailed Surfactants for Creating CO_2-in-Water Macroemulsions for Sweep Enhancement in CO_2-EOR. *SPE*, 137689.

Schlumberger. (2007) Carbonate Reservoirs Meeting Unique Challenges to Maximize Recovery.

Schramm, L.L. (2010) Surfactants Fundamental and Applications in the Petroleum Industry. *Cambridge University Press,* ISBN: 9780521157933.

Schramm, L.L. and Wassmuth, F. (1994) Foams: Basic Principles. *Foams: Fundamentals and Applications in the Petroleum Industry Advances in Chemistry*, ACS, 1-45.

Sheng, J. (2011) Modern Chemical Enhanced Oil Recovery: Theory and Practice. *Elsevier Science*, 978-185-61-7745-0.

Sheng, J. (2013) Surfactant Enhanced Oil Recovery in Carbonate Reservoirs. *Enhanced Oil Recovery Field Case Studies*, Chapter 12, 281-299.

Span, R. and Wagner, W. (1996) A New Equation of State for Carbon Dioxide Covering the Fluid Region from the Triple Point Temperature to 1100 K at Pressures up to 800 MPa. *J. Phys. Chem. Ref. Data.,* 25, 6, 1509-1596.

Stone, M.; da Rocha, S.; Rossky, P.; Johnston, K. (2003) Molecular Difference between Hydrocarbon and Fluorocarbon Surfactants at the CO_2/Water Interface. *J. Phys. Chem. B.,* 107, 10185-10192.

Sydansk, R.D. and Southwell, G.P. (2000) More Than 12 Years of Experience with a Successful Conformance-Control Polymer Gel Technology. SPE Prod. and Fac. 15 (4): 270. SPE-66558-PA.

Talebian, S.H., Masoudi, R., Tan, I.M., Zitha, P.L.J. (2014) Foam Assisted CO_2-EOR: A Review of Concept, Challenges and Future Prospects. *Journal of Petroleum Science and Engineering*, 120.

Than, J. (2016) Hydrophobic Interactions. *UCDavis ChemWIKI*.

Trickett, K. and Eastoe, J. (2008) Surfactant-based Gels. *Advanced in Colloid and Interface Science* 144, 66-74.

Truong, M.T. and Walker, L.M. (2002) Quantifying the Importance of Micellar Microstructure and Electrostatic Interactions on the Shear-Induced Structural Transition of Cylindrical Micelles. *Langmuir*, 18, 2024-2031.

Tung, S.H., Huang, Y.E., Raghavan, S.R. (2007) Contrasting Effects of Temperature on the Rheology of Normal and Reverse Wormlike Micelles. *Langmuir* 2007 (23), 372.

van Zanten, R. (2011) Stabilizing Viscoelastic Surfactants in High-Density Brines. SPE 141447.

Wang, W., Lu, W., Jiang, L. (2008) Influence of pH on the Aggregation Morphology of a Novel Surfactant with Single Hydrocarbon Chain and Multi-Amine Headgroups. *J. Phys. Chem.,* 112, 1409-1413.

Wang, Y., Hong, L., Tapriyal, D., Kim, I.C., Paik, I.H., Crosthwaite, J.M., Hamilton, A.D., Thies, M.C., Beckman, E.J., Enick, R.M., Johnson, J.K. (2009) Deign and Evaluation of Nonfluorous CO_2 soluble Oligomers and Polymers. *J. Phys. Chem. B.*, 113,14971.

Xing, D.; Wei, B.; McLendon, W.; Enick, R.; McNutty, S.; Trickett, K.; Mohamed, A.; Cummings, S.; Eastoe, J.; Rogers, S.; Crandall, D.; Tennant, B.; McLendon, T.; Romanov, V.; Soong, Y. (2010) CO_2 Soluble, Nonionic, Water-Soluble Surfactants that Stabilize CO_2-in-Brine Foams. *Society of Petroleum Engineers,* SPE 129907.

Yang, J. (2002) Viscoelastic Wormlike Micelles and Their Applications. *Current Opinion in Colloid and Interface Science,* 7, 276-281.

Zeng, Z. and Grigg, R. (2006) A Criterion for Non-Darcy Flow in Porous Media. *Transport in Porous Media,* 63, 57-69.

Zheng, X; Panthi, K.; Yunping, F., Johnston, K.; Mohanty, K. (2015) CO_2 Soluble Ionic Surfactant and CO_2 Foams for High Temperature and High Salinity Sandstone Reservoirs. *Energy Fuels,* 29, 5750-5760.

Chapter 4: Solubility References

Adkins, S., Chen, X., Chan, I., Nguyen, Q., Sanders, A., Johnston, K. (2010) Effects of Branching on the Interfacial Properties of Nonionic Hydrocarbon Surfactants at the Air-Water and Carbon Dioxide-Water Interfaces. *Journal of Colloid and Interface Science*, doi: 10.1016/j.jcis.2009.12.059.

AkzoNobel. (2010) Surface Chemistry Catalog.

Liu, J., Han, B., Wang, Z., Zhang, J., Li, G., Yang, G. (2002) Solubility of Ls-36 and Ls-45 Surfactant in Supercritical CO2 and Loading Water in the CO_2/Water/Surfactant Systems. *Langmuir*, 18, 3086-3089.

McClain, J.B., Betts, D.E., Canelas, D.A., Samulski, E.T., DeSimone, J.M., Londona, J.D., Cochran, H.D., Wignall, G.D., Chillura-Martino, D., Triolo, R. (1996) Design of Nonionic Surfactants for Supercritical Carbon Dioxide. *Science*, 274, 2049-2052.

Ren, G., Sanders, A., Nguyen, Q. (2014) New Method for the Determination of Surfactant Solubility and Partitioning Between CO_2 and Brine. *Journal of Supercritical Fluids,* 91, 77-83.

Shervani, Z., Liu, J., Ikushima, Y. (2004) Very High Solubilities of Hydrogenated n-Alkyl CO_2-philes in Supercritical Carbon Dioxide at Moderately Low Temperature and Pressures. *New. J. Chem.,* 28, 666-668.

Shi, Q., Jing, L., Chongqiao, X., Liu, C., Qiao, W. (2015) Solubility of Nonionic Hydrocarbon Surfactants with Different Hydrophobic Tails in Supercritical CO_2. *Journal of Chemical and Engineering Data*, 60, 2469-2476.

Zheng, X, Panthi, K., Yunping, F., Johnston, K., Mohanty, K. (2015) CO_2 Soluble Ionic Surfactant and CO_2 Foams for High Temperature and High Salinity Sandstone Reservoirs. *Energy Fuels,* 29, 5750-5760.

Chapter 5: Rheology References

Acharya, D. (2006) Wormlike Micelles in Mixed Surfactant Solutions. *Advances in Colloid and Interface Science,* 123-126, 401-413.

Anderson, V. (2006) The Rheology of Worm-like Micellar Fluids. *The British Society of Rheology: Rheology Review* 2006, 217-253.

Barentin, C. (2001) Shear Thickening in Dilute Solutions of Wormlike Micelles. *Europhysics Letters,* 55 (3), 432-438.

Berret, J.F. (1997) Rheology of Wormlike Micelles: Equilibrium Properties and Shear Banding Transition. *Wormlike Micelles*. 1-52.

Britton, M.M. and Callaghan, P.T. (1999) Shear Banding Instability in Wormlike Micellar Structure. *The European Physical Journal B,* 7, 237-249.

Calabrese, M.A., Rogers, S.A., Murphy, R., Wagner, N. (2015) The Rheology and Microstructure of Branched Micelles Under Shear. *Journal of Rheology,* 59, 1299.

Cappelaere, E. and Cressely, R. (1997) Shear Banding Structure in Viscoelastic Micellar Solutions. *Colloid Polymer Science,* 275, 407-418.

Cates, M. (1994) Theoretical Modeling of Viscoelastic Phases. *ACS Symposium Series: In Structure and Flow in Surfactant Solutions.* Washington, DC: American Chemical Society, 32-50.

Collura, J. S., Harrison, D.E., Richards, C.J., Kole, T.K., Fisch, M.R. (2001) The Effects of Concentration, Pressure, and Temperature on the Diffusion Coefficient and Correlation Length of SDS Micelles. *J. Phys. Chem. B,* 105, 4846-4852.

Delgado, J., Kriegs, H., Castillo, R. (2009) Flow Velocity Profiles and Shear Banding Onset in a Semi dilute Wormlike Micellar Systems under Couette Flow. *J. Phys. Chem. B.*, 113, 15484-15494.

Dhont, J.K. and Briels, W.J. (2008) Gradient and Vorticity Banding. *Rheol Acta*, 47, 257-281.

Fardin, M.A., Radulescu, O., Morozov, A., Cardoso, O., Browaeys, J., Lerouge, S. (2015) Stress Diffusion in Shear Banding Wormlike Micelles. *Journal of Rheology*, 59, 1335.

Helgeson, M.E., Vasquez, P.A, Kaler, E.W., Wagner, N.J. (2009) Rheology and Spatially Resolved Structure of Cetyltrimethylammonium Bromide Wormlike Micelles Through the Shear Banding Transition. *Journal of Rheology*, 53, 727.

Hoffmann, H. (1994) Viscoelastic Surfactant Solutions. In: *ACS Symposium Series: In Structure and Flow in Surfactant Solutions.* Washington, DC: American Chemical Society, 2-31.

Hu, Y.T., Boltenhagen, P, Pine, D.J. (1998) Shear Thickening in Low-Concentration Solutions of Wormlike Micelles. I. Direct Visualization of Transient Behavior and Phase Transitions. *Journal of Rheology*, 42 (5) 1185-1208.

Hu, Y.T. and Lips, A. (2005) Kinetics and Mechanism of Shear Banding in an Entangled Micellar Solution. *Journal of Rheology*, 49, 1001.

Hu, Y.T., Lips, A., Palla, C. (2008) Comparison Between Shear Banding and Shear Thinning in Entangled Micellar Solutions. *Journal of Rheology*, 52, 379.

Kalur, G.C., Frounfelker, B.D., Cipriano, B.H., Norman, A.I., Raghavan, S.R. (2005) Viscosity Increase with Temperature in Cationic Surfactant Solutions Due to Growth of Wormlike Micelles. *Langmuir* 2005,21, 10998-11004.

Kalur, G.C and Raghavan, S.R (2005) Anionic Wormlike Micellar Fluids that Display Cloud Points: Rheology and Phase Behavior. *J. Phys. Chem. B*, 109, 8599-8604.

Koehler, R.D (2000) Microstructure and Dynamics of Wormlike Micellar Solutions Formed by Mixing Cationic and Anionic Surfactants. *J. Phys. Chem. B*, 104,11035-11044.

Lee, H.Y., Diehn, K.K., Ko, S.W., Tung, S.H., Raghavan, S.R. (2010) Can Simple Salts Influence Self-Assembly in Oil? Multivalent Cations as Efficient Gelators of Lecithin Organosols. *Langmuir Article,* Issue 26(17), 13831-13838.

Liberatore, M.W. (2009) Microstructure and Shear Rheology of Entangled Wormlike Micelles in Solution. *Journal of Rheology*, 53, 441.

Lin, Z., Lu, B., Zakin, J.L., Talmon, Y., Zheng, Y., Davis H.T., Scriven, L.E. (2001) Influence of Surfactant Concentration and Counterion to Surfactant Ratio on Rheology of Wormlike Micelles. *Journal of Colloid and Interface Science,* 239(2), 543-554.

Maeda, H., Yamamoto, A., Souda, M., Kawasaki, H., Hossain, K.S., Norio, N., Almgren, M. (2001) Effects of Protonation on the Viscoelastic Properties of Tetradecyldimethylamine Oxide Micelles. *J. Phys. Chem. B,* 105,5411-5418.

Manneville, S. (2008) Recent Experimental Probes of Shear Banding. *Rheol Acta*, 47, 301-318.

Miller, E. and Rothstein, J.P. (2007) Transient Evolution of Shear-banding Wormlike Micellar Solutions. *Journal of Non-Newtonian Fluid Mechanics*, 143, 22-37.

Mu, J.H. and Li, G.Z. (2001) The Formation of Wormlike MIcelles in Anionic Surfactant Aqueous Solutions in the Presence of Bivalent Counterion. *Chemical Physics Letters,* 345, 100-104.

Pipe, C.J., Kim, N.J., Vasquez, P.A., Cook, L.P., McKinley, G.H. (2010) Wormlike Micellar Solutions: II. Comparison Between Experimental Data and Scission Model Predictions. *Journal of Rheology,* 54, 881.

Raghavan, S. and Kaler, E.W. (2001) Highly Viscoelastic Wormlike Micellar Solutions Formed by Cationic Surfactants with Long Unsaturated Tails. *Langmuir,* 17, 300-306.

Raghavan, S., Fritz, G., Kaler, E.W. (2002) Wormlike Micelles Formed by Synergistic Self-Assembly in Mixtures of Anionic and Cationic Surfactants. *Langmuir,* 18, 3797-3803.

Rehage. H and Hoffmann, H. (1991) Viscoelastic Surfactant Solutions, Model Systems for Rheological Research. *Mol. Phys*. 74(5), 933-973.

Shchipunov, Y. and Hoffmann, H. (2000) Thinning and Thickening Effects Induced by Shearing in Lecithin Solution of Polymer-like Micelles. *Rheol Acta,* 39, 542-553.

Schramm, L.L. and Wassmuth, F. (1994) Foams: Basic Principles. *Foams: Fundamentals and Applications in the Petroleum Industry Advances in Chemistry*, ACS, 1-45.

Sheng, J. (2011) Modern Chemical Enhanced Oil Recovery: Theory and Practice. *Elsevier Science*, 978-185-61-7745-0.

Thareja, P., Hoffmann, I.H., Liberatore, M.W., Helgeson, M.E., Hu, Y.T., Gradzielski, M., Wagner, N.J. (2011) Shear-Induced Phase Separation (SIPS) with Shear Banding in Solutions of Cationic Surfactant and Salt. *Journal of Rheology,* 55, 1375.

Trickett, K. and Eastoe, J. (2008) Surfactant-based Gels. *Advanced in Colloid and Interface Science* 144, 66-74.

Truong M.T. and Walker L.M. (2002) Quantifying the Importance of Micellar Microstructure and Electrostatic Interactions on the Shear-Induced Structural Transition of Cylindrical Micelles. *Langmuir*, 18,2024-2031.

Wang, W., Lu, W., Jiang, L. (2008) Influence of pH on the Aggregation Morphology of a Novel Surfactant with Single Hydrocarbon Chain and Multi-Amine Headgroups. *J. Phys. Chem.*, 112, 1409-1413.

Yesilata, B., Clasen, C., McKinley, G.H. (2006) Nonlinear Shear and Extensional Flow Dynamics of Wormlike Surfactant Solutions. *Journal of Non-Newtonian Fluid Mechanics*, 133, 73-90.

Zhang, Y.M., Zhou, D., Ran, H., He, S. (2016) Rheology behaviors of C22-Tailed Carboxylbetaine in High-Salinity Solution. *Journal of Dispersion Science and Technology*, 37(4),496-503.

Zhao, Y., Haward, S.J., Shen, A.Q. (2015) Rheological Characterizations of Wormlike Micellar Solutions Containing Cationic Surfactant and Anionic Hydrotropic Salt. *Journal of Rheology*, 59(5), 1229.

Chapter 6: Bulk Versus Apparent Viscosity References

Chauveteau, G. and Zaitoun, A. (1981) Basic Rheological Behavior of Xanthan Polysaccharide Solutions in Porous Media: Effects of Pore Size and Polymer Concentration. *Enhanced Oil Recovery: Proceedings of the Third European Symposium on Enhanced Oil Recovery,* 197-212.

Chauveteau, G., Denys, K., and Zaitoun, A. (2002) New Insight on Polymer Adsorption Under High Flow Rates. *SPE/DOE Improved Oil Recovery Symposium*, *SPE 75183*.

Christopher, R.H. and Middlemen, S. (1965) Power-Law Flow Through a Packed Tube. *Ind. Eng. Chem. Fund.,* 4(4), 422-426.

Garrouch, A. and Gharbi, R. (1999) An Empirical Investigation of Polymer Flow in Porous Media. *Ind. Eng. Chem. Res.*, 38, 3564-3571.

Hirasaki, G. and Pope, G.A. (1974) Analysis of Factors Influencing Mobility and Adsorption in the Flow of Polymer Solution Through Porous Media. SPE-4026-PA.

Muller, A.J., Torres, M.F., and Saez, A.E. (2004) Effect of the Flow Field on the Rheological Behavior of Aqueous Cetyltrimethylammonium p-Toluenesulfonate Solutions. *Langmuir,* 20, 3838-3841.

Pope, G. (2007) Overview of Chemical EOR. *Casper EOR Workshop*.

Rojas, M.R., Muller, A.J., Saez, A.E. (2008) Shear Rheology and Porous Media Flow of Wormlike Micelle Solutions Formed by Mixtures of Surfactant of Opposite Charge. *Journal of Colloid and Interface Science,* 326, 221-226.

Rothstein, J.P. (2008) Strong Flows of Viscoelastic Wormlike Micelle Solutions. *Rheology Reviews*.

Savins, J.G. (1969) Non-Newtonian Flow Throughout Porous Media. *Flow Through Porous Media Symposium*, 61 (10), 18.

Sheng, J. (2011) Modern Chemical Enhanced Oil Recovery: Theory and Practice. *Elsevier Science*, 978-185-61-7745-0.

Sun, Y., Saleh, L., Bai, B. (2012) Measurement and Impact Factors of Polymer Rheology in Porous Media. *InTech Europe*, ISBN: 978-953-51-0187-1.

Veerabhadrappa, S.K., Trivedi, J.J., Kuru, E. (2013) Visual Confirmation of the Elasticity Dependence of Unstable Secondary Polymer Floods. *Ind. Eng. Chem. Res.*, 52, 6234-6241.

Chapter 7: Foam Flooding References

Le, V., Nguyen, Q., Sanders, A. (2008) A Novel Foam Concept with CO_2 Dissolved Surfactants. SPE 113370.

Additional References

Bedell, S., Worley, C., Al-Horr, R., McCrery, D. (2010) Quaternaries as Intermediated in the Thermal and Oxidative Degradation of Alkanolamines. *Ind. Eng. Chem. Res.,* 49, 7147-7151.

Chen, H., Zhang, S.H., Chu, Y.B., Yang, H.X., Liu, F.L. (2004) Development and Application of Hydrophobically Associating Polymer Gel in High Temperature and High Salinity Reservoirs for Profile Modification. *Oilfield Chemistry,* 21(4), 343-346.

Chen, X., Adkins, S., Nguyen, Q., Sanders, A., Johnston, K. (2010) Interfacial Tension and the Behavior of Microemulsions and Macroemulsions of Water and Carbon Dioxide with Branched Hydrocarbon Nonionic Surfactant. *J. of Supercritical Fluids*, 55, 712-723.

Chen, Y. (2014) CO_2-in-Water Foam at Elevated Temperature and Salinity Stabilized with a Nonionic Surfactant with a High Degree of Ethoxylation. *Ind. Eng. Chem. Res*.

Cummings, S., Enick, R., Rogers, S., Heenan, R., Eastoe, J. (2010) Amphiphiles for Supercritical CO_2. *Biochimie,* 94, 94-100.

Da Rocha, S., Psathas, P., Klein, E., Johnston, K. (2001) Concentrated CO_2-in-Water Emulsions with Nonionic Polymeric Surfactants. *Journal of Colloid and Interface Science,* 239, 241-253.

Eastoe, J., Dupont, A., Paul, A, Steytler, D., Rumsey, E. (2003) Design and Performance of Surfactants for Carbon Dioxide. *Supercritical Carbon Dioxide; ACS Symposium Series*, Chapter 19, 285-308.

Eastoe, J., Gold, S., Steytler, D. (2007) Hydrocarbon Surfactants for CO_2: An Impossible Dream? *Aust. J. Chem.*, 60, 630-632.

Eastoe, J., Yan, C, Mohamed, A. (2012) Microemulsions with CO_2 as a solvent. *Current Opinion in Colloid and Interface Science,* 17, 266-273.

Gouedard, C., Picq, D., Launay, F., Carrette, P. (2012) Amine Degradation in CO_2 Capture. I. A Review. *International Journal of Greenhouse Gas Control*, 10, 244-270.

O'Callaghan, J., McNamara, H., Copley, M. Hanrahan, J. (2010) Swelling of Ionic and Nonionic Surfactant Micelles by High Pressure Gases. *Langmuir,* 26(11), 7725-7731.

Shen, Z., McHugh, M., Belardi, J., Kilic, S., Mesiano, A., Bane, S., Karnikas, C., Beckman, E., Enick, R. (2003) CO_2 Solubility of Oligomers and Polymers the Contain the Carbonyl Group. *Polymer*, 44, 1491-1498.

Xing, D., Wei, B, Trickett, K., Mohamed, A., Eastoe, J., Soong, Y., Enick, R. (2010) CO_2 Soluble Surfactants for Improved Mobility Control. *Society of Petroleum Engineers,* SPE 129907.

Vita

Madalyn M. Liebum holds a B.S. in Environmental Engineering with a Geology minor from Southern Methodist University in 2013 specializing in surface water treatment and groundwater remediation. She placed 1st regionally and 2nd nationally with her team at the Water and Environment Federation Technical Conference (WEF-Tec) in 2013 focusing on the removal of nitrogen and phosphorus in wastewater treatment plants. The following year, she enrolled at The University of Texas at Austin to seek a M.S. in Petroleum Engineering in order to learn more about subsurface processes and mechanisms for future work in the petroleum or water industry.

This thesis was typed by author.

Email: mliebum@gmail.com